

RICE UNIVERSITY

**Gold Nanoshells for Surface Enhanced Raman Spectroscopy
and Drug Delivery**

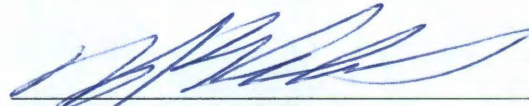
by

Aoune Barhoumi

A THESIS SUBMITTED
IN PARTIAL FULLFILLMENT OF THE
REQUIREMENTS FOR THE DEGREE

Doctor of Philosophy

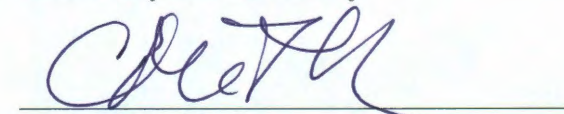
APPROVED, THESIS COMMITTEE:



Naomi J. Halas (Chair)
Professor of Electrical and Computer
Engineering, Professor of Chemistry



Jason H. Hafner
Associate Professor of Physics and
Astronomy and Chemistry



Christy Landes
Norman Hackerman-Welch Young
Investigator, Assistant Professor of
Chemistry

HOUSTON, TEXAS
August 2011

Abstract

• **Gold Nanoshells for Surface Enhanced Raman Spectroscopy and Drug**

Delivery

By

Aoune Barhoumi

Gold nanoshells are tunable plasmonic nanostructures consisting of spherical silica cores wrapped with thin layer of Au. Based on the size of the Au layer with respect to the silica core, gold nanoshells can resonantly absorb or scatter light at any wavelength on the visible or infrared. On resonance, gold nanoshells interact strongly with light to give rise to collective oscillations of the free electrons against the background of the ionic core, phenomena known as localized surface plasmons. The free electron oscillation creates surface plasmon multimodes of various orders. As a result, the average local near field surrounding the Au nanoshell is enhanced. The local field enhancement has been extensively used in different applications. In this work, the local near-field is used to enhance the Raman spectroscopy of DNA and explore the different modes attributed to the base composition and structure of the DNA sequence. We showed that surface enhanced Raman spectroscopy of DNA is dominated by the adenine modes regardless of the base composition of the DNA sequence, a property that we have used to develop a DNA label-free detection system.

As absorbers, plasmon-resonant Au nanoshells can convert absorbed light into heat. As a consequence, the temperature on the Au nanoshell surface increases dramatically. This property is used to light-trigger the release of variety of therapeutic molecules such as

single stranded DNA, siRNA and small molecules. We demonstrated that the local heat can be used to dehybridize double stranded DNA attached to the Au surface via a thiol moiety on one of the DNA strands. The complementary sequence (therapeutic sequence) is released at temperature lower than the standard melting temperature of same DNA sequence. Moreover, small molecules (DAPI) which were initially intercalated on the double stranded DNA attached to the Au surface were successfully released due to the heat generated around the nanoshell surface. Finally, siRNA molecules were also released using a different system made of PLL (polylysine) attached to Au nanoshells. The electrostatic interaction between the negatively charged siRNA and the positively charged PLL was overcome by the thermal perturbation causing the siRNA to be released. *In vitro* experiments successfully showed the release of siRNA, single stranded DNA and small molecules.

Acknowledgements

I would like to first thank my thesis advisor, Dr. Naomi Halas, for her support, assistance and guidance. I highly appreciate the freedom I had on choosing my projects and pursuing them. I also appreciate her help with the critical thinking and constructive criticism on all my projects. Her guidance has inspired me to do extremely well not just in graduate school but in life in general.

I would also like to thank the Halas group members for helping me throughout the past five years. I would like to thank every single member of the group without mentioning names. I appreciate all past group members for their hard work and commitment; it is only because of them that the group is the way it is now. I would like to thank and appreciate all present group members for their continuous hard work and motivation.

I would also like to thank my parents, my brothers and sisters for supporting me throughout all my studies. I thank them for their love, help, and support and I dedicate my success to them

Table of Contents

Abstract	i
Acknowledgements	iii
Table of Contents	iv
List of Figures	viii
List of Tables	xi
Chapter 1: Introduction	1
<i>1.1 Raman Spectroscopy</i>	1
<i>1.1.1 Raman Scattering</i>	1
<i>1.1.2 Surface Enhanced Raman Spectroscopy</i>	4
<i>1.2 Gold Nanoshells</i>	5
<i>1.2.1 Background and physical properties</i>	5
<i>1.2.2 Nanoshells Fabrication</i>	6
<i>1.2.3 Near Field Properties of Au Nanoshells</i>	8
<i>1.2.4 Thermal Properties of Au Nanoshells</i>	12
<i>1.3 Gene Therapy</i>	18
<i>1.3.1 The Challenge of Gene Therapy Vector Design</i>	18
<i>1.3.2 Gold Nanoparticle-based Vectors for gene therapy</i>	19
Chapter 2: Surface Enhanced Raman Spectroscopy of DNA	24
<i>2.1 Introduction</i>	24
<i>2.2 Experimental</i>	27
<i>2.3 Analysis</i>	29

2.4 Results and Discussion.....	31
2.4.1 Adenine Dominated SERS Spectra	34
2.4.2 Detection of DNA Interaction with Cisplatin and Transplatin.....	40
2.5 Conclusion	42
Chapter 3: Correlation of Molecular Orientation and Packing density in a dsDNA self-assembled monolayer observable with Surface Enhanced Raman Spectroscopy	44
3.1 Introduction.....	44
3.2 Results and Discussion.....	45
3.3 Conclusion.....	51
Chapter 4: Label-Free Detection of DNA Hybridization Using Surface Enhanced Raman Spectroscopy.....	53
4.1 Introduction.....	53
4.2 Experimental	55
4.3 Results and Discussion.....	57
4.3.1 Label-free Detection Using Adenine-free Capture Probe.....	57
4.3.2 Label-free Detection Using 2-Aminopurine Substituted capture Probe.....	61
4.3.3 Hybridization Efficiency	63
4.3.4 Target Concentration and Detection limits	66
4.4 Conclusion.....	67
Chapter 5: Detecting Chemically Modified DNA Bases Using Surface Enhanced Raman Spectroscopy	69

5.1 Introduction.....	69
5.2 Experimental Methods.....	71
5.3 Results and Discussion.....	72
5.3.1 Detection of Methylated Adenine.....	72
5.3.2 Detection of Methylated Cytosine.....	77
5.3.3 Detection of hydroxymethylated Cytosine.....	74
5.3.4 Detection of Oxidized Guanine	75
5.4 Conclusion.....	77
Chapter 6: Light-induced Release of DNA from Plasmon-resonant Nanoparticles: Towards Light-controlled Gene Therapy.....	78
6.1 Introduction.....	78
6.1.1 Gold Nanoshells in Photothermal therapy and Drug Delivery	79
6.1.2 Thermal Dehybridization of dsDNA	80
6.2 Experimental	82
6.2.1 Thermal and light-driven DNA Release	82
6.2.2 DNA-nanoshell Coverage and percentage Release.....	82
6.3 Results and Discussions.....	84
6.3.1 DNA Dehybridization Irreversibility.....	84
6.3.2 Thermal Release of ssDNA	87
6.3.3 Light-induced Release of ssDNA.....	89
6.3.4 Surface Coverage and Percentage release.....	91
6.4 Conclusions.....	92

Chapter 7: Visualizing Light-triggered Release of Molecules Inside Living	
Cells.....	94
7.1 <i>Introduction.....</i>	94
7.1.1 <i>Biomedical Applications of Plasmonic Nanoparticles</i>	94
7.1.2 <i>DAPI (4,6-diamino-2-phenylindole).....</i>	96
7.2 <i>Result and Discussion.....</i>	97
7.2.1 <i>DAPI Fluorescence intensity.....</i>	97
7.2.2 <i>Nanoshell Cell Uptake</i>	98
7.2.3 <i>Intracellular Light-induced DAPI Release.....</i>	100
7.2.4 <i>Cytotoxicity Study.....</i>	104
7.3 <i>Conclusion.....</i>	106
Chapter 11: Summary and Perspectives.....	108
References.....	111

List of Figures

Figure 1.1 Model of a molecule.....	1
Figure 1.2 Quantum description of the molecular scattering	3
Figure 1.3 Schematic diagram and corresponding TEM images showing nanoshell fabrication	7
Figure 1.4 SEM sample of synthesized nanoshells.....	8
Figure 1.5 Au nanoshell near field properties.....	10
Figure 1.6 Au Extinction spectra of Au nanoshells showing the maximum absorbance with respect to the IR window (dimensions ~ [120,150] nm). Inset depicts the internal structure of a Au nanoshell.....	15
Figure 1.7 Schematic of the four major types of DNA-based therapies.....	17
Figure 2.1 Typical SERS spectra of untreated and thermally treated ssDNA	32
Figure 2.2 SERS spectra of adenine, thermally pretreated single stranded and double stranded DNA	34
Figure 2.3 Normal Raman of DNA.....	35
Figure 2.4 SERS of thermally treated adenine-free ssDNA and pre-hybridized dsDNA (same sequence with its complement).....	39
Figure 2.5 SERS of cisplatin/transplatin bound to 30 bp dsDNA.....	40
Figure 3.1 SERS detection of DNA orientation. Schematic of the orientation detection strategy based on variation of dsDNA tilt angle and SERS spectra of dsDNA at different concentrations.....	46
Figure 3.2 Guanine to adenine peak intensity ratio as a function of DNA concentration.....	48
Figure 3.3 The ratio of the intensity of the ring-bending mode of adenine at 623 cm^{-1} to the intensity of the breathing mode of adenine at 736 cm^{-1} as a function of the DNA concentration.....	49

Figure 3.4 SERS spectrum of nonthiolated dsDNA.....	50
Figure 3.5 DNA tilt due to incubation with polyT. SERS spectra of dsDNA before and after polyT incubation.....	51
Figure 4.1 SERS of DNA sequences with and without adenine bases.....	58
Figure 4.2 SERS label-free detection of DNA hybridization based on adenine-free probe. SERS of capture probe hybridized with complementary DNA sequence (target) and capture probe hybridized with non-complementary DNA sequence (control).....	60
Figure 4.3 Raman spectroscopy of 2-aminopurine. Surface enhanced and non-enhanced Raman spectroscopy of 2-aminopurine bases.....	62
Figure 4.4 Label-free detection of DNA hybridization based on 2-aminopurine modified DNA prob.....	63
Figure 4.5 Label-free detection calibration curve. Plot shows the hybridization efficiency versus target concentration	65
Figure 5.1 SERS spectra of normal and adenine-methylated DNA sequences.....	72
Figure 5.2 SERS spectra of normal and cytosine-methylated DNA sequences.....	74
Figure 5.3 SERS spectra of normal and cytosine-hydroxymethylated DNA sequences.....	75
Figure 5.4 SERS spectra of normal and guanine-oxidized DNA sequences.....	76
Figure 6.1 Schematic of light-controlled release of ssDNA from Au nanoshells.....	80
Figure 6.2 DNA dehybridization irreversibility. Schematic depicting the released DNA behavior with and without complementary sequence and a graph shows the amount of DNA released versus the temperature based on the released DNA fluorescence intensity.....	86
Figure 6.3 Thermal and light-assisted release of ssDNA from dsDNA-coated nanoshells in solution.....	88
Figure 6.4 Comparison of the light-induced versus thermal dehybridization of dsDNA sequences of different lengths tethered to Au nanoshells.....	90
Figure 7.1 Light-induced DAPI release. Schematic diagram of the light-induced DAPI release and diffusion inside the cell. Fluorescence emission of (i) DAPI only, (ii) DAPI with ssDNA, and (iii) DAPI with dsDNA.....	97

Figure 7.2 Nanoshell-dsDNA-DAPI Cell uptake. Dark field/epifluorescence images of incubated and non-incubated H1299 lung cancer.....99

Figure 7.3 Light-induced DAPI release.....103

Figure 7.4 Flow cytometry cytotoxicity assay. All plots are side-scattered light (SS) versus Propidium Iodide (PI) intensity.....105

List of Tables

Table 1.1 A summary of different Au nanostructures utilized for light activated and non-light activated gene therapy, their wavelength of response, DNA attachment chemistry, and therapeutic target.....	21
Table 2.1 Oligonucleotide sequences used in the described experiments.....	27
Table 2.2 Assignments of normal Raman bands of DNA	35
Table 3.1 DNA sequences used in the described experiments	45
Table 4.1 Oligonucleotide sequences used in the described experiments.....	56
Table 4.2 Raman Assignments.....	58
Table 6.1 DNA sequences used in this study.....	83

Chapter 1: Introduction

1.1 Raman Spectroscopy:

1.1.1 Raman Scattering:

When electromagnetic (EM) waves interact with a molecule, the electron cloud of the molecule oscillates periodically at the same frequency of the incident EM. As a result, an induced dipole is created within the molecule. The dipole can radiate light, mostly at the same frequency of the emitted light (elastic scattering). However, some of the light is radiated at frequencies different than that of the incident light, phenomenon known as non-elastic scattering. Raman scattering is an example of the non-elastic scattering of light due to the interaction of incident EM with a molecule.

Classically, Raman scattering can be explained using the model shown in Figure 1.1. The molecule is modeled as 2 spheres of masses m_1 and m_2 connect by a spring of constant k .

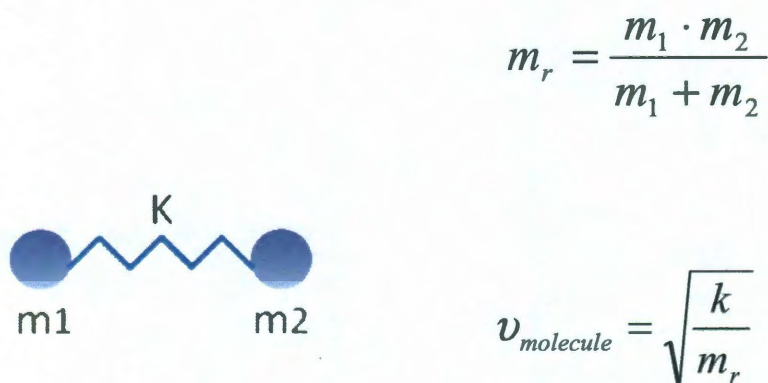


Figure 1.1: Model of a molecule. The vibrational frequency ν is proportional to the square root of the force constant and inversely proportional to the reduced mass of the atoms that are bonded together

- The incident light $E_{(x,t)} = E_0 \cos(\omega_L t - kx)$
- The induced dipole is $\mu = \alpha E$ ($\alpha = \text{polarizability}$)

Substituting in the electric field of light $\mu = \alpha E_0 \cos(\omega_L t)$

Since the polarizability depends on the conformation of the molecule, it will change as the molecule vibrates.

$\alpha = \alpha(Q)$ where Q is the vibrational coordinate

$$\alpha = \alpha_0 + \left[\frac{\partial \alpha}{\partial Q} \right] \cdot dQ + \dots \quad \text{where } Q = Q_0 \cos(\omega_M t)$$

The induced dipole can be calculated as:

$$\mu = \alpha \cdot E_0 \cdot \cos(\omega_L t) + \left[\frac{\partial \alpha}{\partial Q} \right] \cdot Q_0 \cdot E_0 \{ \cos[(\omega_L - \omega_M)t] + \cos[(\omega_L + \omega_M)t] \}$$

The three terms represent frequencies at which light will be emitted. The first emitted frequency equals the frequency of the incident light (elastic scattering, example: Rayleigh scattering), the second and third emitted frequencies are shifted from the incident light (non-elastic scattering, example: Raman scattering).

$\frac{\partial \alpha}{\partial Q}$ has to be non-zero for Raman scattering to occur. Only molecules that interaction with EM can induce a change in molecular polarizability are Raman active molecules.

The quantum picture illustrates better the Raman scattering and explains the phenomenon in terms of transition between electronic states. When the molecule absorbs the incident light, it will be excited from the ground state to a virtual state that is lower than the lowest electronic state. The excited electron will return back to the ground state and three cases are possible. Given that the ground state has energy sub-levels due to the vibrational states of the molecule, the

excited electron can return back to the same sub-level giving off the same frequency of the incident light in that case the scattering is called Rayleigh scattering. If the electron returns back to a different vibrational sub-level (higher or lower in energy than the original sub-level), the scattering is called respectively stokes and anti-stokes.

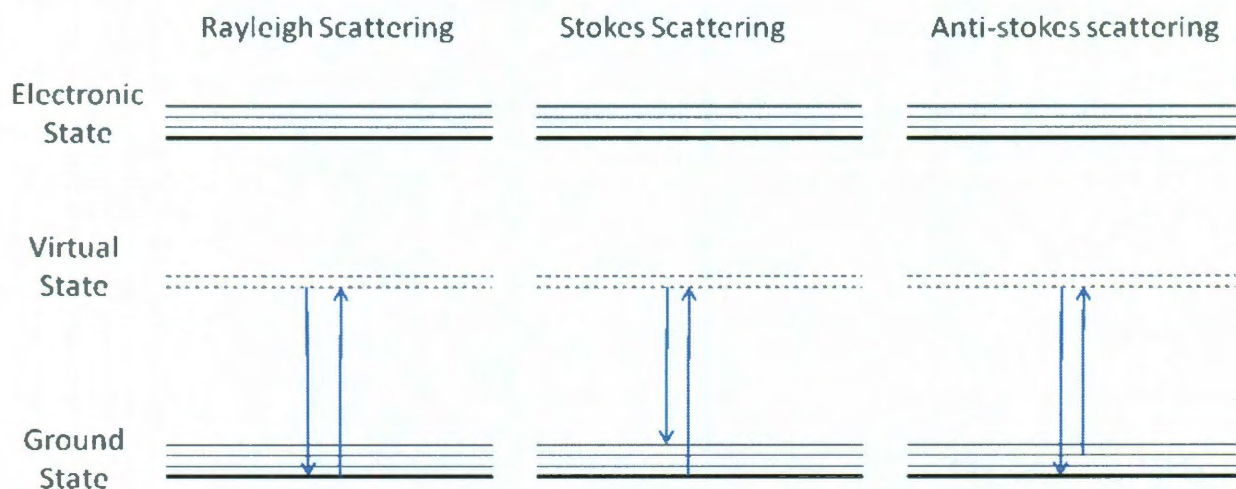


Figure 1.2: Quantum description of the molecular scattering

As discussed earlier and depicted in the Figure 1.2, the Raman scattering depends on the vibrational modes of the molecule. Raman scattering is used as a spectroscopic tool to study simple molecules at different phases (especially solid and gas). Raman scattering is used to study more complex biological molecules such as DNA and proteins¹. It is also used for material identifications and analysis. One major disadvantage of Raman scattering is the signal weakness. Raman signal intensity is orders of magnitude weaker than the elastic scattering. Only 1 in 10^7 photons is scattered inelastically². Because the low probability of detecting the Raman signals, Raman scattering remained under-used for a quite long period of time.

1.1.2 Surface Enhanced Raman Scattering:

In order to overcome the problem of low cross section of Raman scattering, scientists tried to increase the number of probed molecules using a roughened surface. In 1974, Fleischmann *et al* reported the observation of relatively high Raman scattering signals from monolayer of pyridine absorbed on a roughened silver electrode³. The high intensity of the Raman signals which was explained by the increase of the absorbed molecules due to the surface roughness remained a mystery for couple of years since it did not match the predicted calculation. In 1977, Van duyne reported an enhancement factor as high as 10^6 for pyridine on a roughened silver electrode and claimed that the real reason behind the high Raman signal intensity is the surface enhancement effect⁴. Recently SERS has overcome most of the technical problems and become the main techniques used to detect and identify low concentration analytes for chemical sensing and biological applications.

The main reason behind the Raman surface enhancement is the electromagnetic effect⁵. Briefly, the laser excites the roughened metal free electrons creating local charge oscillations. The later generate a high local electric field. Both incident and scattered light are affected by this enhanced field. As a result the Raman signal enhancement is proportional to the E^4 . The second less important contributor to the Raman enhancement is the chemical effect⁶. This effect can be explained by the charge transfer that takes place between the absorbed molecule and the metal surface.

It was predicted that any nanoscale features capable of sustaining surface plasmon excitation can be used as active SERS substrates. Recently, it has been reported that other than roughened metal surfaces, metal nanostructures such as Au nanoparticles and nanorods can form good

Raman active substrate. The collective oscillation of the free electrons on the nanostructure surface generates an enhanced local electric field. Similar to the roughened metal surfaces, the local electric field generated on the close vicinity of metal nanostructures can enhance the weak Raman scattering. Moreover, small aggregates of two or more nanostructures can further enhance the local electric field leading to much higher Raman enhancement. An enormous variety of metal nanostructures were explored as Raman active substrates mostly fabricated using metal nanoparticles deposited on a substrate, chemically roughened surfaces and lithographically fabricated nanostructures. In this thesis, Au nanoshells deposited on silica substrates are used as Raman active substrate.

1.2 Gold Nanoshells

1.2.1 Background and Physical Properties:

Au nanoshells are plasmonic, spherical nanostructures consisting of silica (SiO_2) core wrapped with a thin layer of Au⁷. The interaction between the plasmons of the dielectric core and the metal shell grants Au nanoshell a set of particularly important optical properties. Arguably, the most significant property that distinguishes Au nanoshell from other metal nanostructures is being tunable from the visible to the near infrared (NIR) portion of the spectrum. This tunability can be easily controlled by adjusting the thickness of the Au shell with respect to the silica core during the fabrication process. Au nanoshells like other metal nanostructures support local plasmon oscillation and can form ideal SERS active substrates. The open topography of nanoshells allows detection and identification of large biomolecule such as DNA. Au nanoshells that resonate at the NIR are particularly important for biomedical applications ranging from diagnostic to therapy. Au nanoshells have been used for NIR bioimaging^{8,9} and photothermal cancer therapy¹⁰⁻¹². The ease of conjugation of certain biomolecules such as single stranded

DNA (ssDNA), double stranded DNA (dsDNA) and peptides to the Au surface of nanoshells open doors for new applications in many fields such as drug targeting and delivery. The relative ease of cell uptake and biocompatibility of Au nanoshells allow *in vivo* applications and make nanoshells a potential candidate for future therapies which will allow diagnostic, delivery and controlled release of therapy all done on a single nanostructure.

1.2.2 Nanoshells Fabrication:

Au nanoshells are synthesized according to previously published procedures.^{13, 14} The dimensions of the silica core (120 nm colloidal silica, Precision Colloids LLC, Cartersville GA) and the Au shell were chosen such that the peak plasmon resonance in aqueous suspension was 800 nm, corresponding to the excitation wavelength used in all this work. Briefly, after cleaning commercial silica stobers by multiple washes with ethanol (200 proof), the silica cores are functionalized with 3-aminopropyltriethoxysilane (APTES, Sigma) overnight under vigorous stirring. The silane part of the APTES allowed covalent binding to silica nanospheres and the amine group of the APTES is available to attach to small Au nanoparticles. Separately, small gold nanoparticles ~2 nm in diameter are synthesized using tetrakis(hydroxymethyl)phosphonium chloride (THPC) as the reducing agent from the method reported by Duff, *et al.*¹⁵ After aging for at least 2 weeks, the small Au nanoparticles are incubated with the APTES functionalized silica nanospheres overnight. As a result, the small Au nanoparticles decorate the silica nanospheres serving as nucleation sites for metal growth. The ratio of silica particles to THPC-Au is estimated from the total surface area of the silica particle solution, the concentration and physical cross-section of the THPC-Au, and assuming 25 – 30 % coverage of THPC-Au on the silica surface. Typically, 1 M NaCl is used to increase the isoelectric point of the solution mixture by increasing the ionic strength, thereby decreasing

Coulombic repulsion and increasing surface coverage of THPC-Au nanoparticles on the silica surface. The size of the THPC-Au nanoparticles (the smaller the better) and the surface coverage of THPC-Au on silica nanospheres (the higher the better) are the main contributors to the quality of synthesized nanoshells. The role of these parameters becomes more prominent when thinner Au shell is attempted.

Once the seeds (silica cores decorated with small nanoparticles, Fig. 1.3 (i)) are ready, a plating solution is prepared separately. The plating solution is prepared by mixing 3 mL of 1% HAuCl₄ solution (which was aged for 14 days) with 50 mg K₂CO₃ in 200 mL of deionized H₂O. The plating solution must let set for at least 24–72 hours before being ready to be used. The last step consists of adjusting the ratio of the seed solution to the plating solution. This ratio determines the amount of Au deposited on the surface of the silica spheres thus the thickness of Au shell which determines the optical properties of synthesized nanoshells. It is worth to note that a reducing agent must be added to the seed/plating solution mixture. Formaldehyde has been used as the reducing agent to synthesize nanoshells for a long time, however lately Brinson *et al.*¹⁶ have demonstrated that carbon monoxide (CO) can alternatively used to reduce the Au salt and produce nanoshells of relatively higher quality.

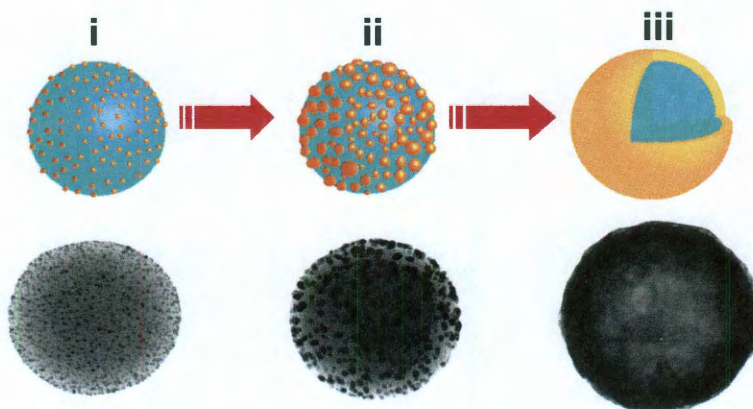


Figure 1.3: Schematic diagram and corresponding TEM images showing nanoshell fabrication: (i) small Au particles attached to amine terminated silica nanospheres, (ii) start of the Au reduction, and (iii) complete Au nanoshell

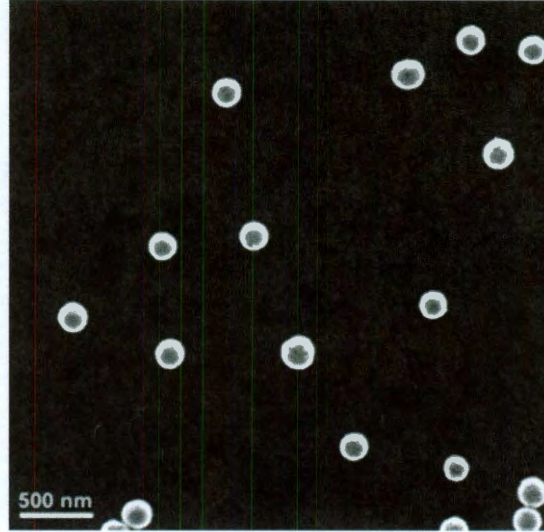


Figure 1.4: SEM sample of synthesized nanoshells using method described above

1.2.3 Near-Field Properties of Au Nanoshells:

As mentioned earlier, the Raman enhancement that takes place at the surface of the Au nanoshell is due to enhanced local field which is a near field property. In order to understand the fundamental physics behind the local field enhancement, this section will give a brief background on the physical properties of Au nanoshell and particularly the near field properties.

In this section Au nanoshell is modeled as shown in Figure 1.5.a. The inner radius (radius of the silica sphere) is r_1 and the outer radius (radius of the nanoshell) is r_2 . ϵ_1 , ϵ_2 and ϵ_3 represent

dielectric constants of silica (2.13), Au ($\epsilon_{Drude-Lorentz}(\omega) = 1 - \frac{\omega_p^2}{\omega^2 + i\Gamma\omega} + L(\omega)$) and the aqueous

medium (1.78), respectively. The interaction between light and Au nanoshell is treated on the quasi-static approximation. The quasi-static approximation simply means that the size of Au

nanoshell is small compared to the incident light wavelength which implies that the incident electric field does not vary spatially over the dimension of the Au nanoshell, the temporal variation is preserved. Practically, the quasi-static approximation is valid for Au nanoshells of diameters less than 80 nm. The quasi-static approximation simplifies tremendously the mathematical calculations and gives a pretty accurate description of the optical properties of Au nanoshell even for diameters larger than 80 nm.

Given the incident electric field $E(r, t) = E_0 e^{-i\omega t}$, the electric field in the three regions of the nanoshell (region 1 = silica, region 2 = gold and region 3 = aqueous medium) is given by the following equation^{17, 18}:

$$E_i = -\nabla\Phi_i(r, \theta)$$

Where

$$\Phi_i(r, \theta) = \left[A_i r + \left(\frac{B_i}{r^2} \right) \right] \cos \theta$$

By adjusting the right boundary conditions, the electric fields at the three regions can be derived:

$$E_1 = \frac{9\varepsilon_2\varepsilon_3}{\varepsilon_2\varepsilon_a + 2\varepsilon_3\varepsilon_b} E_0 (\cos \theta \hat{r} - \sin \theta \hat{\theta})$$

$$E_2 = \frac{3\varepsilon_3}{\varepsilon_2\varepsilon_a + 2\varepsilon_3\varepsilon_b} \left\{ \left[(\varepsilon_1 + 2\varepsilon_2) + 2(\varepsilon_1 - \varepsilon_2) \times \left(\frac{r_1}{r} \right)^3 \right] E_0 \cos \theta \hat{r} - \left[(\varepsilon_1 + 2\varepsilon_2) - (\varepsilon_1 - \varepsilon_2) \times \left(\frac{r_1}{r} \right)^3 \right] E_0 \sin \theta \hat{\theta} \right\}$$

$$E_3 = \left(2 \frac{\varepsilon_2\varepsilon_a - \varepsilon_3\varepsilon_b r_2^3}{\varepsilon_2\varepsilon_a + 2\varepsilon_3\varepsilon_b r^3} + 1 \right) E_0 \cos \theta \hat{r} + \left(\frac{\varepsilon_2\varepsilon_a - \varepsilon_3\varepsilon_b r_2^3}{\varepsilon_2\varepsilon_a + 2\varepsilon_3\varepsilon_b r^3} - 1 \right) E_0 \sin \theta \hat{\theta}$$

$$\begin{aligned} \varepsilon_a &= \varepsilon_1 (3 - 2P) + 2\varepsilon_2 P \\ \varepsilon_b &= \varepsilon_1 P + \varepsilon_2 (3 - P) \end{aligned}$$

Where

$$P = 1 - \left(\frac{r_1}{r_2} \right)^3$$

The important region for Raman enhancement is the region 3 (region outside the shell) where the entire field enhancement is taken place. At the region the induced field as similar to a dipole with an effective dipole moment given by:

$$p = \epsilon_3 \alpha E_{induced}$$

The polarizability is given by:

$$\alpha = 4\pi\epsilon_0 r_2^3 \left[\frac{\epsilon_2 \epsilon_a - \epsilon_3 \epsilon_b}{\epsilon_2 \epsilon_a + 2\epsilon_3 \epsilon_b} \right]$$

This interpretation shows that at the quasi-static approximation, the interaction of the Au nanoshell and the incident electric field generates an oscillating dipole. This dipole resonates when the polarizability α is maximized or the denominator reaches zero.

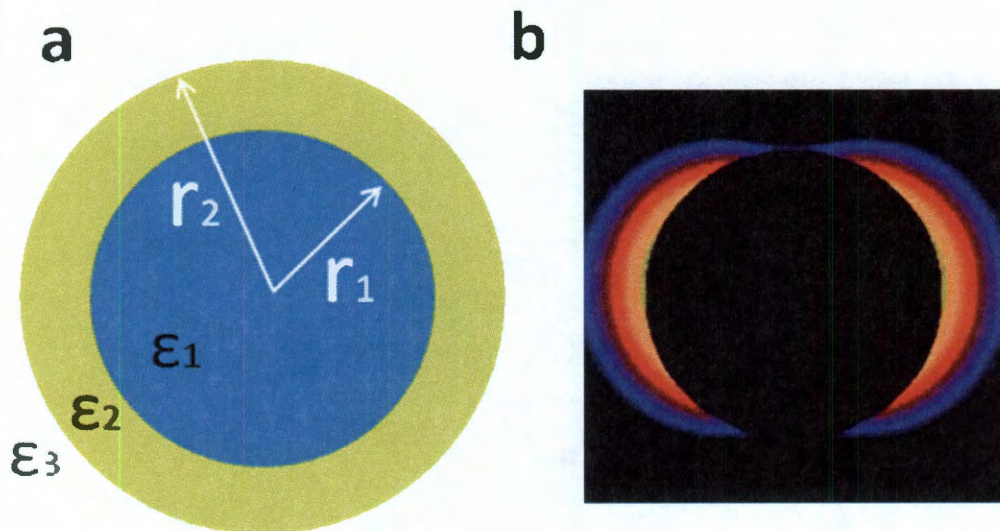


Figure 1.5: Au nanoshell near field properties. (a) schematic depicts the nanoshell parameters. (b) theoretical simulation shows nanoshell near field property.

The local near field at the nanoshell surface is calculated as E_3 (in region 3). The nanoshell near field can be evaluated at appropriate distances from the surface by calculating the average of the field different points on the nanoshell surface. Figure 1.5.b illustrates the local field enhancement on the surface of the nanoshells. It also shows the decay of the local field that extends only few nanometers off the nanoshell surface.¹⁹

Designing the most appropriate SERS substrate that guaranties both high SERS enhancement factor based on high field enhancement as well as high signal reproducibility has been the main challenge on the SERS field. Theoretical calculations showed that interacting plasmon “motifs” such as dimers possess the largest field enhancement at the gap between adjacent particles and rapidly falls as a function of the interparticles distance.²⁰ The debate between using higher order plasmon “motifs” (dimers, trimers, etc) versus single particles has been lately resolved for the use of single particles for these reasons:²¹

1. Even though theoretical calculations shows that the enhancement taking place at the dimers gap exceeds that on single nanoparticles by orders of magnitude, experimental data proves that the SERS enhancement produced by nanosphere dimers is only one order of magnitude greater than isolated nanoshells. Even more surprising, SERS enhancement on nanoshell dimers which theoretically should be one order of magnitude greater than nanosphere dimers, was comparable to isolated nanoshell²². The main reason behind these experimental observations is that the physical size of the gap between adjacent nanospheres (where the all enhancement takes place) is significantly smaller than the physical size of the enhanced area in a single particle. As a consequence increase in the

SERS enhancement in the case of the dimer gap is compensated by the decrease of probed molecule due to the limitation of the physical gap size.

2. The physical size of the gap between adjacent nanoparticles prevents probing larger molecules such as DNA and proteins. The gap area will not be accessible for most large biomolecules which are of great interest.
3. The fabrication of SERS substrates consisting of nanoparticle dimers is extremely challenging and mostly involves the use of lithography which is time and money consuming. On the other hand, substrate consisting of isolated particles is extremely easy and straightforward and requires only few steps of easy and known chemistry as will be described later.

For all these reasons we preferred to use films of isolated nanoshells as SERS active substrates for all the SERS work on this thesis. The fabrication of the substrate will be discussed in detail later on.

1.2.4 Thermal Properties of Au Nanoshells:

The combination of gold nanoparticles and biomolecules has enabled considerable advances in diagnostic and therapeutic nanomedicine.²³ In addition to biocompatibility and ease of fabrication and functionalization, the optical properties of certain noble metal nanoparticles are ideal for biomedical applications. The interaction of light with noble metal nanoparticles results in collective oscillations of the free electrons in the metal known as localized surface plasmons. On resonance, a metallic nanoparticle interacts strongly with incident light, possessing an extinction cross section nominally five times its physical cross section. Resonant illumination can result in strong light scattering (useful in biological sensing and imaging) and strong absorption, with relative magnitudes depending upon absolute nanoparticle size. As absorbers,

plasmon-resonant nanoparticles are unparalleled light-to-heat converters, dissipating energy via their lattice phonons.²⁴

Due to their extraordinarily large absorption cross sections and their inability to re-emit light, the photothermal properties of metallic nanoparticles are arguably their dominant physical characteristic.²⁵⁻²⁷ The physical process underlying the photothermal response of metal-based nanoparticles has been studied quite extensively using time-resolved pulsed laser sources and techniques.²⁸⁻³⁰ Whether a nanoparticle absorbs or scatters light is a function of its size: small nanoparticles are completely absorptive, while with increasing size the ratio of absorption to scattering cross section of a nanoparticle decreases in a complex manner. Ultimately, larger sized micron-scale particles are better scatterers than absorbers of light. Upon resonant illumination with an ultrashort laser pulse, absorptive metallic nanoparticles undergo a very rapid and dramatic increase in temperature (on the subpicosecond timescale). First, there is an initial transient regime where the electrons are at a much higher temperature than the atomic lattice of the nanoparticle. Following this initial rapid heating, the electron and lattice temperatures of the nanoparticle equilibrate on the timescale of a few picoseconds, consistent with the inverse of the highest phonon frequency in the material. Both theoretical and experimental studies indicate that nanoparticle surface temperatures that result can easily exceed the boiling point of water, sometimes by several hundreds of degrees,²⁷ depending on the nanoparticle properties and illumination characteristics. In some cases this can result in a melting/reshaping of the nanoparticle, changing its optical absorption characteristics irreversibly.^{31, 32} If the light-absorbing nanoparticle is immersed in a medium or fluid when illuminated, a nonequilibrium condition will exist between the hot nanoparticle and the cooler surrounding medium. At very low incident powers, this still can result in remarkably large temperature increases in the

surrounding medium due to the presence of the hot nanoparticle.³³ At the lower illumination intensities of interest in biomedical applications, the photothermal response of the nanoparticle can result in heating of the local medium surrounding the nanostructure, which can be used for photothermal tumor ablation by inducing hyperthermia, with resultant cell death.³⁴ For the light-assisted delivery of nucleotides, sufficient incident intensities must be used to initiate the process of DNA melting on the nanoparticle surface, but must be significantly below the intensities where photothermal cell death may result.³⁴⁻³⁷

The plasmon resonant frequencies of metallic nanoparticles depend strongly on particle geometry. The plasmon resonant frequencies of metallic nanoparticles can be tuned through the interaction, or hybridization, of plasmons supported by nanostructure geometry.^{38, 39} This underlying principle, known as plasmon hybridization, has given rise to a large family of plasmonic nanoparticles whose resonances can be tuned to virtually any resonant frequency in the visible and infrared regions of the electromagnetic spectrum. For biomedical applications, a progression of gold nanostructures of various shapes and sizes has been developed with optical resonances in, or that can be tuned to, the near infrared (NIR) water window (690-900 nm).⁴⁰⁻⁴² Blood and tissue are maximally transparent in this NIR spectral window, making it optimal for biomedical applications that utilize light.⁴³

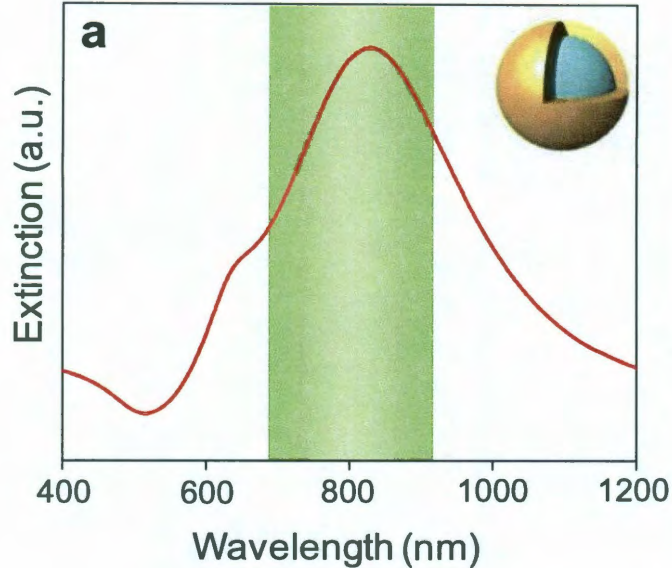


Figure 1.6: Au nanoshell characterization. Extinction spectra of Au nanoshells showing the maximum absorbance with respect to the IR window (dimensions $\sim [120,150]$ nm). Inset depicts the internal structure of a Au nanoshell.

1.3 Gene Therapy:

The fundamental definition of gene therapy is to insert or delete genes- the DNA sequences containing all information needed to express specific proteins- into cells, resulting in therapeutic benefits for specific diseases. The goal is to control and modify the expression of certain specific proteins associated with the cause or occurrence of a disease. When a protein is undesirably expressed by unhealthy cells, inhibiting its functionality or arresting its expression is a process known as downregulation: conversely, enabling protein expression is referred to as upregulation. Following the completion of the sequencing of the human genome, gene therapy is the next logical step in the development of advanced medical treatments for human disease.

Recently, several approaches to gene delivery involving nucleic acids (DNA or RNA) have emerged as potential oligonucleotide-based therapeutic strategies for various diseases.

There are four major classes of oligonucleotide therapy:⁴⁴ (i) Plasmid therapy, (ii) Antisense therapy, (iii) Antisense and short interfering RNA (siRNA) therapy, and (iv) Aptamer therapy (Fig. 1). Plasmid therapy targets DNA and introduces new genes that express proteins missing in cells. Plasmids are long, double-stranded DNA containing the foreign genetic code, delivered inside cells, to diffuse into the nucleus and become incorporated into the cell's genetic material.⁴⁵ Once integrated with the cell's DNA, plasmids become part of the genetic material, allowing continuous expression of a specific missing protein. Antisense therapy directly targets and binds to specific segments of DNA, preventing transcription to the mRNA and thus protein expression. Antisense and siRNA therapies target messenger RNA (mRNA), the intermediary between DNA and functional protein, and can selectively inhibit the expression of a specific protein. Antisense is based on hybridizing a short ssDNA sequence (15 to 30 bases) to its complementary region on the mRNA; once bound, it blocks further translation of the specific mRNA, arresting protein synthesis.⁴⁶ siRNA is a double stranded RNA sequence, nominally 20 bases long, containing the complement of the target mRNA. siRNA therapy involves a more complicated mechanism, where a combination of molecular complexes destroy the target mRNA and result in gene silencing.⁴⁷ Aptamers are short single or double stranded DNA that have been combinatorially selected to recognize and bind to specific target proteins post-translationally, inhibiting their functionality for therapeutic benefit.⁴⁸ Here we focus on antisense oligonucleotide delivery.

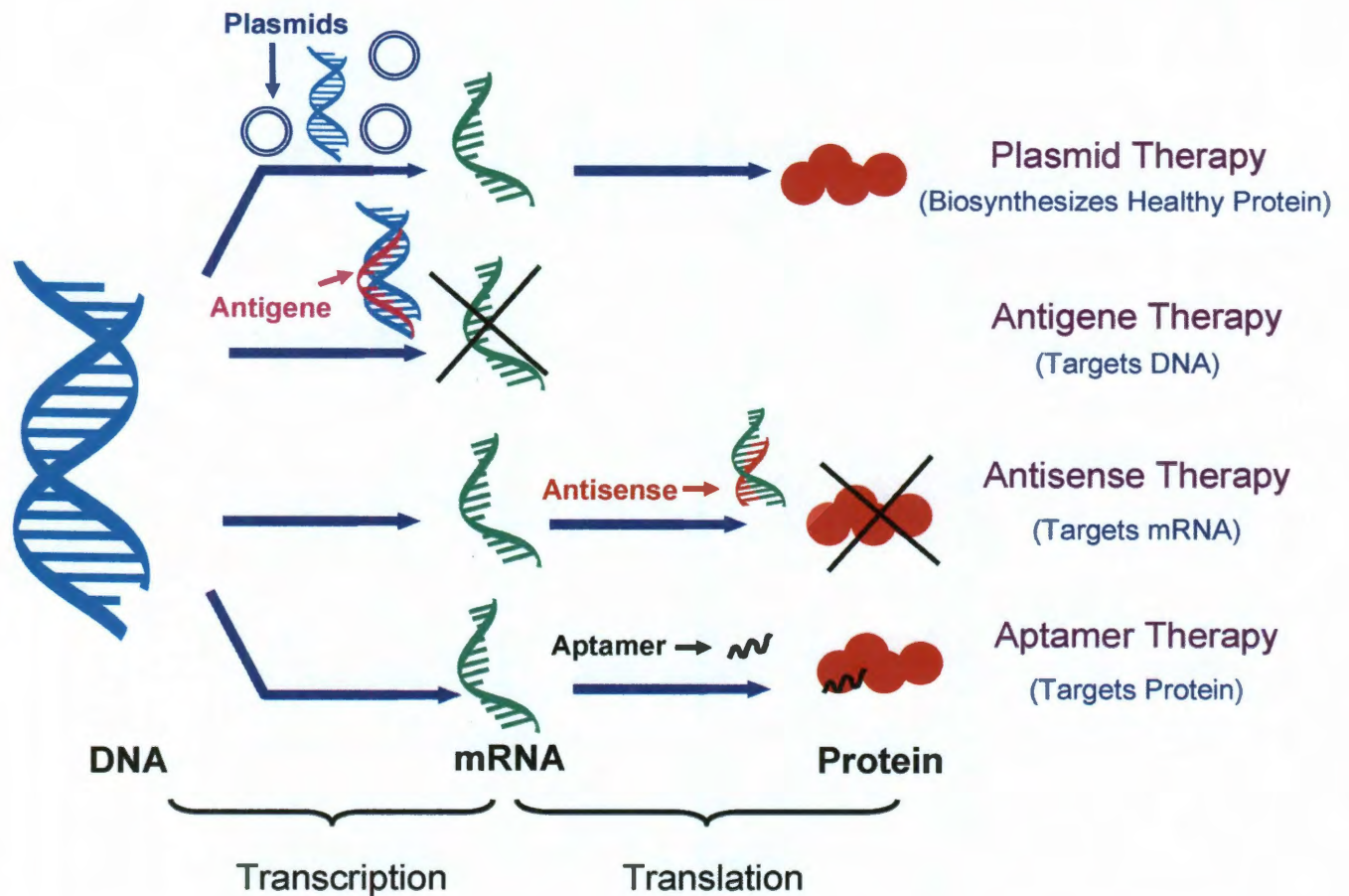


Figure 1.7: Schematic of the four major types of DNA-based therapies. Plasmid DNA enters the nucleus and biosynthesize new healthy protein. Antigen oligonucleotides enter the nucleus, form a triplex with the genomic DNA, and block transcription. Antisense oligonucleotides bind to mRNA, located in the cytoplasm, and block translation. Aptamers act as a conventional type of drug by targeting the malfunctioning protein directly.

Antisense therapy was first suggested by Stephenson and Zamecnik 30 years ago.⁴⁹ The principle of antisense therapy is very simple: design a short single-stranded oligonucleotide to hybridize to a particular messenger RNA (mRNA) target, which then inhibits the translation of that specific mRNA sequence into its corresponding protein. Antisense therapy has been suggested as a therapeutic strategy for cancer, viral infections and inflammatory diseases.⁵⁰

1.3.1 The Challenges of Gene Therapy Vector Design:

However, there are several major inherent challenges to antisense delivery that have impeded its translation into clinical practice.⁵¹ Oligonucleotides by themselves cannot be injected directly into the bloodstream for systemic delivery, due to their rapid degradation (< 20 minutes) by serum nucleases. A carrier that protects the oligonucleotides from enzymatic degradation is therefore essential to any practical delivery strategy. The DNA carrier must also be small enough and possess favorable chemical properties to extravasate (be removed from the bloodstream), be taken up by cells, deliver the oligonucleotide cargo into the cells of interest, and access the cell's genetic material so that it is available to perform its therapeutic mission. Intracellular uptake of foreign materials or structures, a process known as endocytosis, typically results in sequestration of the foreign object within an endosomal compartment inside the cell. Here again, the oligonucleotide may be subject to enzymatic degradation within the endosome. For the oligonucleotide to have its intended therapeutic effect it must be released, or diffused from, the endosomal compartment into the cytosol and within an effective distance of the cell nucleus or ribosome, depending on its specific gene target. Originally, viruses were proposed as delivery vectors for gene therapy, because their own replication requires the injection of their genetic material into cellular hosts. Despite their inherent effectiveness in delivering oligonucleotides *in vivo*, viral vectors have induced unexpected and highly deleterious immune system responses in clinical subjects resulting in death, which is likely to prevent their ultimate approval for clinical use.⁵²

To realize the promise of gene therapy as a new tool in advanced clinical medicine, safe and effective nonviral delivery vectors are critically needed.^{53, 54} An ideal nonviral gene therapy

vector would have several important properties. It would [1] induce no immunogenic response,⁵⁵⁻
⁵⁷ [2] maintain high stability against nucleases in the circulatory system,^{58, 59}
[3] target, and endocytosis into, specific cells of interest,⁶⁰ and [4] provide a means for the
efficient release of oligonucleotide cargo from the endosomal compartment. These requirements
have led to a strong and growing interest in gold nanoparticles of various shapes and sizes as
nonviral vectors for gene therapy. The biocompatibility of gold nanoparticles and nanostructures
is well established. Oligonucleotides can be bound to the surface of a gold nanoparticle in
relatively dense monolayers, greatly increasing their stability against degradation by nucleases.
The facile binding of various types of biomolecules to the surfaces of gold nanoparticles enables
multiple functions to be imparted on the same nanoparticle “platform”: for example, combining
oligonucleotide loading with antibody conjugation for targeting specific cells or tissues is
realizable with this approach. Finally, remote-controlled release of DNA from a nanoparticle
complex is made possible by the resonant optical properties of gold nanoparticles and
nanostructures.⁶¹⁻⁶⁴ Resonant light absorption provides both spatial and temporal control for
oligonucleotide release, which could be highly useful in research as well as in treatment
scenarios. In addition, the energy input due to resonant light absorption and the accompanying
local photothermal heating response may also assist diffusion of the oligonucleotides out of the
endosomal compartment. In particular, nanoparticle-based complexes that respond to near
infrared light, at wavelengths not significantly absorbed by cellular material, and release DNA
upon resonant illumination would provide an ideal platform for light-controlled gene therapy.

1.3.2 Gold Nanoparticle-based Vectors for Gene Therapy:

DNA can be bound to Au nanostructures by simple thiol chemistry or electrostatic attachment. DNA attached to Au nanostructures has an increased half-life from minutes to

hours⁵⁸ against attack by large nucleases due to the increased steric hindrance caused by attachment to the Au surface.⁵⁸ Additionally, polyvalent cations near the Au nanoparticle surface electrostatically repel dications located within the nucleases, also increasing oligonucleotide stability.⁶⁵

Increasing the cellular uptake efficiency of therapeutic DNA is necessary for effective therapy. The attachment of either therapeutic oligonucleotides (DNA, siRNA) or existing transfection agents (cationic liposomes, cationic polymers, dendrimers) to gold nanoparticles has been shown to universally increase cellular uptake and transfection efficiency. DNA/siRNA molecules condense when attached to the gold surface. Attaching other nonviral gene delivery vectors, such as lysine dendrimers, to gold nanoparticles has been shown to increase gene transfection 28-fold relative to the dendrimer alone.⁵⁴ Following cellular uptake, the oligonucleotides must be able to escape from the endosome, diffuse through the cell, and interact with the cell's genetic material. Currently, subsequent to cellular uptake, the DNA-bearing carriers are believed to be sequestered in the endosome. It is currently hypothesized that the use of light activated plasmonic nanostructures can effectively disrupt the endosome and release the DNA into the interior of the cell. Wu *et al.* have observed that light-induced endosomal disruption occurs with pulsed laser irradiation, and suggested that transient cavitation of vapor microbubbles that form between the temperature gradient on the surface of the plasmonic gold nanoparticle and the surrounding medium are responsible for this disruption.⁶⁶

A summary of different Au nanostructure-based gene therapies reported to date is shown in Table 1. Cellular delivery of DNA/RNA conjugated to Au nanoparticles can be effectively accomplished either with or without light activation. Without light activation, when the Au nanostructures are merely serving as carriers for transferring genetic material into cells, they do

elicit a therapeutic response, either downregulation (15, ⁶⁷ or enhanced gene expression.⁶⁸ In general, however, the limited yield of non-light-activated therapy limits this therapeutic strategy. Light-responsive delivery vectors appear to overcome these challenges quite effectively and may be therapeutically more beneficial for controllable gene release than the non-light-activated approach.

Type of Au Nanostructure	Wavelength of Response	DNA/RNA Binding Chemistry	Type of Gene Therapy	Therapeutic Target	Ref
Nanorods	900 nm	Nanorods capped with phosphatidylcholine interact with DNA electrostatically	Light activated	Plasmid DNA release	⁶⁹
Nanorods	780 – 1100 nm	Thiolated DNA covalently attach to Au surface	Light activated	DNA release, GFP gene expression, Block mRNA translation of ERBB2	⁷⁰ ⁷¹ ⁶⁴
Hollow Nanoshells	800 nm	Thiolated polyethylene glycol-RNA chemically bound to Au surface	Light activated	RNA interference	⁷²
Nanospheres	520 nm	Nanoparticles positively charged with dimethylethyl-ammonium interact electrostatically with DNA.	Light activated	T7 RNA polymerase	⁶³
Nanospheres	520 nm	Ethylene glycol-alkylthiol modified RNA attach chemically to Au surface	Non-light activated	Firefly luciferase downregulation	⁶⁷
Nanospheres	520 -560 nm	Plasmid DNA electrostatically attached to Au encapsulated in cationic liposomes	Non-light activated	Enhanced green fluorescent protein expression	⁷³
Nanospheres	520 nm	Positively charged aminated nanoparticles electrostatically attach to plasmid DNA	Non-light activated	Murine IL-2 mRNA expression	⁷⁴
Nanospheres	520 nm	Nanoparticles bearing primary ammonium	Non-light activated	β -galactosidase reporter gene	⁶⁸

		groups bind with anionic DNA via ion-pairing		expression	
--	--	--	--	------------	--

Table 1.1 A summary of different Au nanostructures utilized for light activated and non-light activated gene therapy, their wavelength of response, DNA attachment chemistry, and therapeutic target.

As can be seen in Table 1, the combination of Au nanoparticles and light-activated DNA release has been recently identified by numerous groups as a potentially useful strategy for increased effectiveness in gene therapy. Several variations of this general approach have been demonstrated. DNA has been attached to functionalized Au nanoparticles via photoactive ester linkages, where near-UV irradiation has been used to cleave the ester moieties, releasing the DNA.⁶³ The potential practical biomedical applicability of this specific approach is limited, since for *in vivo* applications, NIR irradiation (650-900 nm) is highly preferable to near-UV light due to its far deeper penetration in tissue,⁷⁵ as well as its negligible mutagenicity relative to near-UV light. Therefore, plasmonic nanoparticles with resonances in the NIR region of the spectrum, such as nanoshells and nanorods, are preferentially being pursued. Nanorods either electrostatically attached to DNA⁶⁹ or covalently bound to thiolated DNA through the Au-S bond^{70, 71} were shown to release DNA when excited with a NIR pulsed laser at the plasmon resonance. However, pulsed laser irradiation may reshape nanorods, which can modify their aspect ratio and their optical properties, including their resonant frequency.⁷¹ Modifications in the nanorod geometry will reduce or eliminate the NIR absorption of these nanoparticles, and could effectively turn off NIR light-controlled release. Moreover, in biomedical applications, the reshaping of nanoparticles may also modify their pharmacokinetics and biodistribution, which may affect their safety and delay or eliminate their ultimate approval for human use. The melting and reshaping of nanorods can be circumvented by using a continuous wave laser.⁶⁴ Lee *et al.*

conjugated thiol-modified dsDNA to nanorods, released the oligonucleotides upon NIR illumination, and successfully blocked the translation of ERBB2 mRNA in BT474 breast carcinoma cells. However, a very low percentage of cells showed protein downregulation: further studies are warranted to quantify this response. Still, the overall strategy of near-IR triggered oligonucleotide release from Au nanoparticle-based vectors is highly promising.

Chapter 2: Surface Enhanced Raman Spectroscopy of DNA

2.1 Introduction:

Detection of DNA, arguably the most important biological molecule, is the basis of numerous technologies ranging from diagnostic screening in clinical medicine to forensic testing in law enforcement.^{76, 77} The vast majority of current DNA detection methods involve the use of fluorescent reporters as part of the signal transduction, requiring costly chemicals and complex chemistry.⁷⁸ Surface-enhanced Raman spectroscopy (SERS), with its demonstrated ability to detect single molecules such as the DNA base adenine, has generated tremendous interest as a potential strategy for label-free biomolecule detection.^{79, 80} While numerous SERS studies of DNA have been performed to date, sensitive and reliable acquisition of SERS spectra from DNA samples remains a significant challenge. For example, in one study it was reported that while all dsDNA samples yielded SERS spectra with good signal to noise ratio, none of the ssDNA oligomers studied yielded detectable SERS signals.⁸¹ Another study reported that the quality of the SERS spectrum of single stranded Calf Thymus DNA was much better than that of the double stranded DNA.⁸² More recently, SERS detection of both single and double stranded DNA was reported, where the observed SERS features appeared to be sequence and/or composition dependent.⁸³

It has now been shown in several detailed investigations that Au nanoshells, spherical nanoparticles whose plasmon resonance frequencies are controlled by the relative inner and outer radius of their metallic shell layer, can be used as highly reproducible SERS substrates.^{19, 22, 84,}
⁸⁵Although nanoparticle dimers separated by nanometer scale gaps are known to produce larger SERS enhancements, known as “hot spots”, fabrication of dimer-based substrates with highly

regular, reproducible hot spots is quite challenging.^{86, 87} A major problem with adjacent nanoparticle pairs as SERS substrates is the very sensitive dependence of the SERS enhancement on interparticle spacing. Fortunately, the amplitude of the integrated SERS enhancement of single nanoshells can be comparable to that of a solid nanoparticle dimer with a nanometer scale gap.²² With the SERS enhancement designed and built into each individual nanoshell particle, the challenging requirement of fabricating nanometer-scale spacing between adjacent nanoparticles is virtually eliminated.^{19, 88,89} For many applications in chemical spectroscopy and sensing, the easily accessible, open surface topology of nanoshells presents a far more preferable substrate for surface-enhanced spectroscopies than the closed topology of nanoparticle dimers or aggregates. This open topology is critically important for biomolecular spectroscopy and sensing, since the spatial extent of many biomolecules of interest, DNA being a prime example, may exceed the nanoscale dimensions of dimer “hot spots”. In addition to the large field enhancements on nanoshell surfaces, the plasmon resonant properties are remarkably insensitive to defects on the particle surface or to nanoscale roughness,⁹⁰ making them ideal substrates for assessing SERS spectral reproducibility. The development and use of highly reproducible substrates is critical in the advancement of SERS as a mainstream spectroscopic technique. This is particularly important in studies of large, complex molecules such as DNA or proteins, since the SERS signal in these molecules already depends significantly on molecular conformation, orientation, and binding specificity to the substrate surface.

In this chapter we report a study of the surface-enhanced Raman spectroscopy of thiolated ssDNA and dsDNA oligomers bound to Au nanoshell-based SERS substrates. In this study the SERS features of DNA are easily recognized. Previous studies have shown that spectral quality and reproducibility can be severely limited by large variations in molecular

conformation and/or packing density of the DNA adsorbate molecules on the substrate. Here we show that a gentle thermal cycling pretreatment of the ssDNA and dsDNA prior to adsorption onto the nanoshell substrate results in a relaxation of the DNA molecules into what we believe to be an extended, “linear” conformation. This protocol results in a dramatic increase in the reproducibility of the SERS spectrum. The spectra obtained using this preparation method show an overwhelming dominance of adenine Stokes modes in the SERS spectra, with much weaker secondary features occasionally observable from other bases, most predominantly guanine. The reproducibility of the SERS spectra decreases slowly over time (several days) as the molecular conformations re-randomize, where an increase in spectral variation consistent with an increased distribution of molecular conformations is observed in the SERS spectra.

In the context of this study we introduce a new quantitative spectral analysis approach useful for SERS. We define a Spectral Correlation Function (SCF), Γ , that provides a metric with which to assess the reproducibility of SERS spectra or, alternatively, to quantify complex changes in the SERS spectrum that may be due to chemical modification of the adsorbate molecules (see Analysis section). We apply this analysis to quantitatively assess the improvements in DNA spectral reproducibility due to our thermal pretreatment protocol. SCF analysis also allows us to monitor complex changes in the SERS spectrum of adsorbate molecules due to chemical modification of the DNA. As an example, we apply SCF analysis to monitor the changes in the SERS spectrum of DNA upon interaction with cisplatin, a chemotherapeutic agent in widespread use for cancer treatment. This class of anticancer compounds is known to induce cell death by binding directly to DNA in cells, arresting cell replication and activating signal transduction pathways that ultimately lead to apoptosis. Our Spectral Correlation Function (SCF) analysis is of direct practical interest in the development

and quantification of high-performance, high-reproducibility SERS substrates. This approach also successfully discriminates changes in the SERS spectrum of DNA upon exposure to cisplatin in comparison with its trans analog, transplatin, known to have a much lower affinity for DNA and therefore useful in this study as a control molecule.

2.2 Experimental:

Nanoshell-based SERS substrates consisting of dispersed nanoshells bound to glass substrates were prepared.^{91, 92} Briefly, a fused quartz microscope slide (Piranha cleaned) was incubated overnight in an (1%) ethanolic solution of poly(4-vinylpyridine) (MW = 160,000 from Sigma-Aldrich) and dried with nitrogen gas; subsequently 100 μ l of aqueous nanoshell suspension was deposited onto the substrate. The substrate was then allowed to sit at room temperature for 3-4 h before rinsing with Milli-Q water (Millipore, Billerica, MA) to remove excess nanoshells, followed by drying with a gentle flow of nitrogen.

Oligonucleotide	Sequence (5'-3')
ST ₂₀ N1 (70 bases)	SH-C ₆ -TTTTTTTTTTTTTTTTTTTTTTCGGCAATCAGGTTGACCG TACATCATAGCAGGCTAGGTTGGTCGCAGTC
SA ₂₀ N2 (70 bases)	SH-C ₆ -AAAAAAAAAAAAAAAAAAAAACGCCGTTAGTCCA ACTGGCATGTAGTATCGTCCGATGCAACCAGCGTCAG
ST ₂₀ N3 (70 bases)	SH-C ₆ -TTTTTTTTTTTTTTTTTTTTTTCGGCTTTCTGGTTGTCCGT TCTTCTTTGCTGGCTTGGTTGGTCGCTGTC
SN4 (50 bases)	SH-C ₆ -GACTGCGACCAACCTAGCCTGCTATGATGTACGGTCAA CCTGATTGCCGC

SN5 (30 bases)	SH-C ₆ -GACTGCGACCAACCTAGCCTGCTATGATGT
SN6 (20 bases)	SH-C ₆ -TCTTGCTGTGTCTGTTCTTT

Table 2.1: Oligonucleotide sequences used in the described experiments.

To study the possible sequence dependence of the SERS of DNA, several DNA oligomers of different lengths and compositions (Table I, purchased from Integrated DNA Technology Inc.) were studied. Prior to use, all thiolated DNA oligomers were reduced with 1,4-Dithio-DL-threitol (DTT, Fluka) and purified with NAP5 purification columns (GE Healthcare). Unthiolated DNA sequences were used as received, having been HPLC-purified by the vendor. DNA uncoiling was achieved *ex-situ* (not on the substrate) by heating the DNA solutions in TE buffer (1x Tris EDTA buffer pH = 7.5 from IDT) to 95°C for 10-15 min. followed by rapid cooling in an ice bath. DNA prehybridization was carried out *ex-situ* by mixing two complementary DNA sequences at a 1:1 molar ratio in DNA hybridization buffer (TE/50mM NaCl, pH = 7.5), heating the solution to 95°C, then allowing it to cool slowly to room temperature in a large water bath. To bind DNA to the nanoshell SERS substrates, 50 μ L of the (typically 40 μ M) target DNA (ssDNA/dsDNA) were deposited onto a freshly made nanoshell SERS substrate. After overnight incubation, the excess ssDNA or dsDNA solution was removed by rinsing with TE or TE/50 mM NaCl buffer, respectively.

For the cisplatin/transplatin experiments, 30 bp prehybridized dsDNA (SN5) was immobilized on nanoshell-SERS substrate and then incubated with 7.5 nM mercaptohexanol (MH, Sigma-Aldrich) for 7 hours to remove nonspecifically bound DNA and prevent the direct

interaction of the cis- and transplatin with the Au surface. Subsequently, 1 mM (aq) cisplatin or transplatin (Sigma-Aldrich) was added. Samples were rinsed with TE/50 mM NaCl buffer prior to SERS acquisition.

SERS spectra were recorded while substrates were immersed in the appropriate buffer (TE for ssDNA and TE/50 mM NaCl for dsDNA) using a Renishaw inVia Raman microscope (Renishaw, U.K.) with 785 nm excitation wavelength. Backscattered light was collected using a 63x water immersion lens (Leitz, Germany), corresponding to a rectangular sampling area of 3 μm x 30 μm . Unless stated otherwise, all the SERS spectra in this work were obtained with an integration time of 20 seconds and a laser power of 0.57 mW before the objective.

Normal Raman spectra of DNA oligomers were acquired with the drop coating deposition Raman (DCDR) method.⁹³ In this protocol, 10 μL of the 40 μM purified DNA sample was deposited onto spectRIM substrates (Sigma-Aldrich). Because of the so-called “coffee ring” effect, the DNA forms a ring on the substrate after drying in a vacuum assisted desiccator. The normal Raman spectra were acquired using a 50x dry objective. An integration time of 900 s and a laser power of 570 mW before objective were used for all the normal Raman spectral acquisitions.

2.3 Analysis:

To quantitatively analyze the reproducibility of the SERS spectra, a dataset of N spectra (in this work, typically N = 8) acquired at randomly selected regions on the same substrate was obtained. Correlation coefficients between all nonidentical spectral pairs ($i \neq j$) in the same dataset were determined from the data using:

$$P_{i,j} = \frac{\sum_{k=1}^w (I_i(k) - \bar{I}_i)(I_j(k) - \bar{I}_j)}{\sigma_i \sigma_j} \quad (1)$$

where i, j is the index of the spectra in the data matrix, k is the wavenumber index of the individual spectra, I is the spectral intensity, W is the spectral range, and σ_i is the standard deviation of the i^{th} spectrum. Once the correlation coefficients $P_{i,j}$ are calculated, a Spectral Correlation Function Γ , the average of the off-diagonal correlation coefficients, can then be determined:

$$\Gamma \equiv \frac{2 \sum_{i=1}^N \sum_{j=i+1}^N P_{i,j}}{N(N-1)} \quad (2).$$

Γ values can be used for quantitative assessment of spectral reproducibility, with values that vary from 1 in the case of identical spectra to 0 in the case of completely uncorrelated spectra.

Changes in SERS spectra can be quantified using the correlation coefficients $P_{i,j}^{\alpha,\beta}$ with all possible spectral pairs originating from spectral measurements α and β respectively.

$$P_{i,j}^{\alpha,\beta} = \frac{\sum_{k=1}^W (I_i^\alpha(k) - \overline{I_i^\alpha})(I_j^\beta(k) - \overline{I_j^\beta})}{\alpha_i^\alpha \sigma_j^\beta} \quad (3)$$

$$\Gamma^{\alpha,\beta} \equiv \frac{\sum_{i=1}^M \sum_{j=1}^N P_{i,j}^{\alpha,\beta}}{M N} \quad (4)$$

In this case, α and β may represent spectra from two different substrates, or spectra obtained from the same sample at two different times. Here i, j index the spectra obtained with substrate α and β respectively, and M and N refer to the total number of spectra analyzed. Prior to correlation analysis, all spectra were processed with a Savitzky-Golay second derivative method (window size of 15 data points with 2nd order polynomial), which can effectively reduce or eliminate possible false correlations resulting from a constant offset or broadband

background.⁹⁴ The larger the $\Gamma^{\alpha,\beta}$ value, the higher the value of the spectral correlation function between the sets of spectra.

Spectral variations induced by cisplatin/transplatin binding to DNA were analyzed using Equations (3) and (4). In this case, α , β refer to the DNA-nanoshell sample before and after cisplatin/transplatin treatment. The average correlation $\Gamma^{\alpha,\beta}$, is a quantitative assessment of spectral variations induced by the sample treatment. Clearly, the smaller the $\Gamma^{\alpha,\beta}$ value, the more significant the spectral changes that have occurred. The spectral range evaluated in this analysis was 350 cm^{-1} to 1700 cm^{-1} .

2.4 Results and Discussion:

Figure 1.1 shows multiple SERS spectra of untreated and thermally cycled ssDNA (SA₂₀N2, Table 1.1). Extremely large variations in SERS spectra are typically obtained for untreated DNA samples (Figure 1.1.a). Following thermal pretreatment (heating of the DNA in solution followed by rapid cooling, then adsorption onto the substrate), the SERS spectra appear dramatically different and highly reproducible (Figure 1.1.b). To evaluate this change in spectral reproducibility, Γ was calculated for the spectra with and without thermal pretreatment (Figure 1.1, inset). Also shown are the Γ values obtained from a series of SERS spectra of prehybridized dsDNA for the same base sequence (with its complement) and a mixture of the same two complement sequences without thermal pretreatment. Using this analytic approach it is clearly seen that the thermally treated ssDNA and the thermally treated, pre-hybridized dsDNA have far higher Γ values ($\Gamma \sim 0.9$) than the untreated samples ($\Gamma \sim 0.1-0.2$). Very similar SERS spectra and spectral reproducibility were observed for all other adenine-containing DNA sequences

listed in Table 1.1, suggesting that the observed increase in spectral reproducibility is remarkably sequence independent, at least for the variety of DNA oligomers studied here.

In the preparation of dsDNA for these studies, the SERS spectra and their spectral reproducibility for the mixture of untreated DNA and its complement in solution were observed to be extremely similar to those observed for untreated ssDNA. From this observation we conclude that without thermal pretreatment it is unlikely that extensive hybridization occurs for these experimental conditions. Substrate-to-substrate spectral reproducibility was also analyzed for thermally pretreated ssDNA and dsDNA samples. Although the overall SERS intensity can vary from substrate to substrate due to variations in nanoparticle density,⁸⁴ the SERS spectral features are highly reproducible, with $\Gamma > 0.98$ in all cases.

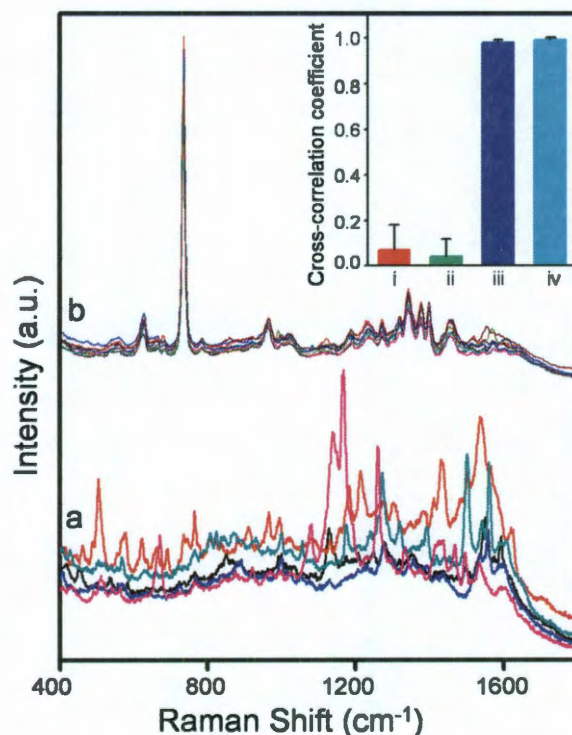


Figure 2.1: Typical SERS spectra of (a) untreated ssDNA and (b) ssDNA following thermal pretreatment. Spectra are offset for clarity. Inset: Γ values for series of 8 SERS spectra for (i) untreated ssDNA from (a), (ii) untreated ssDNA plus complement, (iii) thermally pretreated

ssDNA from (b) and (iv) thermally pretreated dsDNA. Error bars represent one standard deviation.

The dramatic differences in SERS spectra and spectral reproducibility between the untreated and the thermally-pretreated ssDNA samples can be attributed to thermally induced uncoiling of ssDNA prior to attachment to the substrate. We believe this treatment results in extended ssDNA chains with a significantly greater uniformity of molecular conformation than untreated, randomly coiled ssDNA chains. Adsorption of the thermally pretreated, relaxed ssDNA onto the nanoshell substrate surface is quite likely to also result in a more ordered and densely packed monolayer on the nanoparticle surfaces relative to ssDNA adsorbed in randomly coiled conformations. Increased adsorbate order and packing density on the nanoshell substrate surfaces would also enhance the uniformity and reproducibility of the observed SERS signals. Since the persistence length of dsDNA can be as long as 50 nm,⁹⁵ corresponding to ~147 base pairs, all the hybridized dsDNA investigated in these studies are likely to adopt a rigid rodlike structure. Thus, just as with the thermally pretreated ssDNA, the similarly prepared dsDNA is also likely to bind to the nanoshell substrates with increased ordering and a higher packing density.

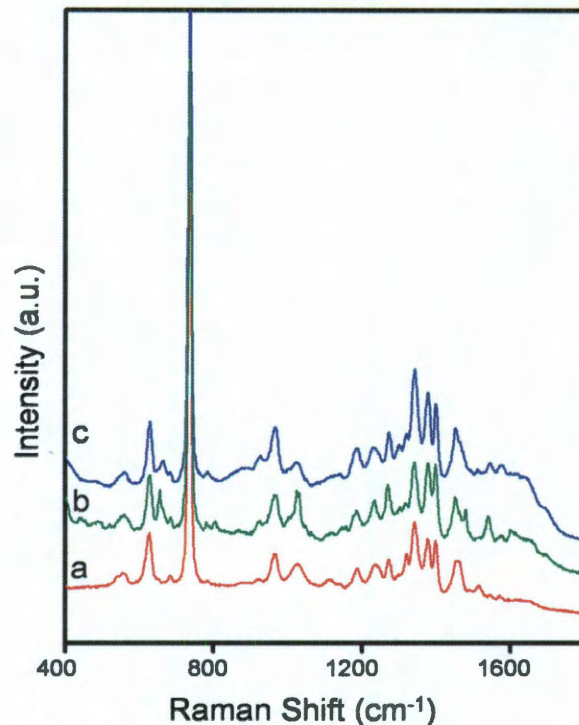


Figure 2.2: SERS spectra of (a) adenine, (b) thermally pretreated single stranded and (c) double stranded SN5. Each spectrum is an average of 8 spectra collected from different spots of the same sample. Spectra are scaled and offset for clarity.

2.4.1 Adenine-Dominated SERS Spectra:

In Figure 2.2, a direct comparison of the SERS spectra of adenine with the SERS spectra of the thermally pretreated thiolated ssDNA and dsDNA (thiolated ssDNA hybridized with its unthiolated complement) SN5, a random sequence 30-base oligonucleotide listed in Table 1.1, is shown. It is clearly observable that both the SERS spectra of ssDNA and dsDNA for SN5 are overwhelmingly dominated by the SERS features of their adenine constituents. This dominance of the adenine features observed in this case was observed in all the SERS spectra of thermally pretreated ssDNA and thermally pretreated, prehybridized dsDNA, regardless of the position or percentage of adenine in the sequence.

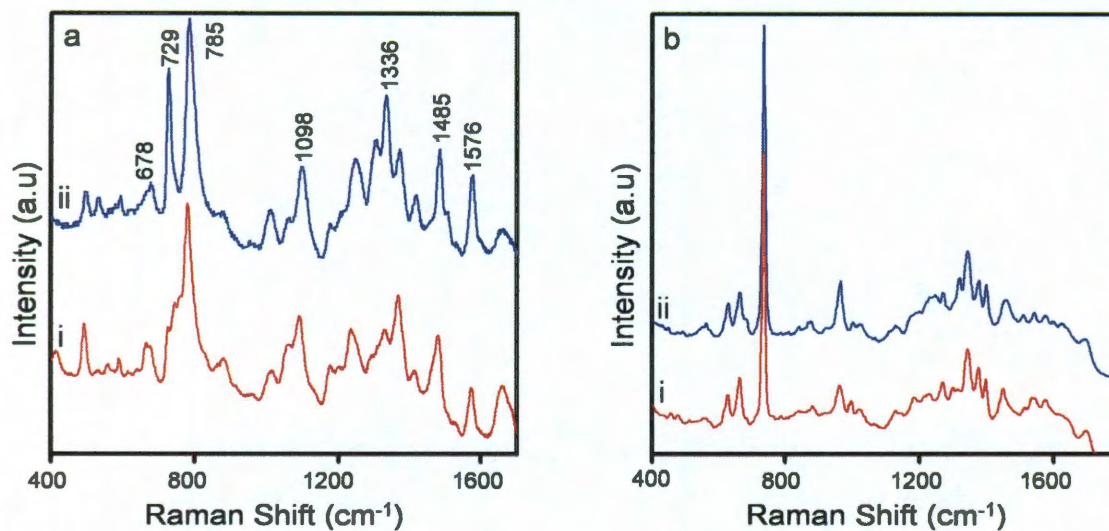


Figure 2.3: (a) Normal Raman of (i) ST₂₀N1 and (ii) SA₂₀N2 (b) SERS spectra of (i) ST₂₀N1 and (ii) SA₂₀N2. Spectra are offset for clarity. Major peaks in the normal Raman spectrum of SA₂₀N2 are assigned.

Wave Number (cm ⁻¹)	Assignments
678	G
729	A
785	T, C
1098	bk (PO ₂ ⁻ st)
1336	A
1485	A, T, C
1576	A (ring st, N6H ₂ df)

A, adenine; T, thymine; G, guanine;

C, cytosine; bk, backbone; st, stretch; df, deformation.

Table 2.2: Assignments of normal Raman bands of SA₂₀N2.

This can be seen quite dramatically in the SERS spectra of thermally pretreated ST₂₀N1 and SA₂₀N2 oligomers, each a 70-base sequence (Figure 2.3). The adenine content in the two DNA sequences, 15.5% and 44.3%, respectively, vary significantly. In addition, the adenine position in each sequence is quite different: for ST₂₀N1, the first adenine is 26 bases away from the thiol group (and therefore the Au surface), where for SA₂₀N2, 20 adenine bases are directly adjacent to the thiol group. Interestingly, the SERS spectra of the two DNA sequences were very similar (Figure 2.3.b), both dominated by adenine modes. Since poly(T) and poly(A) sequences are known to have significantly different packing densities on Au surfaces, a direct comparison of SERS intensities does not yield quantifiable enhancement information, and therefore the SERS spectra in Figure 2.3.b are normalized.^{96, 97} In contrast, their normal Raman spectra (Figure 2.3.a) reveal significant composition dependence. Mode assignments are provided in Table 2.2 for these spectra.

These data suggest that, under our experimental conditions and for the selection of molecules we have studied, that the dominance of the adenine modes in the observed SERS spectra is not due to abundance of adenine base nor to the relative proximity of the adenine bases to the gold surface. The SERS signal itself from the adenine bases appears to be more greatly enhanced than that of the other DNA bases. The only SERS spectral signature from the other DNA bases that is observable is the weak 667 cm⁻¹ peak, attributed to the ring breathing mode of guanine.^{81, 98, 99} This much weaker feature appears in the SERS spectra of both the ssDNA and dsDNA, but is absent from the SERS spectrum of adenine. Stokes modes from thymine and cytosine, and the backbone constituents of ribose and phosphate, are indiscernible.

One may possibly conclude that based on our experimental observations, the thermally pretreated DNA oligomers may be lying down and in direct contact with the Au surface of the

nanoparticle as an explanation of the consistent dominance of the adenine SERS modes. However, we have observed that the SERS of nonthiolated DNA, which is most likely to be lying flat on the gold surface, is quite different in terms of relative intensity of adenine (736 cm^{-1}) and guanine (667 cm^{-1}) peaks than its thiolated DNA counterpart (unpublished). Moreover, experimental¹⁰⁰ and theoretical¹⁰¹ studies have suggested a strong correlation between packing density and DNA conformation. The packing density of DNA chains on the gold nanoshell surface is quite likely to affect their conformation (and vice versa). At higher packing densities both single stranded and double stranded thiolated DNA would preferentially extend from the Au surface. On the other hand, loosely packed DNA chains may prefer to lie flat and in contact with the Au surface, stabilized by DNA/Au interactions.¹⁰² DNA-Au simulation studies taking into consideration DNA base pair stacking, electrostatic interactions, electrolyte effects, in addition to DNA-Au interactions are critically needed to better understand the precise conformation of thiolated and unthiolated DNA on Au surfaces.

To further understand the relative signal contributions of the different DNA bases, SERS spectra of thermally pretreated single stranded ST₂₀N3, a thiolated 70-base oligomer that contains no adenine, and a prehybridized double stranded ST₂₀N3 with its complement, were obtained (Figure 2.4). As expected, in the absence of adenine, the guanine features are seen to dominate the DNA SERS spectra. It is worthwhile to note that there are no detectable features from either cytosine or thymine in the SERS of ST₂₀N3, supporting a conclusion that the SERS cross section of adenine \gg guanine \gg cytosine and thymine.

Several reasons could explain the dominance of adenine in the SERS spectra. One possibility is that DNA degrades during thermal pretreatment of our DNA oligomers, resulting in adenine bases or base containing fragments binding directly to the Au surface thus yielding a

preferentially large SERS signal. This possibility was carefully examined by gel electrophoresis analysis of our DNA oligomers following thermal cycling, which confirmed that the thermal pretreatment is entirely nondestructive and does not compromise DNA integrity. Furthermore, when the pretreated, uncoiled ssDNA samples, now bound to the nanoshell substrates, were reheated then allowed to cool slowly, the reproducibility of the SERS spectra of the reheated samples was measurably decreased. This is most likely due to partial, random DNA recoiling occurring during the slow cooling step. If thermal cycling caused partial DNA dissociation, then additional heating would likely result in further DNA dissociation and an increase in the SERS signal from the additional available adenine, which is not what is observed. These observations lead us to conclude that the most likely reason that adenine dominates the SERS spectra of DNA is that adenine possess a significantly higher SERS cross section than the other DNA bases.

The dominance of adenine due to its higher SERS cross section is consistent with other previously reported SERS studies of DNA. For example, in an equimolar mixture of poly(A), poly(G), poly(C) and poly(T), it was found that the SERS intensities of the ring breathing modes showed an order of $A > C \gg G \geq T$.⁸³ Tip-enhanced Raman spectroscopy (TERS) of single DNA bases in self-assembled monolayers on Au(111) showed the intensity of the adenine breathing mode to be far higher than that of guanine, which in turn was higher than cytosine and thymine.¹⁰³ This observation is consistent with our experiments. It is also important to note that adenine is the only DNA base that exhibits single molecule detectability while the lowest reported detection limits for the other DNA bases are in the sub μM range⁸⁰.

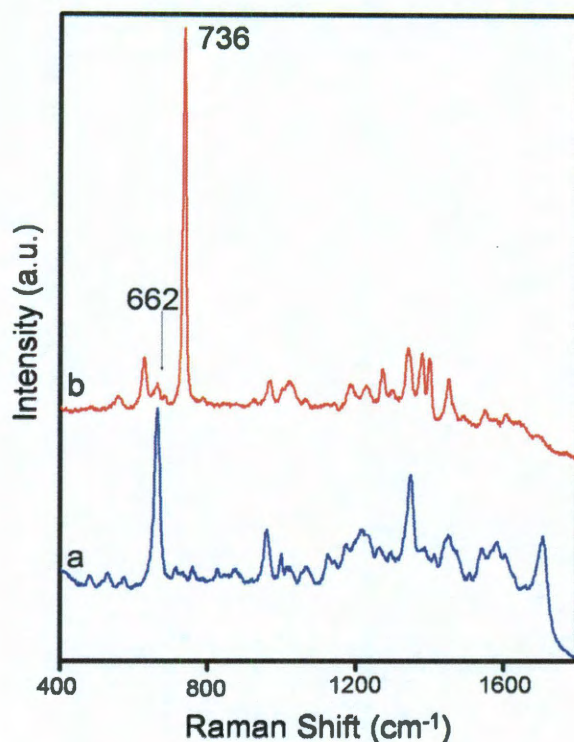


Figure 2.4: (a) SERS of uncoiled ST₂₀N3 (adenine-free 70 base ssDNA). (b) pre-hybridized dsDNA (ST₂₀N3 with its complement).

In previous SERS studies of DNA on nanoshell substrates it was determined that L_{SERS} , the effective $1/e$ distance above the nanoshell surface where SERS enhancement could be detected for nanoshells of this size, is nominally 9 nm.¹⁹ The observations reported here are consistent with this L_{SERS} . Assuming a tilt conformation for thiolated DNA chains on the Au surface supported by simulation studies,¹⁰⁴ approximately the first 30 to 40 bases closest to the Au surface would lie within the L_{SERS} for this substrate. In the case of ST₂₀N1, the first adenine is 26 bases away from the Au surface, still within the L_{SERS} for this nanoshell substrate. In this case, the high SERS cross section of adenine compensates for the weaker SERS enhancement experienced by this moiety at its distance from the nanoshell surface.

2.4.2 Detection of DNA Interaction with Cisplatin and Transplatin:

Having achieved highly reproducible SERS spectra of DNA by this method, we apply this approach to detect and discriminate conformational changes induced by the interaction of DNA with the two platinum ligands cisplatin and transplatin.

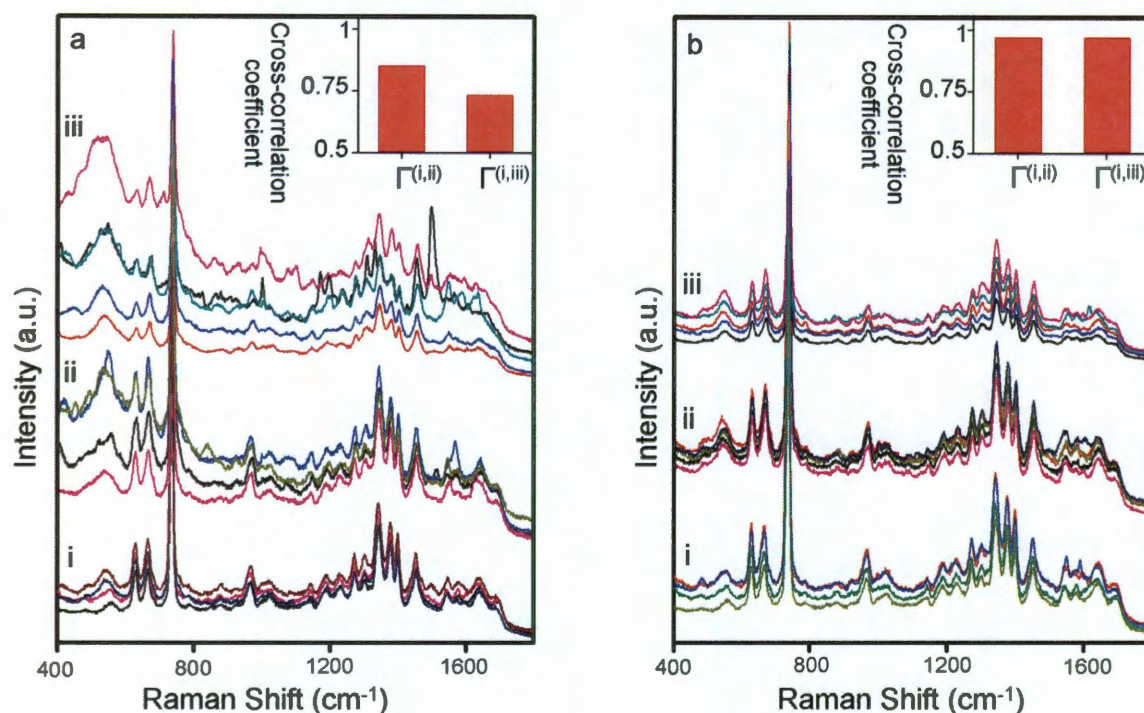


Figure 2.5: SERS of cisplatin/transplatin bound to 30 bp ds-DNA SN5. (a) Spectra (i) before, (ii) immediately following, and (iii) after overnight incubation with cisplatin. (b) Same as (a) for transplatin. Spectra are offset for clarity. Inset: Spectral correlation functions $\Gamma^{\alpha,\beta}$ for different DNA spectra as labeled.

Representative SERS spectra of 30 bp dsDNA (SN5) on mercaptohexanol (MH) passivated nanoshell substrates before and after incubation with cisplatin and transplatin are obtained (Figure 2.5). (MH surface passivation is performed to prevent nonspecific binding of DNA and platinum ligands to the Au nanoshell surface, assuring better DNA-ligand interaction.¹⁰⁵) SERS spectra of DNA before and after incubation with cisplatin or transplatin are similar, with the only recognizable new peak at $\sim 450 \text{ cm}^{-1}$, which can be attributed to the

platinum-amine stretching mode.¹⁰⁶ The appearance of this new peak verifies covalent bonding of the cis-/transplatin to the DNA.

Although the spectra clearly change over time, all the SERS spectra remain reasonably reproducible ($\Gamma > 0.95$), validating the cross-comparison of the SERS spectra between different samples. The reduction in SERS spectral reproducibility is explained by the binding of cisplatin and transplatin to DNA resulting in the formation of monofunctional, interstrand and intrastrand adducts. Since these adducts can form randomly at any purine residues, it is expected that random modifications (“kinks”) in the molecular conformation of the DNA will increase significantly upon adduct formation. The increase in DNA distortion induced by cisplatin binding during incubation does indeed correlate with a decrease in spectral reproducibility (Figure 2.5.a). This observation is consistent with the current understanding of this interaction as a two-step process, where cisplatin initially attaches quickly and preferentially to the N7 atom of guanines and adenines, forming cisplatin/DNA monoadducts. Then, monoadducts are converted into bivalent platinum/DNA complexes in a much slower step that takes up to several hours¹⁰⁷. In contrast, for transplatin, the spectral reproducibility appears time-independent, (Figure 2.5.b). consistent with the fact that transplatin/DNA interaction is a one-step process.¹⁰⁷

It is also clear from our SCF analysis that the spectral changes induced by cisplatin ($\Gamma^{(i,ii)} = 0.85$ immediately after adding cisplatin and $\Gamma^{(i,iii)} = 0.73$ after overnight incubation) are much more significant than those induced by transplatin ($\Gamma^{(i,ii)} = 0.97$ right after adding transplatin and $\Gamma^{(i,iii)} = 0.97$ after overnight incubation). The cross-linking of cisplatin to DNA is believed to be predominantly intrastrand, occurring between two adjacent purines (1,2 intrastrands, d(GpG) or d(ApG), ~90%).¹⁰⁸ Other intrastrand linkages that may occur are between purines separated by one or more nucleotides, and interstrands between purines from opposite DNA strands. A few

adducts are likely to remain monofunctional. It is widely accepted that the 1,2 intrastrand adducts locally unwind and bend double stranded DNA.¹⁰⁹ This is consistent with our observation that cisplatin interaction induces numerous complex changes in the SERS spectrum and a decrease in Γ over time. In the case of transplatin, some of the cross-links formed are interstrands, but most of the adducts remain monofunctional, inducing significantly less DNA distortion. This is consistent with our observation that Γ is unchanged upon DNA-transplatin incubation.

These experiments demonstrate that SERS of DNA can detect ligand binding in two ways: by exciting the Stokes modes of the ligands themselves, but also through the complex conformational changes occurring in the DNA spectra resulting from the conformational distortion due to ligand binding. We believe that this SERS-based approach can be straightforwardly applied to studying the binding affinities of DNA with small molecules. This approach may also be used to develop a new type of all-optical chemical sensor based on optical detection of DNA conformational changes upon binding of the DNA to a ligand of interest.

2.5 Conclusion:

This work demonstrates a successful method for obtaining high quality SERS spectra of single and double stranded DNA. Thermal uncoiling of ssDNA and hybridization of dsDNA dramatically increase the reproducibility of SERS spectra, acquired on nanoshell SERS substrates with highly regular, highly controlled electromagnetic enhancements.

Regardless of the DNA composition, sequence and hybridization state, the SERS spectra of our model DNA exhibit almost identical spectral features dominated by adenine. The high spectral quality and reproducibility of the spectra strongly suggest the possibility of using adenine as an endogenous SERS reporter of DNA. High quality, highly reproducible DNA

spectra may also provide opportunities for label-free DNA detection schemes based on surface enhanced Raman spectroscopy.

The study of the interaction of cis- and transplatin with ds-DNA reveals that spectral changes and reproducibility are highly correlated with DNA-cisplatin binding. These experiments demonstrate the possibility of using SERS to investigate the interaction and kinetics of DNA with various molecules, a topic of high-priority interest in drug discovery, pharmaceutical development and testing.

Chapter 3: Correlation of Molecular Orientation and Packing density in a dsDNA self-assembled monolayer observable with Surface Enhanced Raman Spectroscopy

3.1 Introduction:

DNA, the genetic material of most living systems, has more recently found its way into many novel applications ranging from nanoelectronics¹¹⁰ to DNA-based nanosensors.^{111, 112} In these applications, the binding of DNA to metal surfaces, frequently through the use of a terminal functional group on a DNA oligomer, is prevalent. In particular, the orientation of DNA immobilized on Au surfaces has been extensively studied both experimentally¹¹³ and theoretically¹¹⁴. The ability to monitor the orientation of DNA molecules tethered to metal surfaces is crucial to improving these applications. It has been proposed that the orientation of DNA molecules bound to surfaces correlates with packing density, however, most of these studies were done in the context of determining the optimal packing density of ssDNA for maximum hybridization^{114, 115}. Here we report that the surface-enhanced Raman spectra of a thiolated dsDNA monolayer provide a new level of detail regarding its orientation and packing density on an Au nanoshell surface.

This chapter is an important extension of our previous work in which we demonstrated that a simple protocol based on thermally pretreating DNA prior to binding to Au nanoshell SERS substrates greatly enhances its spectral quality and reproducibility¹¹⁶. Here we use the same experimental procedure to investigate the orientation of dsDNA bound to the Au nanoshell surface. SERS is particularly advantageous for this study since the enhancement depends, in addition to other parameters, on the relative orientation of the investigated molecule with respect

to the substrate surface. However, only few attempts to study DNA orientation on gold surfaces using SERS have been reported¹¹⁷. The high reproducibility of our DNA SERS spectra allows us to monitor variations in DNA orientation with respect to its packing density in significant detail.

3.2 Results and Discussion:

Our detection strategy is based on comparing the relative intensities of the Raman breathing mode of guanine at (667 cm^{-1}) and the Raman ring-bending mode of adenine at (623 cm^{-1})¹¹⁸ in the SERS spectrum of thiolated DNA bound to Au nanoshell surfaces. Adenine and guanine possess the highest Raman cross-sections of the naturally occurring DNA bases: SERS features from thymine and cytosine are much weaker, and are indiscernible in our experiments. For the Au nanoshells used in this study, the L_{SERS} , defined as the effective $1/e$ distance for SERS above the nanoparticle surface, is $\sim 9\text{ nm}$,¹¹⁹ corresponding to ~ 30 bases for a vertical DNA conformation. The DNA sequences used in this study, SA₂₀N1 and SA₁₀N1, were designed specifically with adenine in the first 20 and 10 bases closest to the Au surface, respectively.

Oligonucleotide	Sequence (5'-3')
SA ₂₀ N1 (70 bases)	SH-C ₆ -AAAAAAAAAAAAAAAAAAAAAAAAACGCCGTTAGTCCA ACTGGCATGTAGTATCGTCCGATGCAACCAGCGTCAG
SA ₁₀ N1 (70 bases)	SH-C ₆ -AAAAAAAAAAGCTGCTGTCCCGCCGTTAGTCCAAC TGGCATGTAGTATCGTCCGATGCAACCAGCGTCAG

Table 3.1: DNA sequences used in the described experiments

As a result, for DNA in a near-vertical orientation, the adenine peak has a significantly higher intensity relative to the guanine peak. As the DNA tilt angle increases, more guanine bases enter the fringing field (Figure 3.1.A). Thus the guanine peak intensity gradually increases relative to the adenine peak. The ratio of the guanine to the adenine peak intensity can be correlated quantitatively with an effective tilt angle for the DNA. For simplicity, we will call $R_{G/A}$ the ratio of the intensity of the 667 cm^{-1} guanine peak to the 623 cm^{-1} adenine peak.

$$R_{G/A} = \frac{I^G_{667\text{ cm}^{-1}}}{I^A_{623\text{ cm}^{-1}}}$$

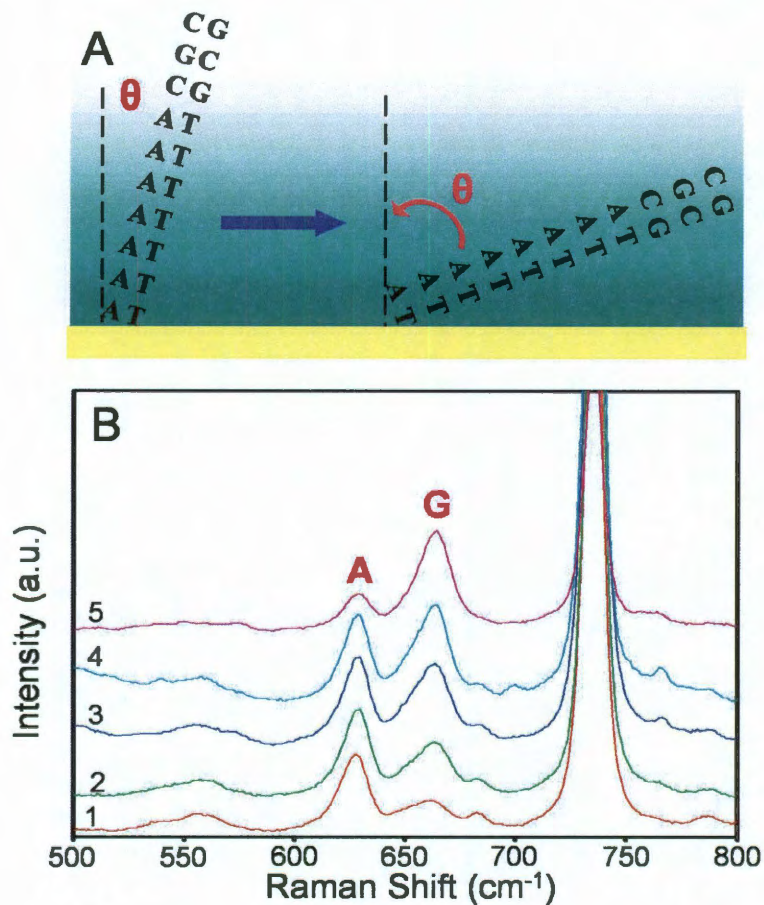


Figure 3.1: SERS detection of DNA orientation. A) schematic of the orientation detection strategy based on variation of dsDNA tilt angle. B) SERS spectra of SA₂₀N1 with its complement at different DNA concentrations. Spectra 1 to 5 correspond to 40, 20, 10, 5 and 1.25 μ M dsDNA, respectively. Spectra are offset for clarity

Figure 3.1.B shows the SERS spectra of dsDNA (SA₂₀N1 with its complement) at different DNA concentrations. For the sample at high DNA concentration, corresponding to a high packing density, the adenine peak intensity is much greater than the guanine peak intensity. The DNA surface density was not directly calculated; however, it could be roughly estimated to be around 18 pmol/cm² at high surface coverage regime¹²⁰. This appears to correspond to a minimum tilt angle. On the other hand, at low DNA concentrations corresponding to low packing densities, the guanine peak intensity significantly increases relative to the adenine peak intensity, suggesting a tilted DNA conformation. These observations are consistent with previous work suggesting that DNA chains tend to stand up at high packing density and lie down at low packing density¹¹⁵.

To better illustrate the correlation between DNA orientation and packing density for SA₂₀N1, we plotted $R_{G/A}$ against DNA concentration (Figure 3.2). $R_{G/A}$ decays asymptotically with increased DNA concentration. This same experiment was also performed with 70 bp DNA with the same sequence as SA₂₀N1 but with 10 adenine (thymine) bases adjacent to the terminal thiol group (and complement) (Figure 3.2).

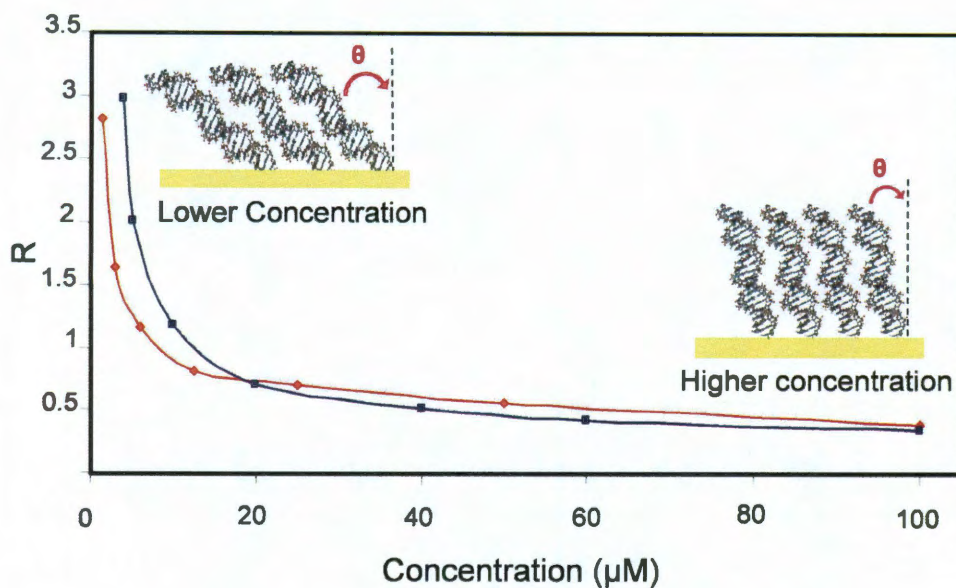


Figure 3.2: Guanine to adenine peak intensity ratio as a function of DNA concentration. Blue and red lines correspond to SA₂₀N1 and SA₁₀N1, respectively, conjugated with their complementary sequences. Insets show schematics of variations of DNA orientation with packing density.

The highly systematic variation of $R_{G/A}$ with DNA concentration strongly suggests that guanine and adenine are changing their relative proximities to the Au surface. Since 70 bp dsDNA is likely to adopt a rigid rodlike structure¹²¹, these measurements are consistent with a variation of the DNA orientation on the Au surface. As a control, we plotted the ratio of the intensity of the ring-bending mode of adenine at (623 cm^{-1}) to the intensity of the breathing mode of adenine at (736 cm^{-1}) as a function of DNA concentration. As would be expected, this ratio was observed to be constant since the two peaks belong to the same DNA base (Figure 3.3)

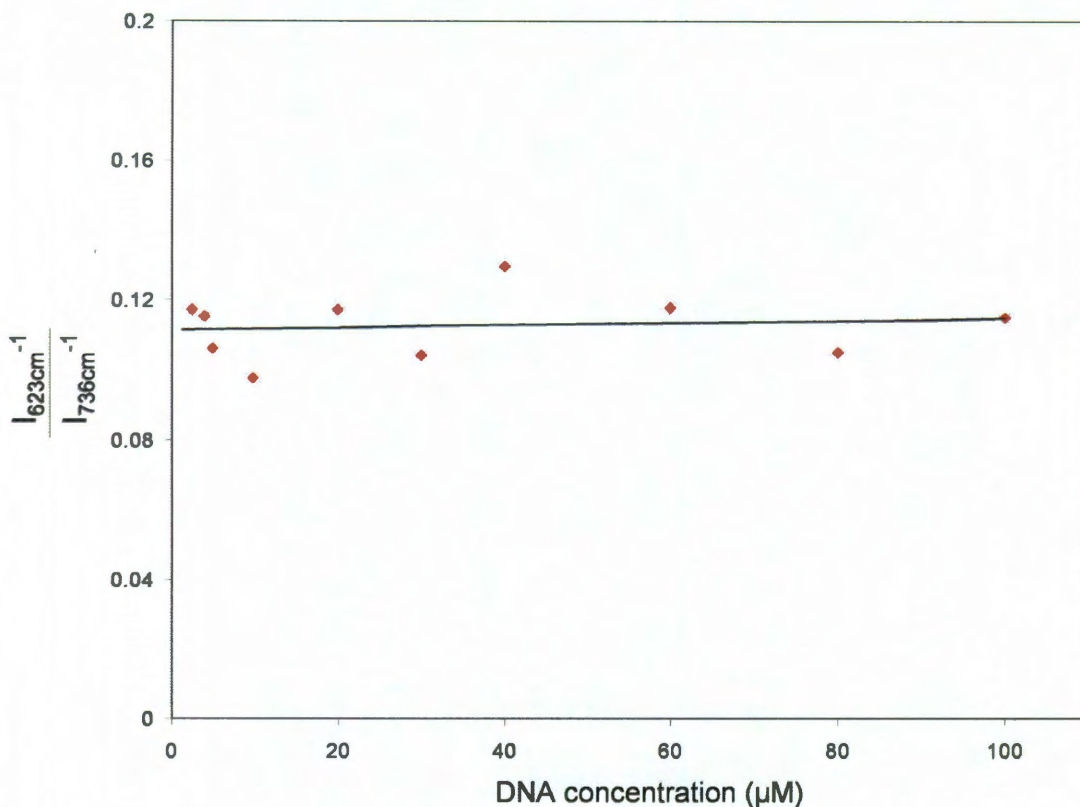


Figure 3.3: The ratio of the intensity of the ring-bending mode of adenine at 623 cm^{-1} to the intensity of the breathing mode of adenine at 736 cm^{-1} as a function of the DNA concentration.

The highly consistent trends in the variation of $R_{G/A}$ with concentration for the two DNA sequences demonstrates a strong likely correlation between DNA packing density on the Au surface and DNA chain orientation (avg. tilt angle). It also suggests that $R_{G/A}$ may be useful as a noninvasive optical monitor to assess packing density of thiolated DNA chains on a SERS-active Au substrate in sensing applications.

Both $R_{G/A}$ plots in Figure 3.2 show dramatic increases at low DNA concentrations, corresponding to DNA chains in close proximity to the Au surface. The asymptotic case would occur for nonthiolated dsDNA lying on the Au surface. For the nonthiolated case, the $R_{G/A}$ value

was found to be much higher than the values measured here for thiolated dsDNA (6.9 compared to ~3, Figure 3.4).

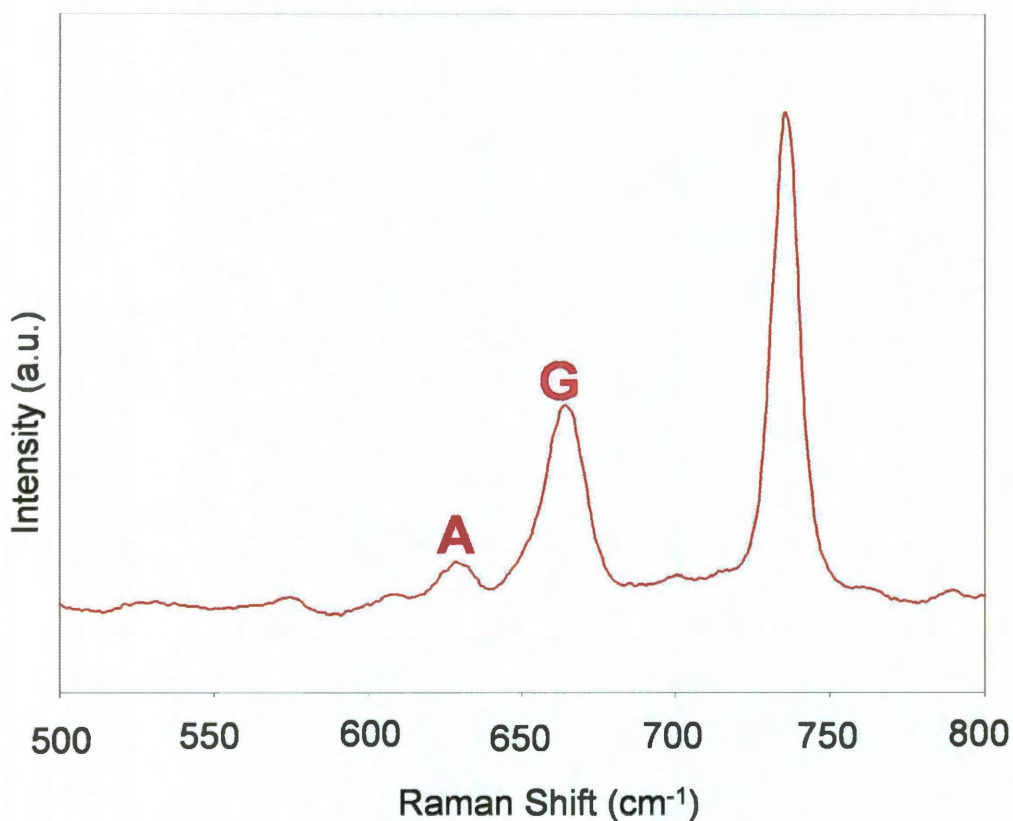


Figure 3.4: SERS spectrum of nonthiolated SA₂₀N1 with its complement

To test the validity of the proposed model, we investigated the possibility of varying the DNA orientation by coadsorbing additional, smaller molecules to the Au surface that would “lift” the DNA chains off the substrate surface. Short thiolated polyT (20 bases) was chosen as a “molecular spacer” for several reasons: its SERS signal is undetectable and would not contribute to the spectrum; it also binds to Au surfaces via its thiol moiety, and it has minimal affinity with the dsDNA, so it is not likely to induce conformational variations in the dsDNA itself.

Figure 3.5 shows a dramatic decrease in $R_{G/A}$ when polyT is coadsorbed with the thiolated dsDNA, (see supporting information for experimental details) corresponding to a decrease in tilt angle due solely to the presence of the coadsorbed molecule. With the polyT bound to the Au surface, the available space for the long DNA chains decreases, causing them to adjust their spatial orientation to a more upright conformation.

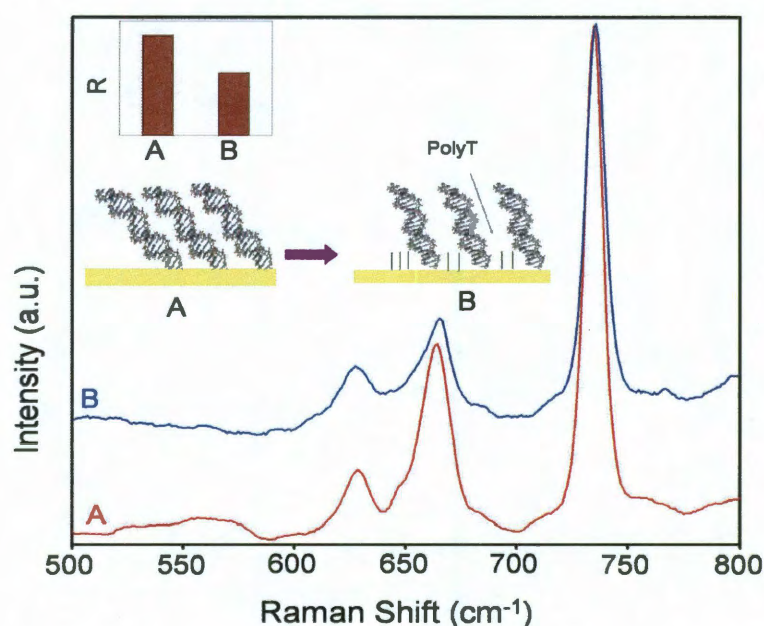


Figure 3.5: DNA tilt due to incubation with polyT. (a) SERS spectra of SA₂₀N1 (2.5 μ M) before polyT incubation, (b) SERS spectra of SA₂₀N1 after polyT incubation, (c) bar plot showing the adenine guanine peak intensity ratio before and after polyT incubation. Insets are schematics depicting the DNA orientation variation caused by polyT incubation.

3.3 Conclusions:

In summary, we have observed that the ratio of two specific features in the SERS spectrum of adenine and guanine in thiolated dsDNA provide highly consistent markers that correlate with DNA chain orientation with respect to the substrate surface. From this analysis, DNA appears to adopt a steeper orientation at higher packing densities, which for decreased packing densities is

reduced. This study will shed light on geometric structure of long chain molecules in general and particularly DNA bound on metal surfaces. Understanding the way this geometrical structure depends on the molecular surface coverage would have great benefit on many technology based on surface chemistry.

Chapter 4: Label-Free Detection of DNA Hybridization Using Surface Enhanced Raman Spectroscopy

4.1 Introduction:

Recently, DNA hybridization has become one of the most frequent applied techniques for clinical laboratory screening of genetic and infectious diseases as well as for forensic testing.¹²²⁻¹²⁴ In a typical DNA hybridization design, probe DNA must be labeled with a radioactive or optical label for detection. The most common DNA array technique employs fluorescent labels^{125, 126}, which, unfortunately, is both chemically and labor intensive. Also, its quantization accuracy is often compromised by the poor photostability of the labeling fluorophores.

Significant progress has been made in the development of alternative DNA assay techniques by using gold nanoparticles,^{127, 128} dye-doped silica nanoparticles¹²⁹, and quantum-dots^{130, 131} as optical tags combined with various modalities of optical detection schemes. Although these approaches have the potential to improve the detection limits, they too, involve costly tagging chemicals and detection instrumentation. On the other hand, label-free detection has been emerging as a potential method for detecting DNA hybridization at high sensitivity with low cost and less preparation time. Whereas several format for label-free detection have been proposed such as electronic¹³², colorimetric^{133, 134}, and electrochemical¹³⁵, surface enhanced Raman spectroscopic (SERS) has not been yet explored as a promising alternative to achieve this goal.

The SERS detection of a single adenine base makes this technique ideal for ultrahigh sensitive label-free detection of DNA hybridization.¹³⁶ Most of the reported SERS-based DNA detection techniques are fundamentally based on detecting labels (SERS active tags) where the presence of the label is an indication of the presence of target DNA.¹³⁷⁻¹³⁹ Two main impediments have

prevented the development of a label-free detection technique based on SERS. First, the spectral reproducibility has been a major challenge for SERS especially for biomolecules such as DNA. Recently, we have reported an experimental procedure based on thermal cycling DNA oligomers which greatly enhances DNA spectral quality and reproducibility¹⁴⁰. Second, since both target and capture probe sequences (capture probe sequence is bound to the SERS-active substrate and complementary to the target sequence) are consisted of the same DNA bases, distinguishing SERS signal resulting from the hybridization of the target sequence is extremely challenging.

Au nanoshells (Au NS), spherical core-shell nanoparticles consisting of a silica core and Au shell with plasmon resonance frequencies controlled by the relative inner and outer radius of the metallic shell layer, have been used as reproducible SERS substrates.^{119, 141-143} In previous reports, we have proved that Au NS-based SERS-active substrates are ideal for large molecules detection such as DNA.^{140, 144} By thermally cycling ssDNA, the spectral quality and reproducibility was greatly enhanced. All DNA sequences were proven to have similar SERS spectra dominated by adenine SERS features regardless sequence length and/or base composition. This step is considered a major achievement towards SERS-based DNA label-free detection technique.

In this chapter I will discuss how we developed a label-free detection technique based on highly reproducible DNA SERS spectra on NS substrates and a substitution of all adenine bases on the capture probe sequence with the artificial base analogue 2-aminopurine. The 2-aminopurine substitution allows for the detection of target hybridization based on the appearance of the dominant SERS peak of adenine bases located within the target sequence. This is the first reported SERS-based label-free DNA detection technique based on DNA base substitution.

4.2 Experimental:

Nanoshell-based SERS substrates consisting of dispersed nanoshells bound to glass substrates were prepared as previously described.^{145, 146} Briefly, a fused quartz microscope slide (Piranha cleaned) was incubated overnight in an (1%) ethanolic solution of poly(4-vinylpyridine) (MW = 160 000 from Sigma-Aldrich) and dried with nitrogen gas; subsequently, 100 μL of aqueous nanoshell suspension was deposited onto the substrate. The substrate was then allowed to sit at room temperature for 3-4 h before being rinsed with Milli-Q water (Millipore, Billerica, MA) to remove excess nanoshells and then dried with a gentle flow of nitrogen.

All DNA sequences (Table 4.1) were purchased from Integrated DNA Technology Inc. (Coralville, IA). Prior to use, all thiolated DNA oligomers were reduced with 1,4-dithio-DL-threitol (Fluka) and purified with NAP5 purification columns (GE Healthcare). Unthiolated DNA sequences were used as received, having been HPLC-purified by the vendor. DNA uncoiling was achieved in solution, prior to binding of the DNA to the substrate by heating the DNA solutions in TE buffer (1 \times Tris EDTA buffer, pH) 7.5, from IDT) to 95 $^{\circ}\text{C}$ for 10-15 min. This step was followed by rapid cooling in an ice bath. DNA prehybridization was carried out *ex situ* by mixing two complementary DNA sequences at a 1:1 molar ratio in DNA hybridization buffer (TE/50 mM NaCl, pH = 7.5), heating the solution to 95 $^{\circ}\text{C}$, and then allowing it to cool slowly to room temperature in a large water bath. To bind DNA to the nanoshell SERS substrates, 50 μL (typically 40 μM) of the target DNA (ssDNA/dsDNA) was deposited onto a freshly made nanoshell SERS substrate. After overnight incubation, the excess ssDNA or dsDNA solution was removed by rinsing with TE or TE/50 mM NaCl buffer, respectively. *In-situ* hybridization was performed by adding 50 μL of the cDNA, corresponding to 1:1 molar ratio, to a SERS substrate that was previously functionalized with thiolated ssDNA, followed by adding 50 μL of

hybridization buffer. After overnight incubation, the excess ssDNA solution was removed by rinsing with TE/50 mM NaCl.

Oligonucleotide	Sequence (5'-3')
ST ₂₀ N1	SH-C6-TTTTTTTTTTTTTTTTTTTTTTTCGCGCAATCAGGTT GACCGTACATCATAGCAGGCTAGGTTGGTCGCAGTC
ST ₂₀ N2	SH-C6-TTTTTTTTTTTTTTTTTTTTTTTCGCGCTTTCTGGTT GTCCGTTCTTCTTTGCTGGCTTGGTTGGTCGCTGTC
SN3	SH-C6-TCTTGCTGTGTCTGTTCTTT
C-SN3	AAAGAACAGACACAGCAAGA
SN4	CATGTGACCTCTTCTAGATC
S2APN5	SH-C6-CGCT/2AP/GG/2AP/TCTG/2AP/CTGCGGCTCCTC C/2AP/T
C-S2APN5	ATGGAGGAGCCGCAGTCAGATCCTAGCG
SN6	CATGTGACCTCTTCTAGATC

Table 4.1: Oligonucleotide sequences used in the described experiments

SERS spectra were recorded while substrates were immersed in the appropriate buffer (TE for ssDNA and TE/50 mM NaCl for dsDNA) by using a Renishaw inVia Raman microscope (Renishaw, U.K.) with 785 nm excitation wavelength. Backscattered light was collected using a 63× water immersion lens (Leitz, Germany), corresponding to a rectangular sampling area of 3 μm × 30 μm. Unless stated otherwise, all the SERS spectra in this work were obtained with an integration time of 20 s and a laser power of 0.57 mW before the objective.

4.3 Results and Discussion:

4.3.1 Label-Free Detection Using Adenine-Free Capture Probe:

All SERS spectra are averages of at least 8 spectra acquired from different spots of the same substrate to ensure SERS spectral reproducibility. Typical Γ^{140} (spectral correlation function) of ~ 1 is calculated for all SERS spectra. The overwhelming dominance of adenine spectral features is supported by previous studies and is primarily attributed to the higher SERS cross section of adenine.¹³⁶ The DNA SERS spectrum looks extremely similar to adenine SERS spectrum, dominated by the 736 cm^{-1} peak (adenine breathing mode) (Figure 4.1.a). In the presence of adenine, spectral features from other DNA bases (guanine, thymine and cytosine) are inconsequential. SERS of adenine-free DNA, DNA sequence that does not contain adenine bases (ST₂₀N2), shows SERS modes of other bases especially guanine (Figure 4.1.b). The main SERS feature of the adenine-free DNA spectrum appeared at 663 cm^{-1} (guanine breathing mode).

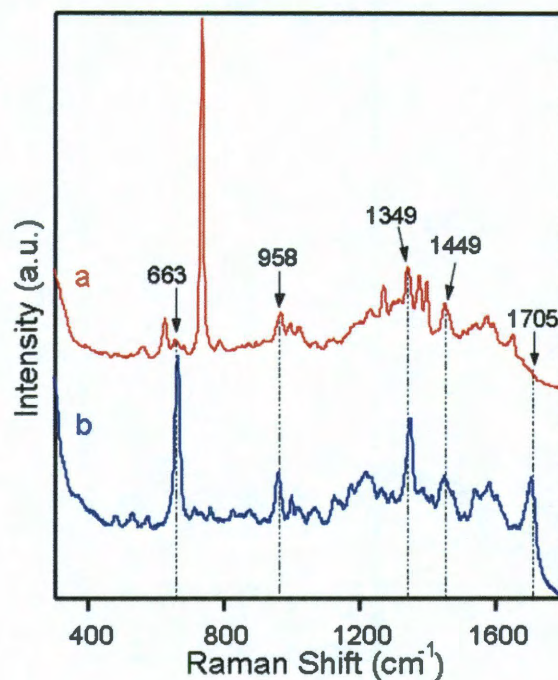


Figure 4.1: SERS of DNA sequences (a) with adenine bases and (b) with no adenine bases

Peak	Assignment
663	G breathing mode
958	NH bending
1349	A and G stretching
1449	A and G stretching
1705	Carbonyl group

Table 4.2: Raman Assignments

This result proves that the overwhelming 736 cm^{-1} mode is very distinctive for adenine bases. This 736 cm^{-1} strong adenine SERS mode can be used to detect the presence of a target sequence (containing adenine) that would hybridize to a capture probe which is adenine free. The SERS of the adenine-free capture probe is missing the 736 cm^{-1} mode as shown in Figure 4.1.b.

In the adenine-free capture probe format, single stranded adenine-free DNA sequences (capture strand) were first immobilized on the Au NS SERS active substrate through a thiol moiety on their 5' end, the rest of the DNA sequences are available for hybridizing with the complementary strands. SERS of the capture probe sequences is shown in Figure 2 with the main peak being at 663 cm^{-1} (guanine breathing mode). A target sequence (complementary to the capture probe) and a random sequence (non-complementary to the capture probe) were separately hybridized with the capture probe. The hybridization of the target sequence is evident by the appearance of the 736 cm^{-1} adenine peak (Figure 4.2.a). For the control sequence, a very small peak appeared at 736 cm^{-1} due to DNA/DNA interaction as well as DNA/surface non-specific binding (Figure 4.2.b).

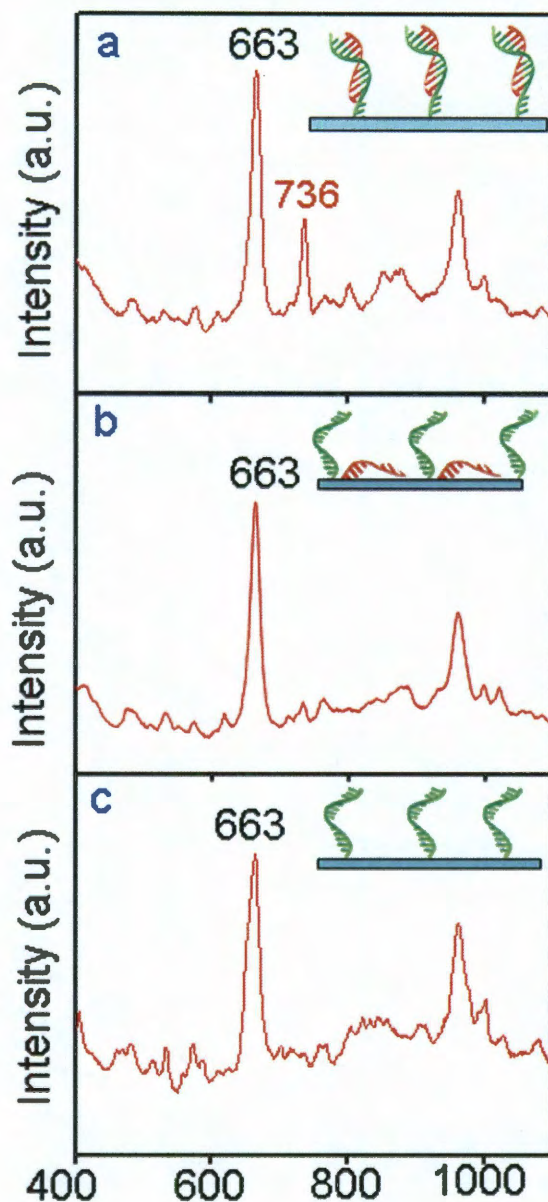


Figure 4.2: SERS label-free detection of DNA hybridization based on adenine-free probe. SERS of: (a) capture probe hybridized with complementary DNA sequence (target), (b) capture probe hybridized with non-complementary DNA sequence (control) and (c) DNA capture probe (adenine-free)

It has been reported that, for on-surface DNA hybridization, the packing density of the capture probe greatly affects the hybridization efficiency⁹⁶. Lower capture probe packing density significantly increases the hybridization efficiency since it allows for better interaction between

the capture probe and the DNA target. On the other hand, lower packing density provides more free space between DNA probe sequences for DNA/surface non-specific binding. This non-specific binding is significant for Au surfaces due to the high affinity between single stranded DNA and Au. To overcome this problem, mercaptohexanol was used to passivate the free surface which prevents target single stranded DNA from interacting with the Au surface.

Label-free detection of DNA hybridization has been proven using SERS and adenine as a SERS biomarker. Since the hybridization is indicated by the appearance of the main adenine peak, the capture strand has to be adenine-free. A convolution of adenine spectral features from capture and target DNA sequences is undesirable. Whereas this result is very promising, limitation in the detected DNA sequences is very unpractical.

4.3.2 Label-Free Detection Using 2-Aminopurine Substituted Capture Probe

To overcome the problem of sequence limitation substitution of adenine bases in the capture probe rather than completely eliminating them has been considered. 2-aminopurine have been found to be widely used as an artificial adenine substitution.¹⁴⁷ The substitution of adenine by its isomer 2-aminopurine, preserves the same characteristics of the substituted sequence. Very similar to adenine, 2-aminopurine binds to thymine through hydrogen bonding.^{148, 149} The substitution only causes a very small perturbation of the nucleic acid structure.¹⁵⁰

The SERS of the 2-aminopurine bases, however, is quite different than adenine bases. Most importantly, 2-aminopurine does not have SERS features at 736 cm^{-1} region (Figure 4.3.a) which means that it can be used as an ideal adenine substitution. SERS of DNA sequence containing 2-aminopurine shows only two main features at 807 cm^{-1} (breathing mode of 2-aminopurine) and 663 cm^{-1} (breathing mode of guanine) (Figure 4.3.b). A 2-aminopurine substituted DNA capture

probe can be used as a label-free adenine-based detection system where the hybridization of the target sequence is marked by the 736 cm^{-1} adenine peak.

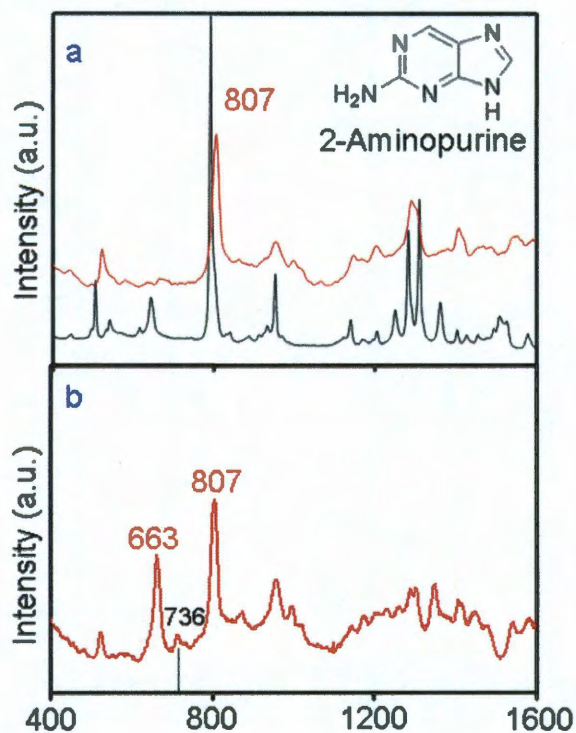


Figure 4.3: Raman spectroscopy of 2-aminopurine. (a) Surface enhanced (black) and non-enhanced (red) Raman spectroscopy of 2-aminopurine bases. (b) SERS of DNA containing 2-aminopurine bases. All adenine bases are substituted with 2-aminopurine. Inset is structural formula of 2-aminopurine.

Figure 4.4 shows the SERS spectra of the target (a) and a non-complementary control (b) DNA sequences hybridized to the 2-aminopurine substituted capture probe. The hybridization of the target sequence is identified by the 736 cm^{-1} adenine peak.

Further spectral proof of the target sequence hybridization, in addition to the 736 cm^{-1} adenine peak, is demonstrated by comparing the intensity of the guanine peak (663 cm^{-1}):2-aminopurine peak (807 cm^{-1}) ratio between the target and the non-complementary control sequence. A significant increase of this ratio is observed in the case of target hybridization. A relative

increase in intensity of the guanine peak indicates the hybridization of the target sequence, which contains guanine bases. The hybridization of the target sequence is verified by the appearance of a new peak at 736 cm^{-1} (adenine peak) and the relative increase of the guanine peak.

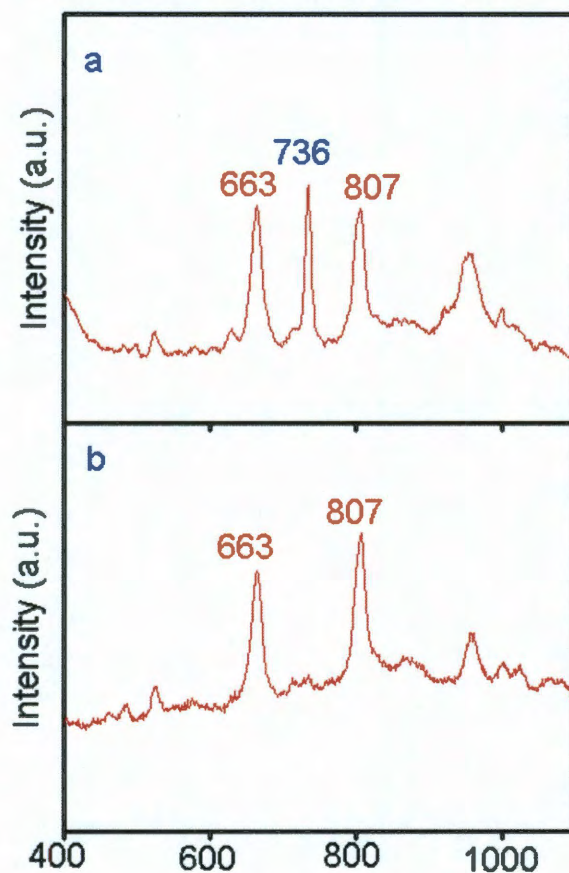


Figure 4.4: Label-free detection of DNA hybridization based on 2-aminopurine modified DNA probe. (a) complementary DNA sequence hybridized to 2-aminopurine probe (target). (b) non-complementary DNA sequence hybridized to 2-aminopurine probe (control).

4.3.3 Hybridization Efficiency:

On-surface DNA hybridization has been extensively studied for different surfaces, capture probe sequences and packing densities, buffers and so on. Experimentally determining the DNA hybridization is a very time consuming task. It usually requires dye-labeling the target sequence and determining the number of hybridized DNA sequences after displacing the DNA target and

capture probe from surface⁹⁶. Since the fluorescence of these label dyes is very pH dependent, keeping experimental solutions at the optimum buffer conditions (pH and salt concentration) for dye fluorescence is tedious, difficult and typically introduces some experimental errors.

The SERS label free detection technique described provides a more straightforward way to determine hybridization efficiency. The DNA hybridization efficiency can be simply calculated based on the ratio of the 736 cm^{-1} adenine peak intensity to the 807 cm^{-1} 2-aminopurine peak intensity. The intensity of the 807 cm^{-1} 2-aminopurine peak is constant and determined only based on the capture probe packing density. The peak ratio is 0 for non-hybridization. When capture probe and target sequences are prehybridized prior to binding to the NS substrate, the peak ratio would be maximum corresponding to A100% hybridization efficiency. Different hybridization efficiencies can be extrapolated from the different peak ratios and correlated to the target concentration. The hybridization efficiency is normalized for all substrates since it only depends on the ratio of intensities of the two peaks.

Figure 4.5 shows that the hybridization efficiency is fairly low even at high target concentration ($\sim 11\%$ at $80\text{ }\mu\text{M}$). The low hybridization efficiency is consistent with previous reports⁹⁶ and is mainly due to the capture probe packing density and hybridization conditions (buffer, temperature). Mercaptohexanol was used as a spacer molecule which increases the hybridization efficiency and decreases the non-specific DNA/surface interaction (result not shown). In addition, it was suggested that using a spacer short DNA sequence could further improve the hybridization efficiency.⁹⁶

This system provides a straightforward approach to study DNA hybridization efficiency for different DNA sequences, buffer conditions, spacers and so on. This could help improve other DNA detection techniques as well as on on-surface DNA hybridization technologies

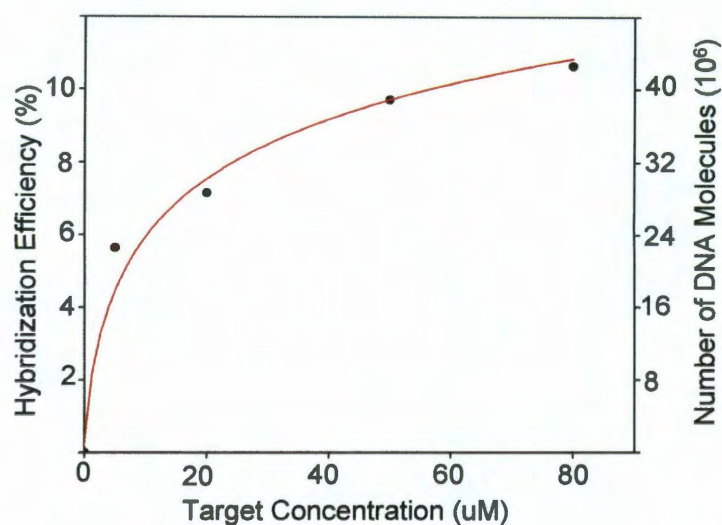


Figure 4.5: Label-free detection calibration curve. Plot shows the hybridization efficiency versus target concentration

In addition, since, the DNA mutations decrease the hybridization efficiency,¹³² this technique can be used to detect DNA mutations such as SNP (single nucleotide polymorphism). Introducing a mutation on the target sequence should decrease the hybridization efficiency which can be determined as a decrease in the peak ratio. Moreover, chemically modified DNA (oxidized or methylated) should also have a lower hybridization efficiency which could be detected as well. Particularly, DNA oxidation, which occurs most readily at guanine and correlated to aging-related diseases such as cancer could be detected. SERS of oxidized guanine will be different than normal guanine. The presence of oxidized guanine on the target sequence can be indicated by: (i) decrease in the adenine to 2-aminopurine peak ratio due to lower hybridization efficiency associated with sequence perturbation. (ii) decrease in the guanine to 2-aminopurine peak ratio since oxidized guanine will not have the same SERS features as native guanine. (iii) possibility of the appearance of new SERS features associated with the oxidized guanine.

One advantage of using SERS for DNA detection is the tremendous amount of information that could be derived from the SERS spectra. Whereas other DNA detection techniques are based on detecting tags, our detection scheme is based on detecting DNA itself. As a result the slightest variation on DNA target base composition and/or chemical structure can be easily detected. This technique can be extended beyond simple DNA detection to detecting mutated and chemically modified DNA, which could be used for many biomedical applications.

4.3.4 Target Concentration and Detection Limits:

The system allows measurement of the target concentration based on the calibration curve (Figure 4.5). Whereas in other DNA detection techniques, target concentration is typically determined through a comparative study, in this system, target sequence concentration could be directly extrapolated from the calibration curve. The adenine to 2-aminopurine peak intensity ratio is directly correlated to the target concentration. We have reported that thermal relaxation of DNA provides high substrate to substrate SERS spectral reproducibility in terms of peak position but not peak intensity. In SERS, peak intensity depends not only on number, conformation and relative proximity of molecules to the surface, but mostly on substrate quality. Comparing intensities of spectra acquired on different substrates requires high substrate reproducibility which is experimentally hard to achieve. The described label-free detection technique allows substrate to substrate comparison since it is based on the peak ratio regardless of the absolute intensity. The peak ratio depends only on the number of target molecules with respect to the number of probe molecules which represent the hybridization efficiency.

To determine the detection limit of the SERS label-free detection technique, we performed the hybridization experiment with decreasing DNA target concentrations. SERS of different samples was then acquired. Data shows that the minimum target concentration that could be detected and

discriminated versus a control sequence based on the peak ratios is ~ 80 nM corresponding to only 1.2×10^6 detected DNA molecules. 1.2×10^6 is the number of molecules on the $30 \mu\text{m} \times 3 \mu\text{m}$ sampling area and it is based on the DNA surface coverage (determined based on previous reports¹⁵¹) and DNA hybridization efficiency. It is worth to note that for 80 nM target concentration, the hybridization efficiency is only 0.3 %, this value could be easily improved by developing appropriate hybridization buffer and/or altering the capture strand packing density. The detection limit for the described technique is not determined by the target concentration rather by the hybridization efficiency, increasing the hybridization efficiency to 30 % will decrease the detection limit to the femto molar range.

The packing density of single stranded DNA on a Au surface which is easily predicted from previous studies is related to the number of hybridized DNA molecules through the hybridization efficiency. This technique is able to determine the absolute number of DNA molecules hybridized to the substrate which is relevant to all biomedical applications involving DNA detection. Number of molecules detected is reported for different target DNA concentration in Figure 4.5.

4.4: Conclusion

We observe that adenine can be used as a Raman marker for detecting DNA hybridization. The SERS high sensitivity to adenine bases (single molecule detection) makes adenine an optimum marker for label-free detection of DNA hybridization. We showed that an adenine-free DNA sequence can be used as a capture probe to label-free detect DNA hybridization. The appearance of the adenine peak is an evidence of the target hybridization. To overcome the limitation on detecting only thymine-free DNA, we substituted all adenine bases with 2-aminopurine bases. Whereas 2-aminopurine is chemically similar to adenine, SERS signal of 2-

aminopurine is quite different. Most importantly 2-aminopurine does not have any SERS feature at 736 cm^{-1} (breathing mode of adenine). The appearance of the adenine peak is still distinctive to the hybridization of the target sequence. Since the ratio of the adenine peak to the 2-aminopurine peak depends only on the number of the target sequences with respect to the number of the probe sequences, this technique can be used to determine both hybridization efficiency and target concentration. The high sensitivity to the hybridization efficiency allows the technique to be extended to detect DNA mutation such as SNP (single nucleotide polymorphism) and DNA base modification such as oxidation and methylation which will all decrease DNA hybridization efficiency. The detection limit is demonstrated to be $\sim 80\text{ nM}$ which corresponds to only 1.2×10^6 DNA molecules under SERS sampling area. Given that the detection of a single adenine base is attainable by SERS, ultra sensitive label-free detection technique based on SERS is approachable by experimentally improving the hybridization efficiency.

Chapter 5: Detecting Chemically Modified DNA Bases Using Surface Enhanced Raman Spectroscopy

5.1 Introduction:

The chemical modification of DNA bases has become a topic of rapidly increasing interest in the assessment of human disease. There are two major types of DNA base chemical modifications of interest in this context. The first occurs in epigenetics, the study of alterations in gene expression induced by changes other than modifications in the genetic code. Chemically modified bases can alter phenotype without changing DNA sequence.¹⁵² Epigenetic markers are thought to arise due to the influence of environmental factors influential in the onset of diseases such as cancer. In eukaryotic cells, methylated cytosine (mC) is the most common epigenetic marker.¹⁵³ In addition to its role in controlling gene expression, DNA methylation has been shown to strongly correlate with cancer in humans. Hypomethylation of DNA in human tumors,¹⁵⁴ hypermethylation of tumor-suppressor genes^{155, 156} and the inactivation of microRNA genes by DNA methylation¹⁵⁷ are all strong evidentiary factors of a relationship between the presence of chemically modified DNA bases and various human cancers. Hydroxymethylcytosine (hmC) is a stable DNA modification of great interest as a new epigenetic marker that has recently been discovered^{158, 159}. Hmc is highly abundant in the brain and believed to be important in neuronal function. It is currently accepted that hmC performs a fundamentally different epigenetic function than mC, making discrimination between hmC and mC extremely important; however, distinguishing hmC from mC is very challenging. Common

methods such as enzymatic approaches and bisulfite sequencing have proven unable to distinguish mC from hmC in DNA¹⁶⁰.

A second type of chemically modified DNA that is also extremely important is oxidized DNA. DNA oxidation occurs as a result of the interaction of reactive species of oxygen or nitrogen with genomic DNA¹⁶¹. The most common form of DNA oxidation in eukaryotes is guanine oxidation¹⁶², resulting most commonly in G to T transverse mutation¹⁶³. Despite the absence of a firm correlation between guanine oxidation and cancer, there is strong evidence that the level of guanine oxidation in genomic DNA is a relevant biomarker for assessing antioxidant status and cancer risk¹⁶⁴.

Typical methods for detecting DNA base modifications include single cell gel electrophoresis assay¹⁶⁴ for guanine oxidation detection, and bisulfite-based^{165,166,167} or enrichment-based methods^{166,167} for DNA methylation. All these methods require multiple-step sample preparation with chemicals that may induce additional chemical modifications in the DNA or interfere with the detection of modified DNA. In addition, most of these methods fail to distinguish between hmC and mC. The low throughput of these methods makes them unreliable strategies for the development of clinical diagnostic assays. Therefore the need for robust, streamlined methods for detecting chemically modified DNA bases is an important goal for analytical research, with the promise of clinical applications and technological impact.

Surface enhanced Raman spectroscopy (SERS) has been extensively explored to detect different types of biomolecules using broad range of nanostructures¹⁶⁸⁻¹⁷¹. In particular, Au nanoshells have shown great success as an active SERS substrate¹⁷²⁻¹⁷⁴. In this chapter, I report a simple and direct method for detecting the DNA base chemical modifications of adenine and cytosine methylation and hydroxymethylation, and guanine oxidation, using SERS. This method

is based on identifying SERS spectral variations due to DNA base modifications. No chemical treatments are needed, which eliminates the interaction of DNA with other chemicals, minimizing unwanted chemical modifications due to sample preparation. Applying this method would make detection of DNA base modification straightforward.

5.2 Experimental and Methods:

All DNA sequences used in this study were custom synthesized (Integrated DNA Technology, Inc). Modified bases were inserted during the sequence synthesis such that the number and position of modified bases was well determined. All DNA sequences were only thermally pretreated¹⁷² before SERS spectral acquisition with no further chemical treatment. All SERS spectra shown are the average of at least 5 individual spectra acquired from different spots on the same substrate. All SERS spectra are highly reproducible, with a spectral correlation function (Γ) close to 1.^{172, 175}

5.3: Results and Discussion:

5.3.1 Detection of Methylated Adenine:

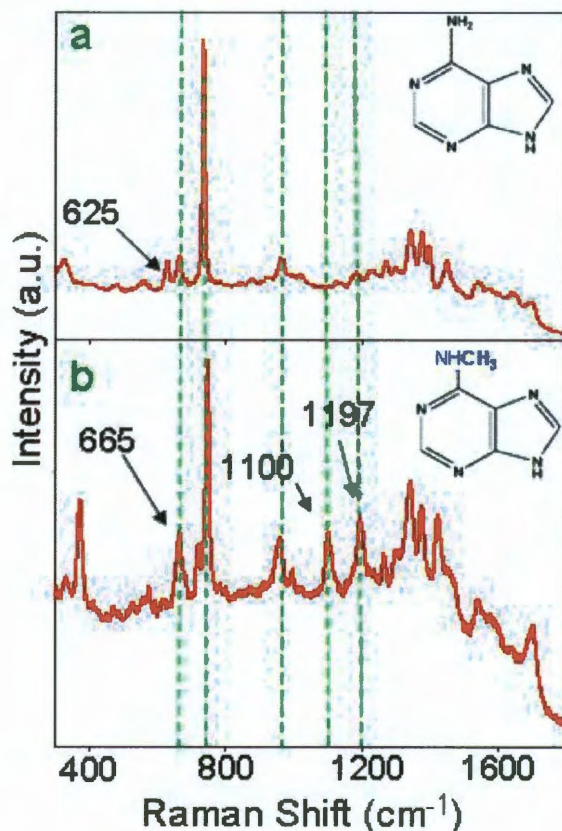


Figure 5.1: SERS spectra of (a) normal DNA sequence, and (b) adenine-methylated DNA sequence. Inset: molecular structures of adenine (top) and 6-methyladenine (bottom).

The spectrum of thermally pretreated 12 base single stranded DNA sequences (TCAAGCTGTGAC) is shown in Figure 5.1.a. As expected, the SERS spectrum is dominated by the 736 cm^{-1} peak (adenine breathing mode)¹⁷². When all adenine bases are substituted by 6-methyladenine (TCA*A*GCTGTGA*C) two new peaks appeared on the SERS spectrum, at 1100 and 1197 cm^{-1} (Figure 5.1.b). The 625 cm^{-1} adenine peak disappears, and the 665 cm^{-1} peak

(guanine breathing mode) has higher intensity. The appearance of these two new peaks is a confirmative marker indicating the methylation of adenine bases.

5.3.2 Detection of Methylated Cytosine:

Cytosine methylation is the most abundant epigenetic marker in eukaryotes. Unfortunately, cytosine bases possess a significantly weak Raman cross section compared to adenine and guanine.¹⁷⁶ Cytosine SERS features can barely be distinguished in the DNA SERS spectrum. Therefore, it is expected that the methylation of cytosine bases would not introduce large spectral variations in the DNA spectrum. Figure 5.2 shows that the substitution of cytosine by 5-methylcytosine (TC*AAGC*TGTGAC*) causes a slight increase in the 786 cm⁻¹ intensity (cytosine breathing mode).

Cytosine methylation of many eukaryotes frequently occurs at the CpG nucleotide sequences and 60 to 90 % of all CpGs in mammals are methylated^{177, 178}. Given this high degree of cytosine methylation, mC SERS detection is still possible although changes in the SERS DNA spectrum of this base are relatively minor.

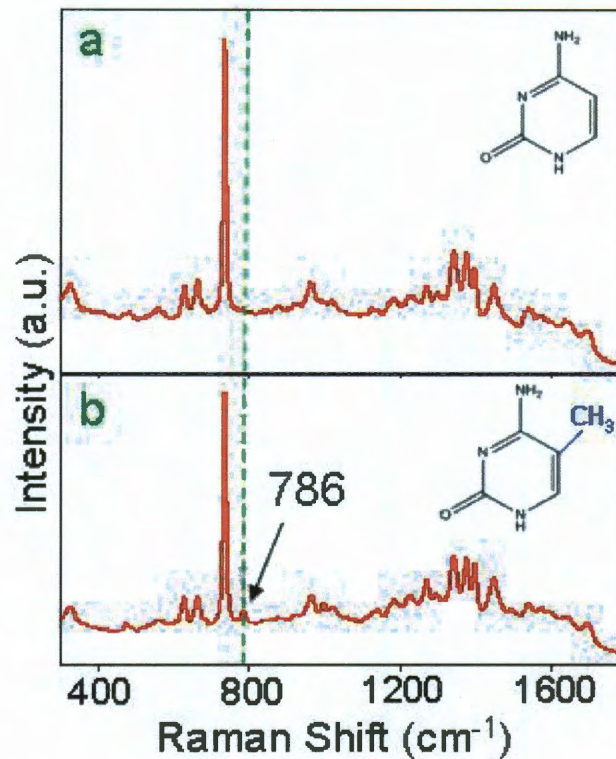


Figure 5.2: SERS spectra of (a) normal DNA sequence, and (b) cytosine-methylated DNA sequence. Inset: molecular structures of cytosine (top) and 5-methylcytosine (bottom).

5.3.3 Detection of hydroxymethylated Cytosine:

In contrast, however, the hydroxymethylation of cytosine introduces a significant change in the DNA SERS spectrum. It is worth noting that this particular DNA sequence has only one hmC due to synthesis limitations (TGAC*AGTTGTGATAG). Figure 5.3.b shows a significant intensity increase of the 665 cm^{-1} mode as well as the 963 cm^{-1} feature. Most importantly, the 1397 cm^{-1} is greatly suppressed as a result of the presence of the hmc base in the DNA sequence. The spectral variations between normal DNA and hydroxymethylated DNA are significant and dramatic, making verification of the presence of hmCs in a DNA sequence using SERS very straightforward. This data clearly indicates that a discrimination between mC and hmC is possible using SERS. The significant increase of the 665 cm^{-1} peak is an obvious marker of the

presence of hmC. The relative increase of the 786 cm^{-1} peak intensity for cytosine methylated DNA is still larger than the same peak increase for hydroxymethylated cytosine, rendering the detection of mC in the presence of hmC possible as well. To better elucidate this specific detection problem would require a DNA sequence containing both modifications.

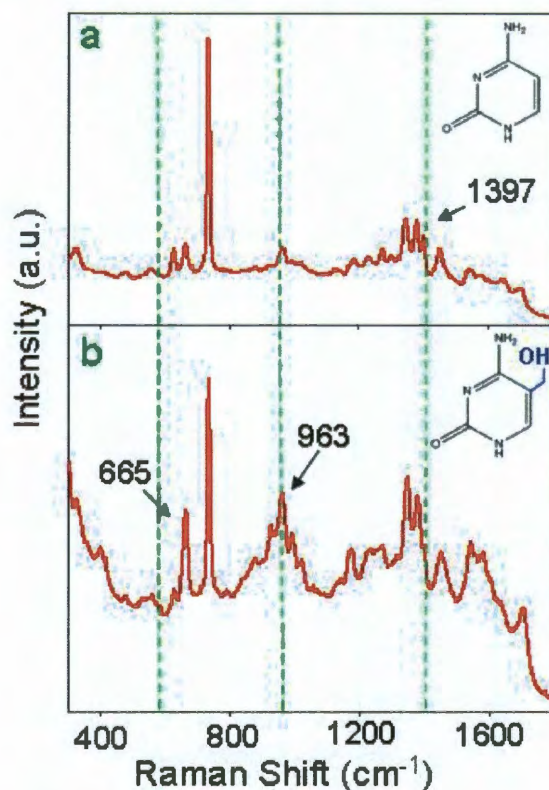


Figure 5.3: SERS spectra of (a) normal DNA sequence, and (b) cytosine-hydroxymethylated DNA sequence. Inset: molecular structures of (top) cytosine, (bottom) 5-hydroxymethylcytosine.

5.3.4 Detection of Oxidized Guanine:

The SERS spectrum of guanine oxidized DNA (where all guanine bases are substituted with 8-oxo-guanine, (TCAAG*CTG*TG*AC) was acquired (Figure 5.4). Here there are two significant markers indicating guanine oxidation: the appearance of a new mode at 1079 cm^{-1} and the disappearance of the guanine breathing mode (665 cm^{-1}). More detailed experimental studies

coupled with theoretical analysis are needed to identify the specific structural origin of these observed changes in the SERS spectrum. It is possible that the presence of modified DNA bases may affect the overall DNA spectrum by introducing new modes as well as suppressing or enhancing existing modes related to the modified base itself. Also, modified bases may affect the DNA/ surface interaction causing enhancement and/or suppression of modes not related to the modified base itself. The scope of this study is limited to the experimental demonstration of SERS detection and the identification of spectral markers for specific DNA base modifications.

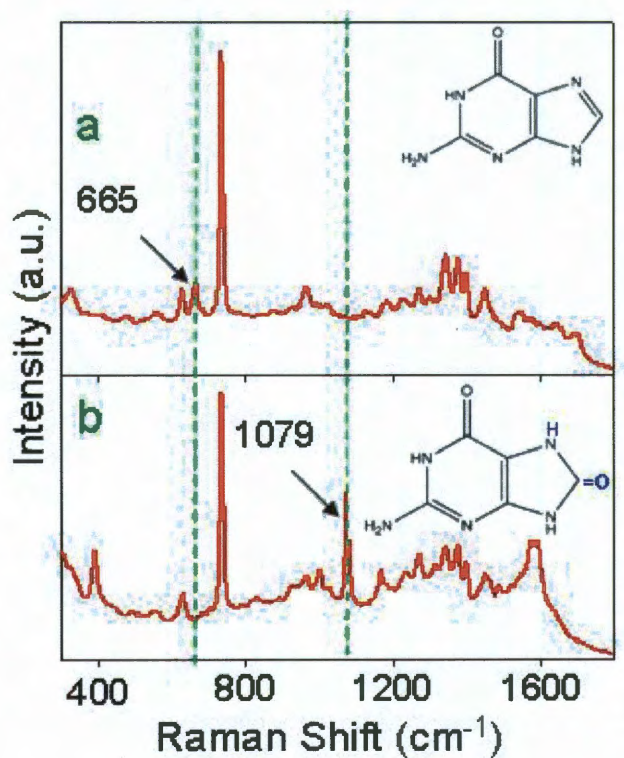


Figure 5.4: SERS spectra of (a) normal DNA sequence, and (b) guanine-oxidized DNA sequence. Inset: molecular structures of guanine (top) and 8-oxo-guanine (bottom).

5.4 Conclusion:

In conclusion, we demonstrated that SERS can be used to identify chemically modified DNA bases, including methylated adenine, methylated and hydroxymethylated cytosine, and oxidized guanine. All identified markers are unique and evident for discrimination of the specific modification. No chemical pretreatment was used, maintaining the integrity of the DNA sequence and making this a potentially promising approach for diagnostic applications.

Chapter 6: Light-induced Release of DNA from Plasmon-resonant Nanoparticles: Towards Light-controlled Gene Therapy

6.1 Introduction:

Recently, many reported results proving the potential role of nanoparticles in therapeutic molecules delivery and controlled release. That is an excellent motivation for quantitative studies of the light-induced release process of DNA from plasmon-resonant nanoparticle surfaces. In this chapter we develop a Au-nanoparticle-based nonviral vector for antisense gene delivery consisting of double stranded DNA (dsDNA) covalently attached to NIR-absorbing, plasmon-resonant Au nanoshells. Light-controlled release of ssDNA from Au nanoshells induced by resonant light absorption is demonstrated for oligonucleotide sequences of differing lengths and base compositions. The dehybridization temperatures of these sequences have been determined experimentally for both thermal and light-controlled dehybridization. Light-controlled oligonucleotide release is found to occur with essentially no temperature increase of the nanoparticle solution ambient, in stark contrast to thermal release, which occurs significantly at higher temperatures. Both dehybridization temperatures are found to be significantly below the solution-phase T_m for the same oligonucleotide. The maximum dsDNA coverage, as well as the percentage of DNA released from the nanoparticle surface, are determined for both light-controlled and thermal DNA dehybridization, and are found to be quite different for these processes. This work is the first study quantifying the effects of light-controlled DNA release from plasmon-resonant nanoparticles relative to thermally driven DNA release: the characteristics observed here are likely to provide general insight and stimulus for further study of light-induced DNA release from other plasmonic nanoparticles.

6.1.1 Gold Nanoshells in Photothermal Therapy and Drug Delivery:

Au nanoshells are spherical core-shell nanoparticles consisting of a silica core and Au shell with plasmon resonance frequencies controlled by the relative inner and outer radius of the metallic shell layer.^{38, 39, 179} Au nanoshells can be designed to have their maximum absorbance in the NIR region of the spectrum.¹⁸⁰ This absorbance wavelength is particularly important for biomedical applications since it falls within the near infrared spectral water window where tissue is nearly transparent. When illuminated with NIR light of resonant wavelength Au nanoshells absorb a portion of the total electromagnetic energy incident on the nanoparticle complex and convert the light into heat, resulting in an increased temperature on the Au nanoshell surface. This nanoparticle-based light-to-heat conversion has been explored in other therapeutic applications, in particular for photothermal cancer therapy.¹⁸¹ In this chapter, we study both purely thermal and light-controlled DNA dehybridization for DNA bound to nanoshell surfaces. The dsDNA has two strands: [1] a sense oligonucleotide with a thiol group on its 5' end for covalent bonding to the Au nanoshell surface, and [2] a complementary antisense oligonucleotide, which is the therapeutic sequence. These two complementary oligonucleotides hybridize through Watson-Crick base pairing. In this study, the therapeutic payload is the antisense oligonucleotide (ssDNA), and the principle is the same as antisense oligonucleotide therapy except Au nanoshells are the therapeutic carriers and light excitation controls the ssDNA release. Figure 6.1 shows a schematic of the Au nanoshell-based delivery system.

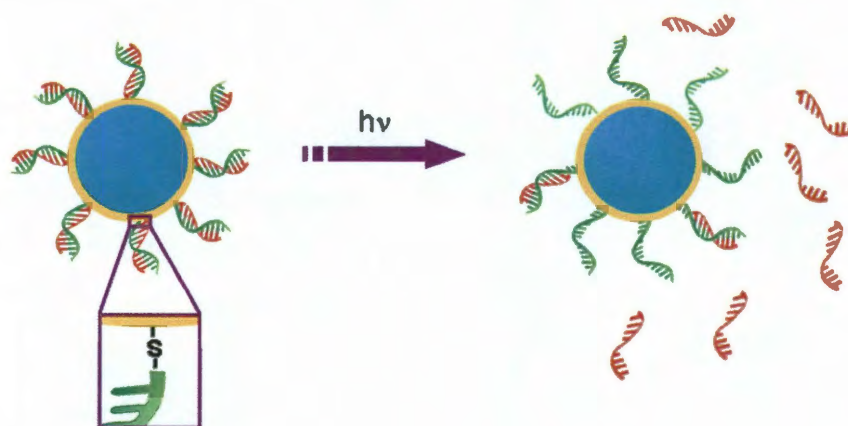


Figure 6.1: Schematic of light-controlled release of ssDNA from Au nanoshells. Green sequences are the thiolated sense sequences bound to the Au nanoshell surface, red sequences are the antisense sequences, released when nanoshells are illuminated with NIR light at their plasmon resonant frequency.

6.1.2 Thermal Dehybridization of dsDNA:

The temperature at which melting, or dehybridization, of double stranded DNA in solution occurs is influenced by many factors, including composition and orientation of neighboring base pairs, sequence length, and salt concentration. For example, dsDNA with a higher percentage of Guanine-Cytosine (GC) pairs will have a higher melting temperature, because the GC pair compared to the Adenine-Tymine (AT) has greater stacking interactions and an additional third hydrogen bond. To predict the melting temperature of dsDNA in solution, the nearest neighbor (NN) model is used to determine nucleic acid stability based upon the composition and orientation of neighboring base pairs¹⁸²⁻¹⁸⁶. The NN model is based largely on experimental work over more than two decades that provided precise measurements of thermodynamic parameters.¹⁸⁷⁻¹⁹³ These included specifically the binding free energy (ΔG), enthalpy (ΔH), and entropy (ΔS) for the 10 possible neighboring base pair combinations:

AA/TT, AT/TA, TA/AT, CA/GT, GT/CA, CT/GA, GA/CT, CG/GC, GC/CG, GG/CC. So, by knowing the composition of dsDNA, the predicted ΔG can be calculated by summing the ΔG values of each neighboring base pair plus a ΔG initiation value (ΔG_{int}).

$$\Delta G_{\text{Predicted}} = \Delta G_{\text{int}} + \sum \Delta G_n \quad (1)$$

Similarly, ΔH and ΔS are calculated and used to predict the melting temperature (T_m) of complementary oligonucleotides. The total oligonucleotide strand molar concentration (C_T), and the theoretical ΔH and ΔS , are used:

$$T_m(1MNa^+) = \frac{\Delta H}{\left[\Delta S + R \ln \left(\frac{C_T}{4} \right) \right]} \quad (2)$$

where R is the gas constant (1.987 cal/K·mol). The salt concentration also plays a critical role in dsDNA melting temperature. The T_m increases with increasing salt ion concentration due to the salt ions shielding the Coulombic repulsion between the negatively charged phosphate backbones of the oligonucleotides. If the salt ion concentration is low, the shielding decreases, so the dsDNA becomes less stable and the T_m decreases. There has been much debate whether the salt effect is sequence or length dependent; however, the most accurate empirical equation is a quadratic salt correction function that is sequence, composition, and length dependent. Because of this extensive research effort the T_m of dsDNA in solution is considered to be a relatively straightforward-to-predict value. However, binding dsDNA to nanoparticle surfaces for either

thermal or light-induced release introduces a new local environment for the DNA molecules which dramatically modifies solution phase T_m values.

6.2 Experimental:

6.2.1 Thermal and Light-driven DNA Release:

To demonstrate thermal and light-controlled release of ssDNA, several DNA oligomers of varying lengths and compositions (purchased from Integrated DNA Technology Inc.) were utilized (Table 6.1). Prior to use, all thiolated DNA oligomers were reduced with 1,4-Dithio-DL-threitol (DTT, Fluka) and purified with NAP5 purification columns (GE Healthcare). Unthiolated DNA sequences were used as received, having been HPLC-purified by the vendor. DNA hybridization was performed by mixing two complementary DNA sequences in a 1:1 molar ratio in DNA hybridization buffer (TE/50mM NaCl, pH = 7.5), heating the solution to 95 °C, then allowing it to cool slowly to room temperature in a large water bath. To ensure the maximum surface dsDNA coverage on the nanoshells, excess hybridized dsDNA was incubated with an aqueous suspension of Au nanoshells for at least 8 hours. The dsDNA was first precipitated with ethanol to minimize salt concentration and avoid nanoshell aggregation.

Oligonucleotide	Sequence (5'-3')
ST ₂₀ N1 (70 bases)	CTGACGCTGGTTGCATCGGACGATACTACATGCCAGTTGGACTA ACGGCGGGACAGCAGCTTTTTTTTTT
SN2 (50 bases)	GCGGCAATCAGGTTGACCGTACATCATAGCAGGCTAGGTTGGTC GCAGTC

SN3 (30 bases)	TATGATCTGTCACAGCTTGATACTACTTCA
SN4 (20 bases)	TATGATCTGTCACAGCTTGA
SN3-comp (30 bases)	TGAAGTAGTATCAAGCTGTGACAGATCATA

Table 6.1: DNA sequences used in this study. The released sequences are shown: the capture sequences are complements of these sequences with a thiol on the 5' end to ensure binding to the Au nanoshell surface. Labeled-sequences are the same released sequences with fluorescein on the 5' end.

Before the thermal or light-assisted dehybridization of dsDNA, the DNA/nanoshell mixture was centrifuged at least twice and resuspended in fresh buffer to remove excess free DNA in solution. Light-assisted release was performed as follows: 1 ml of nanoshells/DNA suspension was illuminated with a continuous wave laser (DioMed, $\lambda = 800$ nm, 1 W incident power). The temperature of the suspension (ambient temperature) was monitored with a thermocouple. For non-labeled DNA sequences, 1 mL aliquots were taken at different temperatures and run in a 3% agarose gel. For fluorescein-labeled DNA samples, fluorescence measurements of the supernatant were performed. For thermal dehybridization, DNA/nanoshell suspension was heated in a water bath. Similarly, aliquots were obtained and run in gel electrophoresis or checked for fluorescence intensity.

6.2.2 DNA-nanoshell Coverage and Percentage Release:

To quantify the number of oligonucleotides on the nanoshell surface, a 12 mM mercaptoethanol solution (Sigma Aldrich) was used as a DNA-displacing solution. Mercaptoethanol rapidly displaces hybridized surface-bound oligonucleotide via a thiol

exchange reaction.¹⁹⁴ This process is rapid and efficient because the oligonucleotide self-assembled monolayer (SAM) cannot block access of the mercaptoethanol to the gold surface and mercaptoethanol forms a more tightly packed SAM due to its greater packing energy via Van der Waals forces than the DNA monolayer it displaces.

First, a standard curve of fluorescein-labeled DNA fluorescence intensity versus DNA concentration was experimentally determined. The amount of DNA bound to the nanoshell surface in a sample was determined by taking a fluorescence measurement of the supernatant before the mercaptoethanol displacing solution was added (background fluorescence) and after 24 hours incubation with mercaptoethanol. Subtraction of the background fluorescence allowed us to obtain a value for the amount of DNA displaced. Nanoshell concentration was determined by using the Beer-Lambert law, the extinction coefficient was determined by Mie theory. Finally, the amount of DNA per nanoshell was calculated. Since the antisense strand was tagged with fluorescein, the amount of DNA released was easily quantified. After thermal or light-driven release of DNA, the difference in fluorescence intensity was calculated and the percentage of DNA released was determined. In these experiments the displacing solution was not used.

6.3 Results and Discussion:

6.3.1 DNA Dehybridization Irreversibility:

The purpose of this study was to compare the amount of ssDNA released by light-controlled and thermal dehybridization, and to obtain the effective DNA-ambient melting temperature for both processes. Dehybridization reversibility is a critical concern for these processes, since rehybridization of the released ssDNA back to the nanoparticle once the laser

irradiation has ceased, if it occurs to a significant extent, would greatly limit the effectiveness of this strategy for gene delivery.

In the first experiment, a suspension of Au nanoshell/dsDNA (SN3 prehybridized with its thiolated complement) was prepared as described. The ssDNA antisense strand has a fluorescein label on its 5' end. The prepared nanoparticles were divided into two samples. For both samples, DNA dehybridization was thermally induced. In one sample, an excess of the nonthiolated SN3-complement was added to solution. In the presence of the excess of the SN3-complement, the released SN3 DNA will preferentially hybridize to the excess SN3-complement in solution. For the other sample, no additional DNA was added to the solution. After thermal dehybridization of both samples under the same experimental conditions, the aliquots were centrifuged and the fluorescence intensity of the supernatant was measured. The released sequence was the only source of a fluorescence signal. If the released DNA rehybridizes with its complementary sequences left behind on the Au nanoshell surface, the amount of fluorescent DNA in solution will be significantly higher for the sample with the excess DNA complement in solution and a measureably lower fluorescent signal when no SN3-complement is available in solution for competitive binding.

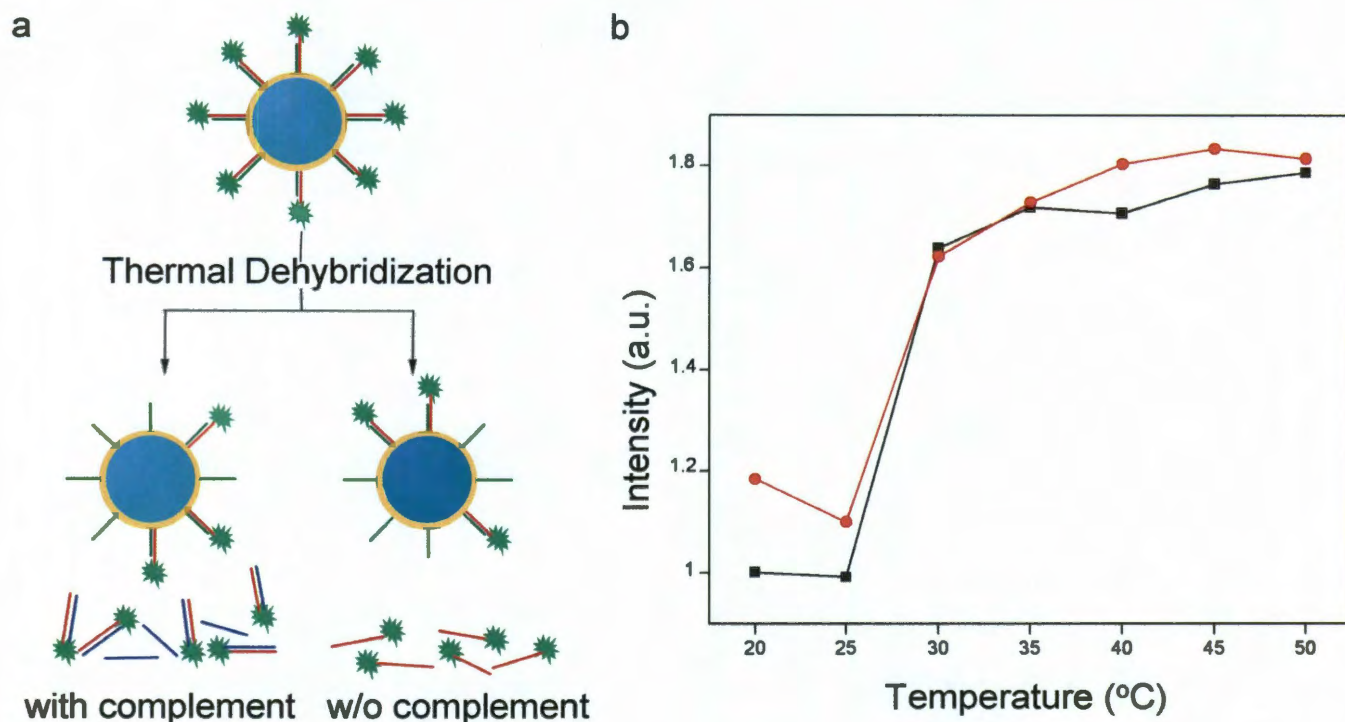


Figure 6.2: DNA dehybridization irreversibility. (a) Schematic depicting the released DNA behavior with and without complementary sequence. (b) Graph shows the amount of DNA released versus the temperature based on the released DNA fluorescence intensity with (red) and without (black) complementary sequence.

The results of this experiment are shown in Figure 6.2. Here it can be seen that the fluorescent signal due to the released DNA agrees for the two release conditions within experimental error, and that the DNA dehybridization on the Au nanoshell surface is an essentially irreversible process. This dehybridization irreversibility is critical for biological applications, and must be the case for the released DNA to be delivered to proceed to mRNA binding, in the case of antisense oligonucleotide therapy.

Two main factors contribute to the dehybridization irreversibility. First, rehybridization of the released ssDNA would require it to hybridize with the complementary sequences on the Au surface, a process well documented to be of low efficiency.¹⁹⁴ In addition, after dehybridization, the sense sequence on the nanoparticle surface may loop and bind non-specifically directly onto

the Au surface, preventing rehybridization. This effect would be likely for all metal surfaces with high affinity to DNA. It is worth noting that the presence of the SN3-complement in solution did not appreciably affect either the DNA melting temperature (around 35 °C) or the amount of DNA released. At low temperatures, however, the amount of DNA released in the presence of the excess SN3-complement sequence is slightly higher due to non-thermal DNA release, either due to nonthermal dehybridization or the presence of some nonspecifically bound ssDNA on the nanoparticle surface.

6.3.2 *Thermal Release of ssDNA:*

dsDNA dehybridization is an essential process in all biological systems as well as many DNA-based nanotechnology applications. The mechanism of dsDNA thermal dehybridization has been thoroughly studied¹⁹⁵. It has been shown that dsDNA attached to surfaces, in particular Au surfaces, behaves differently than free dsDNA in terms of melting temperature and phase transition.¹⁹⁶

We first studied the thermal dehybridization of dsDNA attached to Au nanoshell surfaces. Gel electrophoresis has been used to determine the amount of ssDNA released, a process requiring no fluorescent labeling of the DNA. In the 3% agarose gel used in this work, the pore size is much smaller than the nanoshell diameter. Consequently, the nanoshells in the DNA/nanoshell suspension are trapped in the gel electrophoresis wells. Only free DNA will migrate through the gel matrix. Comparing the bands intensities of the released ssDNA from aliquots taken at different temperatures reveals the progression of the DNA release in the DNA/nanoshell sample, since the band intensity is proportional to the concentration of DNA.

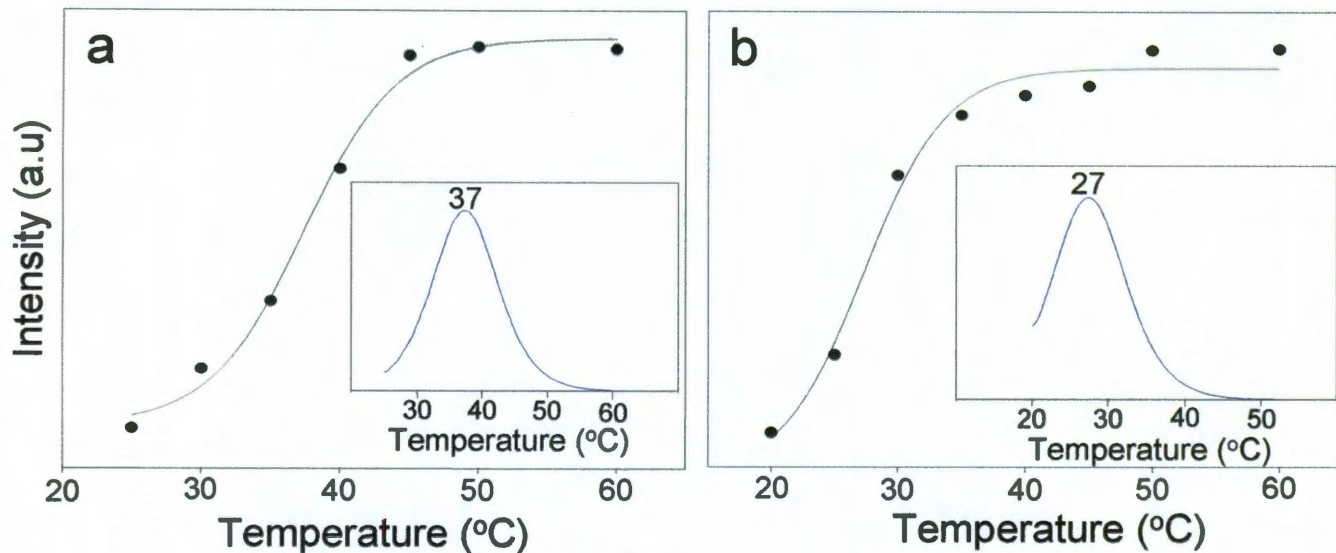


Figure 6.3: Thermal (a) and light-assisted (b) release of ssDNA from dsDNA-coated nanoshells in solution. The melting curves for 20 base dsDNA attached to Au nanoshell surface are shown. Insets show the first derivatives of the melting curves, depicting the melting temperatures T_m of each process.

DNA melting curves, obtained by monitoring the UV fluorescence (from the DNA-associated dye Syber green) in the gel column as a function of solution-ambient temperature, are shown for thermal DNA dehybridization (Figure 6.3.a) and for light-induced DNA dehybridization (Figure 6.3.b). The UV absorption intensity is directly proportional to the amount of DNA released. The maximum of the first derivative of these curves, corresponding to the temperature of maximum DNA release, is defined as the DNA melting temperature, T_m . For both thermal and nonthermal DNA release, the derivative plots are shown as insets. The melting temperature of the 20 base dsDNA (SN4 with its thiolated complement) attached to Au nanoshells was experimentally determined to be 37 °C (Figure 6.3.a). The melting temperature of the same dsDNA sequence in solution, not confined to Au surface, is expected to be nominally 50 °C at 50 mM salt concentration (IDT DNA). Although the salt concentration on the nanoshell/DNA solution is likely to be somewhat lower than 50 mM due to ethanol precipitation of the DNA prior to

binding to the nanoshell surfaces, there is still clearly a significant decrease in the DNA melting temperature when DNA is bound to the Au surface relative to the anticipated solution phase T_m . The same trend was consistent for all DNA sequences investigated in this study. It is interesting to note that DNA melting temperature depression for DNA bound to an Au surface is still a matter of debate: both increasing and decreasing T_m for DNA on Au nanoparticles relative to the corresponding solution phase value have been reported.^{196, 197}

Under the experimental conditions described above, the T_m of the dsDNA sequence attached to Au nanoshell surfaces has shown a significant decrease.¹⁹⁶ Most likely, the high affinity of DNA to the Au surface is playing an essential role in the T_m reduction. In solution, the T_m depends solely on DNA strand length and base composition. However, when one strand of the duplex is attached to a surface, the T_m may be affected by the influence of the surface on the duplex stability. Because of the high affinity of ssDNA to the Au surface, the single-stranded DNA form is more favorable than when in solution, which would result in a decrease in DNA melting temperature.

6.3.3 Light-induced Release of ssDNA:

The DNA melting curve for light-assisted DNA dehybridization is shown in Figure 6.3.b, with the first derivative of the melting curve shown in the inset. Here the T_m of the 20 base DNA sequence, the same sequence used in thermal dehybridization, is 27 °C. This corresponds closely to the ambient temperature of the DNA-nanoshell suspension. This lack of temperature increase corresponds to two possible mechanisms for DNA release. These are: [1] a nonequilibrium thermal mechanism, where the irradiated nanoparticle undergoes a strong and rapid temperature increase at its surface sufficient to melt the DNA but not sufficient to raise the ambient solution temperature, or [2] a nonthermal mechanism, such as charge transfer to the DNA adsorbate,

resulting in DNA dehybridization driven by Coulomb repulsion. Further experimentation would be needed to specifically identify which mechanism or mechanisms may be responsible for the DNA release.

To examine this ambient-temperature light-induced dehybridization further, both thermal and light-assisted dehybridization experiments were performed on three other sequences (30, 50, and 70 bases). Correspondingly, similar distinct decreases in the T_m due to thermal dehybridization and to light-assisted dehybridization of dsDNA attached to nanoshells were observed (Figure 6.4). For all sequences studied, light-assisted DNA dehybridization is observed to occur at essentially ambient temperature. While further studies are warranted to determine the specific light-induced release mechanism, the fact that release occurs at ambient temperature over a range of oligonucleotide lengths and compositions is extremely encouraging for gene therapy applications. The fact that laser-induced gene release can occur in a regime where the laser irradiation does not increase the ambient temperature indicates that this process may be useful for the safe release of oligonucleotides in cells without inadvertently compromising cell viability.

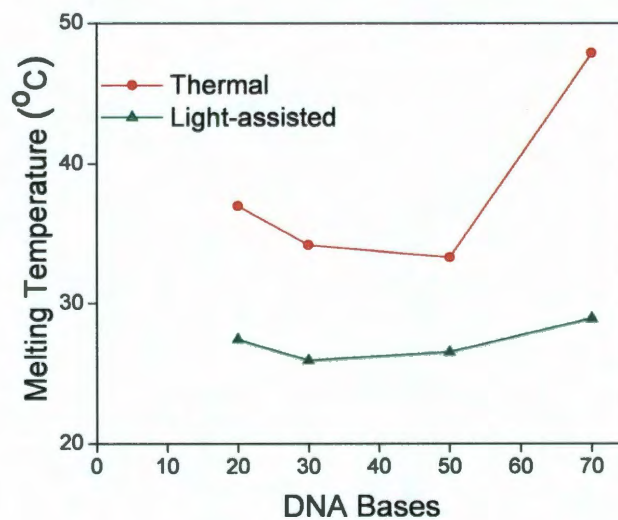


Figure 6.4: Comparison of the light-induced (green) versus thermal (red) dehybridization of dsDNA sequences of different lengths tethered to Au nanoshells. For all DNA sequences studied,

the light-assisted melting temperatures are lower than 30 °C which makes this system suitable for releasing ssDNA as long as 70 bases in biological applications.

6.3.4 Surface coverage and percentage release:

DNA surface coverage on nanoshells was determined using a previously reported protocol with minor modifications.¹⁹⁴ In this procedure, (i) the concentration of nanoshells is determined from the extinction spectra and Mie theory, (ii) the emission intensity of fluorescence-labeled DNA displaced from the nanoshell surface is measured, and (iii) the fluorescence intensity is correlated to the DNA concentration through a standard, previously determined curve. The number of molecules and the percentage of ssDNA released from the nanoshell surface can be determined by comparing the fluorescence intensity before and after thermal or light illuminated DNA release.

The coverage of dsDNA molecules on Au nanoshells was determined to be 6400 dsDNA molecules/nanoshell which corresponds to 14.6 pmol/cm². This coverage is consistent with previous results of oligonucleotide surface coverage on Au films (18.1 ±3 pmol/cm²).¹⁹⁴ Due to the 150 nm diameter size of the NS particle, its surface is more analogous to a gold film compared to a small gold nanoparticle. This observation is consistent with published results indicating that the packing density of oligonucleotides on the surface becomes analogous to packing densities on a gold film when a spherical gold nanoparticle substrate approaches 150 nm in diameter.^{198, 199} The decrease in packing density determined for DNA on nanoshells relative to that reported for planar Au surfaces may be due to: [1] the use of dsDNA in our studies instead of ssDNA, and [2] a decreased salt concentration needed to prevent nanoshell aggregation, which reduces electrostatic repulsion between DNA chains and decreases overall packing density.¹⁹⁴

The percentage of DNA released was determined for the cases of both thermal and light-induced DNA dehybridization. While ~90% of the ssDNA is released for thermal dehybridization, only ~50 % of the total available ssDNA is released for the light-induced process. The fact that these release percentages are so remarkably different provides strong support for a fundamental difference between the thermal and light-induced DNA dehybridization process. While it is not surprising that the thermal release process, conducted under equilibrium conditions, results in the greatest percentage of ssDNA released from the nanoshell surface, it raises significant further questions regarding the actual release mechanism or mechanisms involved in light-driven DNA release. It is also important to note that the number of ssDNA molecules released per nanoshell in the case of light-induced release (3169 ssDNA/nanoshell) is considerably larger than the number of molecules released by the same process on nanorods (250 molecules/nanorod).⁶⁴ This possible dependence of yield on the aspect ratio of the nanoparticle also suggests that this process occurs under highly nonequilibrium conditions on the nanorods surface, or that a charge-transfer mechanism may be important in the release process.

6.4 Conclusion:

Both thermal and light-triggered dehybridization of dsDNA where one complementary strand was covalently bound to Au nanoshells was investigated. In contrast to dehybridized ssDNA in solution, dehybridization of dsDNA bound to an Au nanoparticle surface is shown to be essentially irreversible. The melting temperatures of dsDNA bound to nanoshell surfaces was assessed for both thermally-induced and resonant light-induced dehybridization. A large difference in T_m was observed for each process, and each process occurs at a T_m substantially lower than the corresponding melting temperature of the same oligonucleotide in solution.

The light-induced dehybridization of dsDNA bound to Au nanoshells appears to occur at the solution-ambient temperature for all dsDNA sequences and lengths studied. The coverage of dsDNA on Au nanoshell surfaces was quantified and shown to correspond closely to packing densities obtainable on planar Au films. By quantifying surface coverage of dsDNA, we were also able to determine the percentage of ssDNA released for both the thermal (~90%) and the light-induced (~50%) release process. These studies point to some very interesting and dramatic differences between thermal and light-induced processes on plasmon-resonant nanoparticle surfaces. Not only does this system provide a promising potential for light-controlled gene release for gene therapy, it also provides a new and exciting context where the rich chemical physics of substrate-adsorbate interactions may prove relevant to our understanding of light-actuating nanoparticle complexes.

Chapter 7: Visualizing Light-triggered Release of Molecules Inside Living Cells

7.1 Introduction:

7.1.1 Biomedical Applications of Plasmonic Nanoparticles:

Strategies for the directed release of controlled quantities of molecules inside living cells are in high demand for drug delivery,²⁰⁰ gene therapy,^{201, 202} and tissue engineering.^{203, 204} The release mechanisms of most delivery vectors depend on processes such as diffusion, dissolution, chemical and enzymatic reactions, or changes in various environmental factors such as temperature, pH, solvent, and ionic concentrations.^{201, 205-208} For example, transfection reagents such as polyethylenimine act as a proton sponges following endocytosis, absorbing protons in the low-pH environment of the endosome, causing it to swell and eventually rupture, facilitating gene delivery.²⁰⁹ This type of environmental control of molecular release varies with cellular location and cell type, and can result in unpredictable release. A physical release mechanism that does not rely on the specific chemical properties of the cellular environment would be highly useful and more easily generalizable to various cell types.²¹⁰ Light-induced release is a particularly attractive option: the high spatial and temporal control that lasers provide would be highly useful for initiating and following intracellular processes dynamically, at the single cell level.²¹¹⁻²¹⁷

Plasmonic nanoparticles, metal-based nanostructures supporting collective electronic oscillations, are highly promising potential candidates for facilitating controlled light-triggered release, due to their large optical cross sections, their geometrically-tunable optical resonances^{218,}

²¹⁹ and their strong photothermal response.^{220, 221} Because of their large cross sections and extremely low quantum yield, metallic nanoparticles convert optical energy to thermal energy with high efficiency upon resonant optical illumination.^{27, 222} Resonant optical illumination of the nanoparticle triggers the controlled dehybridization and release of DNA molecules adsorbed onto the nanoparticle surface.^{215, 217} Gold nanoparticles are also biocompatible, easy to fabricate, and can be functionalized with a wide variety of host-carrier molecules capable of noncovalent accommodation of guest molecules.^{205, 217}

In the previous chapter I described light-induced dehybridization of double-stranded DNA (*dsDNA*) attached to Au nanoshells.²¹⁷ Nanoshells with plasmon resonance wavelength at 800 nm were coated with *dsDNA*, where one strand of the DNA had a thiol moiety on its 5' end, facilitating covalent attachment to the nanoshell surface by a Au-thiol bond. The complement DNA sequence was nonthiolated, and therefore bound only to its complementary DNA sequence and not to the nanoparticle surface. Upon illumination with NIR light at the nanoshell plasmon resonance wavelength, the *dsDNA* was dehybridized, releasing the antisense sequence. This process is highly efficient, resulting in the dehybridization and release of nominally 50% of the DNA from the complexes upon illumination, with no apparent temperature increase in the solution ambient. DNA antisense therapy has been explored extensively as a class of gene therapy and has highly promising potential to provide safe and effective treatments for a multitude of diseases and genetic disorders.²²³

Here we show that, in addition to light-controlled release of DNA, the nanoshell-*dsDNA* complex serves as an effective host and light-triggered release vector for other types of molecules. Many types of guest molecules can associate with *dsDNA*, either by intercalating between adjacent base pairs or by binding in either the major or minor groove of the DNA

double helix.²²⁴ The driving forces for association can include π -stacking, hydrogen bonding, van der Waals forces, hydrophobic and polar interactions, and electrostatic attractions; therefore, dsDNA can host a large variety of guest molecules via noncovalent bonds.^{224, 225}

7.1.2 DAPI (4',6-diamidino-2-phenylindole)

DAPI (4',6-diamidino-2-phenylindole), a water soluble blue fluorescent dye that binds reversibly with dsDNA (Figure S4) is the molecule we chose to deliver, to demonstrate and clearly visualize the light-induced intracellular release. DAPI was chosen because of its bright fluorescent properties, stability and negligible toxicity.²²⁶ DAPI binds preferentially to the minor grooves of dsDNA: its association with DNA causes a large increase in its quantum yield.²²⁶⁻²³⁰ The selectivity of DAPI to dsDNA makes it a frequently used, standard stain for cell nuclei in fluorescence microscopy.^{229, 230}

A schematic of the light-triggered molecular release is shown in Figure 7.1. Initially, nanoshell-dsDNA complexes were loaded with DAPI by incubation of DAPI with the nanoshell-dsDNA complexes. Next, the nanoshell-dsDNA-DAPI complexes were incubated with H1299 lung cancer cells, where intracellular uptake was verified using both dark-field and bright-field microscopy. Upon illumination with an 800 nm CW laser, corresponding to the peak resonant wavelength of the nanoshell complexes, the DAPI molecules were released from the nanoshell complexes. Subsequent to release, the DAPI diffused through the cytoplasm and into the cell nucleus, where it preferentially bound and stained the nuclear DNA. To the best of our knowledge, this is the first light-controlled delivery system that can be tailored to release quantifiable amounts of nonbiological molecules, within living cells by remote means, on demand.

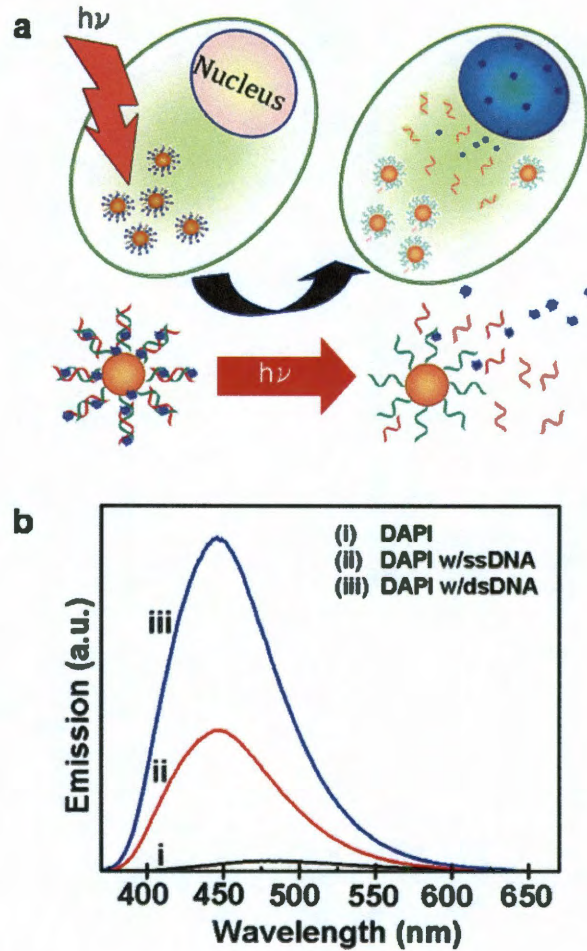


Figure 7.1 Light-induced DAPI release. (a) Schematic diagram of the light-induced DAPI release and diffusion inside the cell. (b) Fluorescence emission of (i) DAPI only, (ii) DAPI with ssDNA, and (iii) DAPI with dsDNA.

7.2 Results and Discussion:

7.2.1 DAPI Fluorescence Emission:

The DAPI fluorescence emission intensity drastically increases as a result of DAPI molecules binding to DNA (Figure 7.1.b). As an isolated molecule, DAPI has a low quantum yield (Figure 7.1.b, i),²²⁷ however, when DAPI is attached to single stranded DNA (ssDNA) (Figure 7.1.b, ii), a weak electrostatic attraction binds the cationic DAPI molecules to the negatively charged

phosphate backbone of the DNA, resulting in a slight increase in its fluorescence intensity.²²⁷ When the DAPI molecules bind to the minor grooves of the dsDNA (Figure 7.1.b, iii),^{227, 230} the increased rigidity and stabilization significantly increases its quantum yield.²²⁶ DAPI binding to the dsDNA also displaces H₂O molecules initially solvating the DNA oligomers, significantly reducing intermolecular proton transfer between H₂O and DAPI, resulting in an additional increase of DAPI fluorescence intensity.^{227, 228, 231}

The specific base-pair composition of the dsDNA plays an important role in determining the number of DAPI molecules that will bind to the dsDNA.²³² Previous studies have shown that DAPI preferentially binds to regions rich with adenine (A) and thymine (T) nucleotide bases because DAPI forms hydrogen bonds with A-T bases pairs.²³⁰ The DAPI molecule is 14-15 Å long, corresponding to an overlap of three base pairs.^{227-229, 232} In our experiments, since it is desirable to bind as many DAPI molecules as possible to improve the staining of the nucleus after light-induced release, we designed a 26-base pair sequence with multiple A-T-rich regions with segments of three or more consecutive A-T base pairs to specifically enhance DAPI loading.

7.2.2 Nanoshell Cell Uptake:

To use this light-triggerable complex for molecular release in live cells, the complex must first be effectively taken up by the cells of interest. To facilitate cell uptake, the nanoshell-dsDNA-DAPI complexes were incubated with H1299 lung cancer cells in serum containing cell culture medium for 1 hour. After incubation, the cells were fixed and internalization of the nanoshell-dsDNA-DAPI complexes was imaged using both dark field (Figure 7.2.a-b) and bright field (Figure 7.2.c) microscopy. Nanoshells in this size range both absorb and scatter light: their strong scattering cross section enables them to be easily visualized by optical microscopy. In

Figure 7.2.a, a H1299 cell with its cell membrane marked by the green fluorescence dye Alexa Fluor 488 WGA (wheat germ agglutinin) is shown. Internalized nanoshells are easily seen as diffraction-limited bright spots in this image. As a control, cells not incubated with the nanoshell-dsDNA-DAPI complexes showed no observable bright spots when imaged in the same manner (Figure 7.2.b).

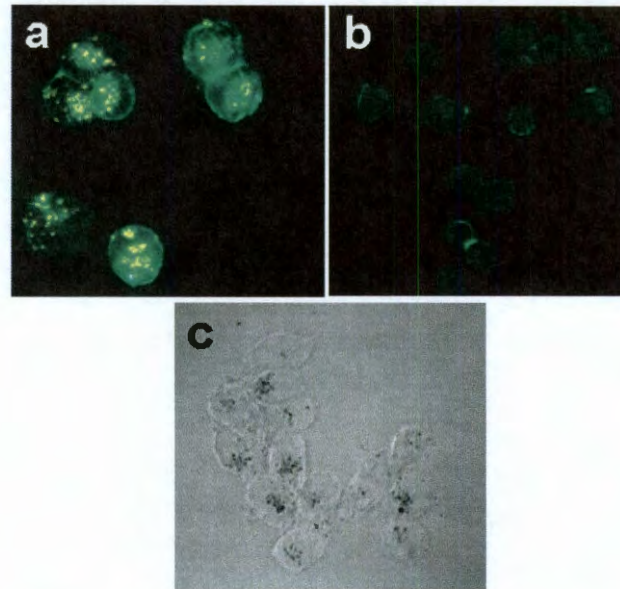


Figure 7.2 Nanoshell-dsDNA-DAPI Cell uptake. Dark field/epifluorescence images of (a) H1299 lung cancer cells incubated with nanoshell-dsDNA-DAPI complexes, (b) nonincubated cells (control). (c) Bright field image of middle slice of H1299 lung cancer cells incubated with nanoshell-dsDNA-DAPI complex.

Because the dark-field images are two-dimensional, these images alone do not give clear evidence whether the nanoshell complexes have been endocytosed, or are merely adsorbed onto the outer membrane of the cell. Bright-field imaging was used to further investigate cellular uptake. Obtaining images at varying depths of field within an individual cell allows us to clearly visualize in three dimensions the nanoshell distribution within the cell. Figure 7.2.c is a slice from the middle of the cell showing clear diffraction-limited dark spots corresponding to

nanoshell complexes, verifying that the nanoparticles are internalized within the cell. A video sequence of two-dimensional projections obtained as the depth of field is scanned through the cell resolves the 3D distribution of nanoshell. Internalization of nanoshells is in agreement with observations by Ochsenkühn *et al*, who used TEM sections of NIH-3T3 fibroblast cells to confirm nanoshell uptake.²³³

At first thought, it is surprising that the nanoshell-dsDNA-DAPI complex is internalized into cells because the negatively-charged phosphate backbone on the DNA should experience electrostatic repulsions with the negatively-charged cell membrane.²³⁴ However, previous studies by Chithrani *et al* and Giljohann *et al* suggest that Au nanoparticles functionalized both with and without DNA adsorb extracellular serum proteins from the cell culture media.^{234, 235} The adsorbed extracellular proteins then interact with the cell membrane and facilitate cellular uptake in an adsorptive endocytosis pathway. Conversely, recent studies by Ochsenkühn *et al* show that nanoshell uptake increases in the absence of extracellular proteins, suggesting the possibility of a passive, nonendocytotic uptake mechanism.²³³ While in our studies nanoshell complex uptake is clearly visualizable in H1299 cells, the precise uptake mechanism is not clearly identifiable, and is likely to depend on a variety of factors including cell type, functionalization of the nanoparticle, and incubation conditions.

7.2.3 Intracellular Light-Induced DAPI Release:

To investigate intracellular light-induced molecular release, the H1299 cells incubated with nanoshell-dsDNA-DAPI complexes were illuminated with a NIR CW laser (1 W/cm², 800 nm) for 5 minutes. This irradiation time and laser power level were determined from previous experiments,²¹⁷ which demonstrated after 5 minutes of laser irradiation no additional dehybridization of the DNA occurred. This laser power and time allow the DAPI to be released

while minimizing laser exposure to the H1299 cells. After laser irradiation, samples were placed in an incubator for one hour to allow time for released DAPI molecules to diffuse to the nucleus. Next, the nuclei of the cells were isolated by lysing the cell membrane (see supplemental information) and the DAPI fluorescence intensity was quantified by flow cytometry. Nuclei isolation is necessary to ensure that flow cytometry only measures fluorescence from DAPI molecules bound to genomic DNA in the nucleus and does not measure fluorescence from DAPI molecules in the cytoplasm.

Evidence of DAPI release is shown by the normalized flow cytometry histograms of DAPI fluorescence intensity versus number of nuclei from H1299 cells incubated with nanoshell-*ds*DNA-DAPI before and after laser treatment (Figure 7.3). After laser treatment, the fluorescence intensity of the nuclei increased, demonstrating that DAPI molecules were released from the nanoshells, diffused through the cytoplasm and into the cell nuclei, binding with the genomic DNA. Prior to laser irradiation, some DAPI fluorescence is observed within the cells (Figure 7.3.c, left) and measured by flow cytometry (Figure 7.3.a-b, before laser). This DAPI fluorescence signal originates from both excess DAPI molecules present in the sample and DAPI molecules which were non-controllably released from the complexes during the incubation and prior to laser irradiation.

The bar graph depicts the mean DAPI fluorescence intensity \pm SEM (standard error of the mean) increase from before laser (59.7 ± 0.21) to after laser (79.8 ± 0.33) (Fig. 3a). A ~33% increase in fluorescence intensity. An unpaired t-test of the two means was performed at a 95% confidence level, which resulted in a two-tailed p value of $p < 0.0001$, which is statistically significant. This observed increase in DAPI fluorescence after laser treatment (~33%) demonstrates that the nanoshell-*ds*DNA complex effectively released its guest molecules from

the dsDNA host carriers inside the cells. Epifluorescence images of H1299 cells incubated with nanoshell-dsDNA-DAPI before (Figure 3c, left) and after (Figure 7.3.c, right) laser treatment visually show the increase in DAPI fluorescence intensity. The cell membrane is marked by the green dye, Alexa-Fluor 488 wheat germ agglutinin.

The plasmon resonant illumination of the nanoshells is crucial for DAPI release into the cells. To test this hypothesis, a control experiment consisting of H1299 cells incubated with DAPI only (no nanoshells) was conducted (Figure 7.3.b). The cells were irradiated with the NIR laser under conditions identical to the previous experiment. The mean DAPI fluorescence intensity \pm SEM did not significantly increase after laser irradiation (237 ± 0.86 to 239 ± 0.95 , $p = 0.1188$), indicating that DAPI release does not occur without the presence of the nanoshell-dsDNA complex. It is important to note that the mean fluorescence intensity is higher for the control (Figure 7.3.b) compared to the nanoshell-dsDNA-DAPI sample (Figure 7.3.a) due to multiple washings of the nanoshell-dsDNA-DAPI sample.

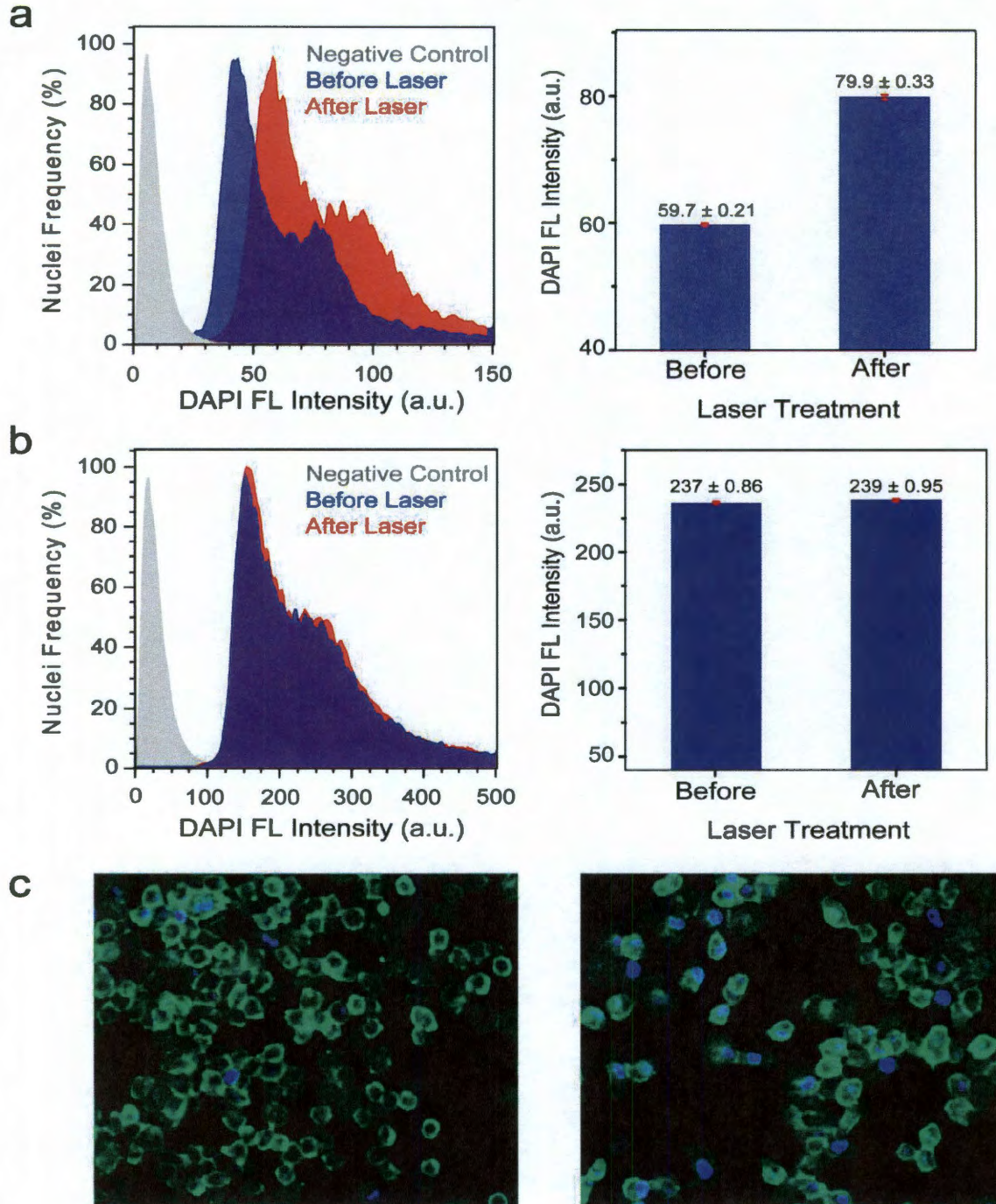


Figure 7.3 Light-induced DAPI release. (a-b) Flow cytometry histograms of DAPI Fluorescence (Ex: 355nm/Em: 460 nm) versus number of isolated nuclei from H1299 cells incubated with a) nanoshell-dsDNA-DAPI and b) DAPI (control). Negative control (gray), treated cells without laser irradiation (blue) and treated cells with laser irradiation (red). Bar graphs display the mean DAPI fluorescence intensity \pm SEM before and after laser irradiation. (c) Epifluorescence images of H1299 cells incubated with nanoshell-dsDNA-DAPI (left) before and (right) after laser treatment. The cell membrane is marked by the green dye, Alexa-Fluor 488.

The shape of the flow cytometry histograms for both before laser and after laser are consistent with nuclei stained with DAPI. DAPI is routinely used to study the cell cycle because it binds to DNA stoichiometrically. Looking at the before laser histogram in Figure 7.3.a as an example, the tallest peak (~40) originates from nuclei with two sets of chromosomes. This peak is the tallest because in a typical cell cycle, a cell spends the longest portion of time with two sets of chromosomes; therefore, the probability of a cell having two sets of chromosomes is the highest. The second, smaller peak (~80), double the fluorescence intensity of the tallest peak, indicates nuclei which have exactly double the amount of DNA, four sets of chromosomes, and are ready to enter mitosis and divide. The nuclei with fluorescence intensities in between these two peaks indicate cells which are currently synthesizing DNA prior to mitosis. The negative control histogram (gray) has a single peak because in the absence of DAPI every nuclei essentially fluoresces identically resulting in a signal which is attributed to autofluorescence (background).

7.2.4 Cytotoxicity Study:

To ensure that this method for light-triggered intracellular molecular release would be useful for biomedical applications, such as drug delivery, a cytotoxicity assay was performed to investigate both the effects of nanoshells and laser irradiation on cell viability. Propidium iodide (PI) was chosen as a marker to distinguish viable from non-viable cells, because it is a membrane-impermeable dye which is excluded from viable healthy cells.²³⁶ When a cell membrane is damaged, PI enters the cell, stains the dsDNA in the nuclei and emits red fluorescence; however, undamaged cells will not fluoresce. Flow cytometry was used to observe changes in PI fluorescence intensity for a large sample size of 30,000 cells. The negative control (Figure 7.4.a) consisted of cells which were not incubated with nanoshell-dsDNA-DAPI and did

not undergo laser treatment. The fluorescence observed in Figure 4a is attributed to autofluorescence and PI staining caused by apoptotic and necrotic cells already present in the experiment, with damaged membranes. The nanoshell-dsDNA-DAPI complexes were then incubated with H1299 cells for 12 hours. Following incubation, the cells were divided into two samples: cells not treated with the laser (Figure 7.4.b) and cells treated with the laser for 10 minutes (Figure 7.4.c). Figure 7.4.b shows no significant increase in PI fluorescence intensity, demonstrating that nanoshell-dsDNA-DAPI complexes are not cytotoxic under the experimental conditions of the study.

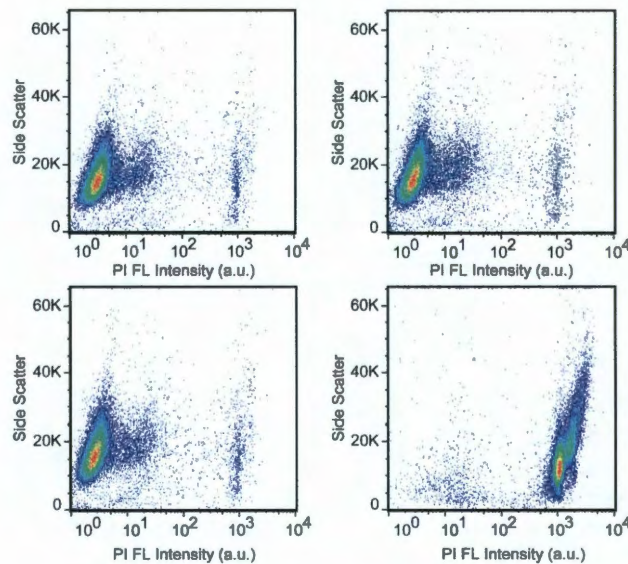


Figure 7.4 Flow cytometry cytotoxicity assay. All plots are side-scattered light (SS) versus Propidium Iodide (PI) intensity. (a) Negative control: H1299 cells not incubated with nanoshell-dsDNA-DAPI and no laser treatment. Cells incubated with nanoshell-dsDNA-DAPI for 12 hours: (b) without laser treatment and (c) with laser treatment. (d) Positive Control: Cells were treated with 0.1% Citrate/0.1% Triton, which permeates the cell membrane, allowing PI to stain the dsDNA in the nucleus.

More interestingly, cells incubated with nanoshell-dsDNA-DAPI complexes and irradiated with the laser for 10 minutes also show no significant increase in PI fluorescence intensity. This demonstrates that the light-triggered release procedure did not adversely affect the cells.

Considering nanoshells are well-known for their use in photothermal therapy, this result may be surprising; however, the illumination conditions for this experiment ($1\text{W}/\text{cm}^2$, 5 minutes) were significantly below those used for photothermal induction of cell death in cell culture ($4\text{W}/\text{cm}^2$, 4-6 minutes).²²¹ Figure 7.4.d represents a positive control sample of cells treated with 0.1% Citrate/0.1% Triton solution, which permeates the cell membrane, allowing PI to enter the cell and stain the nucleus, resulting in a large increase in PI fluorescence intensity.

7.3 Conclusion:

In conclusion, nanoshells functionalized with dsDNA were successfully used to transport DAPI molecules into living cells. Successful uptake of nanoshells into H1299 cells was achieved. DAPI molecules, initially bound to the dsDNA on the NS surface, are released due to the illumination of the nanoshell-dsDNA-DAPI complex with the appropriate NIR light. DAPI molecules initially released in the cell cytoplasm diffuse into the cell nucleus and bind to the genomic DNA of the cell. The staining of the cell nucleus with the released DAPI was quantified using flow cytometry. A cytotoxicity assay demonstrated that nanoshell uptake is nontoxic and that laser irradiation of nanoshell-laden cells under the conditions where DAPI release occurs does not induce cell death.

This nanoshell-dsDNA system could be extended to a multitude of other guest molecules that associate with the host dsDNA carrier including small organic fluorophores,²²⁵ steroid hormones,²³⁷ and therapeutic molecules.^{224, 225, 237} For example, the quest to find dsDNA intercalators that inhibit the uncontrollable replication of tumor cells comprises an entire field of cancer research. Currently, there are more than 130 FDA approved anti-cancer drugs that specifically target DNA.²³⁸ For *in vivo* clinical applications, however, before the DNA intercalator can reach the genomic DNA, it must overcome several hurdles, such as metabolic

pathways and cytoplasmic and nuclear membranes. As a result, the failure of DNA therapies to offer successful clinical treatments is primarily due a lack of viable delivery methods rather than effectiveness of the DNA intercalator to treat cancer.²²⁴ This nanoshell-dsDNA delivery vector preserves the guest molecule by minimizing non-desired interactions with other molecules and it provides light-triggered release with controllable delivery.

Chapter 7: Conclusions and perspectives

In this thesis, Gold nanoshells were used as SERS active substrates to investigate spectral properties of DNA molecules. The SERS spectra obtained from untreated DNA were very non-reproducible and varies based on DNA base composition and state (single or double stranded). After DNA thermal treatment, the SERS DNA spectral quality and reproducibility were greatly enhanced. All DNA spectra acquired were very identical and dominated by the adenine modes regardless of base composition, DNA length or state. After thermal treatment DNA molecules are more rigid and adopt a more linear structure causing a great improvement in surface coverage. As a result, the reproducibility of SERS spectra is tremendously improved.

The high reproducibility of DNA spectra allowed the detection of DNA perturbation caused by the binding of small molecules to DNA. The binding of small molecules to DNA strands initiates kinks and bends in the DNA strands causing a significant decrease in the spectral reproducibility. The detection of the real time binding of cisplatin, commonly used chemotherapy, to DNA was achieved using SERS. The discrimination between cisplatin and transplatin (structurally similar to cisplatin but does not bind to DNA) interactions with DNA was very obvious. The DNA SERS system can be further developed to be used for screening potential new chemotherapeutic molecules and assess their binding to DNA.

A label-free DNA detection system was developed using SERS. The new system is based on the adenine SERS spectral dominance. When the capture strand is adenine-free or adenine substituted, the SERS of the capture strands is missing all adenine features. The target binding event is detected by the appearance of a strong peak from adenine bases on the target sequence.

It turns out that the intensity of the adenine peak is directly related to the DNA target concentration which makes the developed system not only label-free but also self calibrated.

SERS was also used to detect and identify DNA base chemical modifications on DNA strands. DNA base modifications have been proven to be related to certain diseases such as cancer as well as playing main role in epigenetic. Four different base modifications: adenine methylation, cytosine methylation and hydroxymethylation and guanine oxidation were all detected using SERS. Each base modification causes the appearance or disappearance of certain SERS features unique for that modification, which make the system reliable for detecting single or multiple base modifications. The SERS detection is very straightforward and does not require any sample preparation eliminating possible chemical modifications caused by interaction of DNA with various chemicals. SERS detection enabled discrimination between cytosine methylation and hydroxymethylation on the DNA strands investigated. The discriminations between these two bases is considered particularly challenging in the field of epigenetic due to their chemical and structural similarity and complexity of detection using common methods . The described method is the first attempt in using SERS in epigenetic research. The simplicity of the SERS detection may introduce SERS-bases DNA chemical modifications screening as routine in clinical diagnosis.

On the second part of this thesis, Au nanoshells were used as non-viral, controllable drug delivery systems. Au nanoshells can be promising triggered non-viral drug delivery systems owing to their exceptional photothermal property. Upon light illumination, Au annoshells efficiently convert part of that light into heat which is used to dehybridize double stranded DNA attached to the nanoshell surface. Single stranded DNA can then be delivered for antisense gene

therapy or small DNA intercalators for conventional therapy as well as *in vivo* intracellular imaging.

Investigated cells can uptake Au nanoshells at very high efficiency and the DNA can be dehybridized and delivered at temperature lower than 37°C upon light irradiation which makes the system ideal for intracellular drug delivery and controlled release of ssDNA and small molecules. DAPI molecules, typically used to stain cell nuclei, were bound to the dsDNA initially tethered to the Au nanoshells. After incubation with H1299 cancer cells and upon light irradiation, Au nanoshells were able to release their DAPI payloads. DAPI, then, diffused in the cytoplasm, crossed the nuclear membrane and stained the nuclear DNA. Brighter cellular nuclei were seen after Au NS/DNA/DAPI uptake and DAPI release. The Au nanoshell system efficiently holds the DAPI payload, carries it into the cell cytoplasm and releases it upon light illumination. The system can be further developed to span other potential therapeutic agents such as siRNA, dsDNA, etc.

The field of plasmonics has been largely expanding bringing new applications that affected many areas such as medicine, sensing, and energy. The applications of plasmonics in medicine are particularly essential as I believe the fight against diseases is the main goal of science. The plasmonic nanostructures can combine the efficiency of delivery and the control of release to form ideal drug delivery systems. Finally, I hope that this work will be a contribution to reach our global goal to improve human health and life in general.

Appendix: Publications and Patents

PUBLICATIONS

- Yu Zhang, **Aoune Barhoumi**, J. Britt Lassiter, Naomi J. Halas, “Orientation-Preserving Transfer and Directional Light Scattering from Individual Light-Bending Nanoparticles” *Nano Lett.* **ASAP**.
- **Aoune Barhoumi**, Naomi Halas, “Label-Free detection of DNA hybridization Using Surface Enhanced Raman Spectroscopy” *J. Am. Chem. Soc.* **2010**, 132, 12792-12793.
- Ryan Hushka, Oara Newman, **Aoune Barhoumi**, and Naomi Halas “Visualizing Light-Triggered Release of Molecules Inside Living Cells” *Nano Lett.* **2010**, 10, 4117-22.
- **Aoune Barhoumi**, Ryan M. Hushka, Rizia Bardhan, Mark W. Knight, Naomi Halas, “Light-Induced Release of DNA from Plasmon-Resonant Nanoparticles: Towards Light-Controlled Gene Therapy” *Chem. Phys. Lett.* **2009**, 482, 171-179. **COVER ARTICLE**
- Carly S. Levin, Janardan Kundu, **Aoune Barhoumi**, Naomi Halas “Nanoshell-Based Substrates for Biomolecular Spectroscopic detection” *Analyst* **2009**, 134, 1745-1750.
- Janardan Kundu*, Oara Neumann*, Benjamin Janesko, Dongmao Zhang, Surbhi Lal, **Aoune Barhoumi**, Gustavo Scuseria, Naomi J. Halas “Adenine- and Adenosine Monophosphate (AMP)- Gold Binding Interactions Studied by Surface Enhanced Raman and Infrared Spectroscopies” *J. Phys. Chem. C* **2009**, 113, 14390-14397.
- Dongmao Zhang, Hui Wang, Oara Neumann, **Aoune Barhoumi**, Michael Perham, Jeffrey Hartgerink, Pernilla Wittung-Stafshede, Naomi J. Halas “Gold Nanoparticles can Induce the Formation of Protein-Based Aggregates at Physiological pH” *Nano Lett.* **2009**, 9, 666-671.
- **Aoune Barhoumi**, Dongmao Zhang, Felicia Tam, Naomi Halas “Surface-Enhanced Raman Spectroscopy of DNA” *J. Am. Chem. Soc.* **2008**, 130, 5523-5529.
- **Aoune Barhoumi**, Dongmao Zhang, Naomi Halas, “Correlation of Molecular Orientation and Packing Density in a dsDNA Self-Assembled Monolayer Observable with Surface-Enhanced Raman Spectroscopy” *J. Am. Chem. Soc.* **2008**, 130, 14040-14041.

PATENTS

- **Aoune Barhoumi**, Dongmao Zhang and Naomi Halas, “Composition for Targeted Drug Delivery and Controlled Release” United States Patent, 20100040549.
- **Aoune Barhoumi**, Dongmao Zhang and Naomi Halas, “Device and Method for Label-free Detection of DNA Hybridization” Filed on 08/16/2010.
- **Aoune Barhoumi**, Ryan Hushka, Oara Newman, and Naomi Halas “Triggered-release of DNA absorbed and/or intercalated from nanoparticles” Filed on 09/15/2010.

References

1. Painless laser device could spot early signs of disease
BBC news **27 September 2010**.
2. Sands, B. L.; Welsh, M. J.; Kin, S.; Marhatta, R.; Hinkle, J. D.; Bayram, S. B., Raman scattering spectroscopy of liquid nitrogen molecules: An advanced undergraduate physics laboratory experiment. *Am. J. Phys* **2007**, *75*, 488-95.
3. M. Fleischmann, P. J. H. a. A. J. M., Raman Spectra Of Pyridine Adsorbed At A Silver Electrode. *Chem. Phys. Lett.* **1974**, *26*, 163-66.
4. Jeanmaire, D. L.; Duayne, R. P. V., Surface Raman electrochemistry. Part 1. Heterocyclic, aromatic and aliphatic amines adsorbed on the anodised silver electrode
J. Electroanal. Chem. **1977**, *84*, 1-20.
5. King, F. W.; Duayne, R. P. V.; Schatz, G. C., Theory of Raman scattering by molecules adsorbed on electrode surfaces. *J. Chem. Phys.* **1978**, *69*.
6. Albrecht, M. G.; Creighton, J. A., Anomalously intense Raman spectra of pyridine at a silver electrode
J. Am. Chem. Soc. **1977**, *99*, 5215-17.
7. Oldenburg, S. J.; Averitt, R. D.; Westcott, S. L.; Halas, N. J., Nanoengineering of optical resonances. *Chem. Phys. Lett.* **1998**, *288* 243-247.
8. Gobin, A. M.; Lee, M. H.; Halas, N. J.; James, W. D.; Drezek, R. A.; West, J. L., Near-Infrared Resonant Nanoshells for Combined Optical Imaging and Photothermal Cancer Therapy. *Nano Lett.* **2007**, *7*, 1929-34.
9. Loo, C.; Lowery, A.; Halas, N.; West, J.; Drezek, R., Immunotargeted Nanoshells for Integrated Cancer Imaging and Therapy. *Nano Lett.* **2005**, *5*, 709-11.
10. Choi, M.-R.; Stanton-Maxey, K. J.; Stanley, J. K.; Levin, C. S.; Bardhan, R.; Akin, D.; Badve, S.; Sturgis, J.; Robinson, J. P.; Bashir, R.; Halas, N. J.; Clare, S. E., A Cellular Trojan Horse for Delivery of Therapeutic Nanoparticles into Tumors. *Nano Lett.* **2007**, *7*, 3759-65.
11. Gobin, A. M.; Moon, J. J.; West, J. L., EphrinA1-targeted nanoshells for photothermal ablation of prostate cancer cells. *Int. J. Nanomed.* **2008**, *3*, 351-8.
12. Hirsch, L. R.; Stafford, R. J.; Bankson, J. A.; Sershen, S. R.; Rivera, B.; Price, R. E.; Hazle, J. D.; Halas, N. J.; West, J. L., Nanoshell-mediated near-infrared thermal therapy of tumors under magnetic resonance guidance. *PNAS* **2003**, *100*, 13549-54.
13. Oldenburg, S. J.; Averitt, R. D.; Westcott, S. L.; Halas, N. J., Nanoengineering of optical resonances. *Chem. Phys. Lett.* **1998**, *288*, 243-247.
14. Oldenburg, S. J.; Westcott, S. L.; Averitt, R. D.; Halas, N. J., Surface enhanced Raman scattering in the near infrared using metal nanoshell substrates. *J. Chem. Phys.* **1999**, *111*, 4729-4735.
15. Edwards, P. P., A New Hydrosol of Gold Clusters. 1. Formation and Particle Size Variation. *Langmuir* **1993**, *9*, 2301-9.
16. Brinson, B. E.; Lassiter, J. B.; Levin, C. S.; Bardhan, R.; Mirin, N.; Halas, N. J., Nanoshells Made Easy: Improving Au Layer Growth on Nanoparticle Surfaces. *Langmuir* **2008**, *24*, 14166-71.

17. Erickson, T. A.; Tunnell, J. W., Gold Nanoshells in Biomedical Applications. **2009**.
18. Averitt, R. D.; Westcott, S. L.; Halas, N. J., Linear optical properties of gold nanoshells. *J. Opt. Soc. Am. B* **1999**, *16*, 1824-32.
19. Lal, S.; Grady, N. K.; Goodrich, G. P.; Halas, N. J., Profiling the Near Field of a Plasmonic Nanoparticle with Raman-Based Molecular Rulers. *Nano Lett.* **2006**, 2338-2343.
20. Jain, P. K.; El-Sayed, M. A., Universal Scaling of Plasmon Coupling in Metal Nanostructures: Extension from Particle Pairs to Nanoshells. *Nano Lett.* **2007**, *7*, 2854-8.
21. Lal, S.; Grady, N. K.; Kundu, J.; Levin, C. S.; Lassiter, J. B.; Halas, N. J., Tailoring plasmonic substrates for surface enhanced spectroscopies. *Chem. Soc. Rev.* **2008**, *37*, 898-911.
22. Talley, C. E.; Jackson, J. B.; Oubre, C.; Grady, N. K.; Hollars, C. W.; Lane, S. M.; Huser, T. R.; Nordlander, P.; Halas, N. J., Surface-Enhanced Raman Scattering from Individual Au Nanoparticles and Nanoparticle Dimer Substrates. *Nano Lett.* **2005**, *5*, 1569-1574.
23. Hu, M.; Chen, J.; Li, Z.-Y.; Au, L.; Hartland, G. V.; Li, X.; Marquez, M.; Xia, Y., Gold nanostructures: engineering their plasmonic properties for biomedical applications. *Chem. Soc. Rev.* **2006**, *35*, 1084-1094.
24. Link, S.; El-Sayed, M. A., Optical Properties and Ultrafast Dynamics of Metallic Nanocrystals. *Annu. Rev. Phys. Chem.* **2003**, *54*, 331-336.
25. Govorov, A. O.; Zhang, W.; Skeini, T.; Richardson, H.; Lee, J.; Kotov, N. A., Gold nanoparticle ensembles as heaters and actuators: melting and collective plasmon resonances. *Nanoscale Res Lett.* **2006**, *1*, 84-90.
26. Richardson, H. H.; Carlson, M. T.; Tandler, P. J.; Hernandez, P.; Govorov, A. O., Experimental and Theoretical Studies of Light-to-Heat Conversion and Collective Heating Effects in Metal Nanoparticle Solutions. *Nano Letters* **2009**, *9*, 1139-1146.
27. Govorov, A. O.; Richardson, H. H., Generating heat with metal nanoparticles. *Nano Today* **2007**, *2* (1), 30-38.
28. Hu, M.; Hartland, G. V., Heat Dissipation for Au Particles in Aqueous Solution: Relaxation Time versus Size. *J. Phys. Chem. B* **2002**, *106*, 7029-7033.
29. Fu, A.; Micheel, C. M.; Cha, J.; Chang, H.; Yang, H.; Alivisatos, A. P., Discrete Nanostructures of Quantum Dots/Au with DNA. *J. Am. Chem. Soc.* **2004**, *126*, 10832-10833.
30. Yavas, O.; Leiderer, P.; Park, H. K.; Grigoropoulos, C. P.; Poon, C. C.; Leung, W. P.; Do, N.; Tam, A. C., Optical Reflectance and Scattering Studies of Nucleation and Growth of Bubbles at a Liquid-Solid Interface Induced by Pulsed Laser Heating. *Physical Review Letters* **1993**, *70*, 1830-1833.
31. Link, S.; Burda, C.; Nikoobakht, B.; El-Sayed, M. A., How long does it take to melt a gold nanorod? A femtosecond pump-probe absorption spectroscopic study. *Chem. Phys. Lett.* **1999**, *315*, 12-18.
32. Aguirre, C. M.; Moran, C. E.; Young, J. F.; Halas, N. J., Laser-induced reshaping of metallodielectric nanoshells under femtosecond and nanosecond plasmon resonant illumination. *Journal of Physical Chemistry B* **2004**, *108*, 7040-7045.
33. Huttman, G.; Birngruber, R., On the possibility of High-Precision Photothermal Microeffects and the Measurement of Fast Thermal Denaturation of Proteins. *IEEE Journal of Selected Topics in Quantum Electronics* **1999**, *5*, 954-962.
34. Hirsch, L. R.; Stafford, R. J.; Bankson, J. A.; Sershen, S. R.; Rivera, B.; Price, R. E.; Hazle, J. D.; Halas, N. J.; West, J. L., Nanoshell-mediated near-infrared thermal therapy of tumors under magnetic resonance guidance. *Proc. Natl. Acad. Sci.* **2003**, *100*, 13549-13554.

35. Jain, P. K.; Huang, X.; El-Sayed, I. H.; El-Sayed, M. A., Review of Some Interesting Surface Plasmon Resonance-enhanced Properties of Noble Metal Nanoparticles and Their Applications to Biosystems. *Plasmonics* **2007**, *2*, 107-118.
36. Gobin, A. M.; Lee, M. H.; Halas, N. J.; James, W. D.; Drezek, R. A.; West, J. L., Near-Infrared Resonant Nanoshells for Combined Optical Imaging and Photothermal Cancer Therapy. *Nano Lett.* **2007**, *7*, 1929-1934.
37. Pissuwan, D.; Valenzuela, S. M.; Cortie, M. B., Therapeutic possibilities of plasmonically heated gold nanoparticles *Trends in Biotech.* **2006**, *24*, 62-67.
38. Prodan, E.; Radloff, C.; Halas, N. J.; Nordlander, P., A hybridization model for the plasmon response of complex nanostructures. *Science* **2003**, *302*, 419-422.
39. Wang, H.; Brandl, D. W.; Nordlander, P.; Halas, N. J., Plasmonic Nanostructures: Artificial Molecules. *Acc. Chem. Res.* **2007**, *40*, 53-62.
40. Oldenburg, S. J.; Averitt, R. D.; Westcott, S. L.; Halas, N. J., Nanoengineering of optical resonances *Chem. Phys. Lett.* **1998**, *288*, 243-247.
41. Nikoobakht, B.; El-Sayed, M. A., Preparation and Growth Mechanism of Gold Nanorods (NRs) Using Seed-Mediated Growth Method. *Chem. Mater.* **2003**, *15*, 1957-1962.
42. Schwartzberg, A. M.; Olson, T. Y.; Talley, C. E.; Zhang, J. Z., Synthesis, Characterization, and Tunable Optical Properties of Hollow Gold Nanospheres. *J. Phys. Chem. B* **2006**, *110*, 19935-19944.
43. Weissleder, R., A clearer vision for in vivo imaging. *Nature Biotech.* **2001**, *19*, 316-317.
44. Patil, S. D.; Rhodes, D. G.; Burgess, D. J., DNA-based Therapeutics and DNA Delivery Systems: A Comprehensive Review. *AAPS J.* **2005**, *7*, 61-77.
45. Uherek, C.; Wels, W., DNA-carrier proteins for targeted gene delivery. *Adv. Drug Delivery Rev.* **2000**, *44*, 153-166.
46. Crooke, S. T., Molecular mechanisms of action of antisense drugs. *Biochim. Biophys. Acta* **1999**, *1489* 31-44.
47. Whitehead, K. A.; Langer, R.; Anderson, D. G., Knocking down barriers: advances in siRNA delivery. *Nature Reviews* **2009**, *8*, 129-139.
48. Stull, R. A.; Francis C. Szoka, J., Antigene, Ribozyme and Aptamer Nucleic Acid Drugs: Progress and Prospects *Pharm. Res.* **1995**, *12*, 465-483.
49. Stephenson, M.; Zamecnik, P. C., Inhibition of Rous sarcoma viral RNA translation by a specific oligodeoxyribonucleotide. *Proc. Natl. Acad. Sci.* **1978**, *75*, 285-288.
50. Stephens, A. C.; Rivers, R. P., Antisense oligonucleotide therapy in cancer. *Curr. Opin. Mol. Ther.* **2003**, *5*, 118-122.
51. Gewirtz, A. M., Oligonucleotide Therapeutics: A Step Forward. *J. Clin. Oncology* **2000**, *18*, 1809-1811.
52. Israel, Z. H.; Domb, A. J., Polymers in Gene Therapy: Antisense Delivery Systems. *Polym. Adv. Technol.* **1998**, *9*, 799-805.
53. Langer, R.; Tirrell, D. A., Designing materials for biology and medicine *Nature* **2004**, *428*, 487-492
54. Ghosh, P.; Han, G.; De, M.; Kim, C. K.; Rotello, V. M., Gold nanoparticles in delivey applications. *Adv. Drug Deliver. Rev.* **2008**, *60*, 1307-1315.
55. Carter, P. J.; Samulski, R. J., Adeno-associated viral vectors as gene delivery vehicles. *Int. J. Mol. Med.* **2000**, *6*, 17-27.

56. Pouton, C. W.; Seymour, L. W., Key issues in non-viral gene delivery. *Adv. Drug Deliver. Rev.* **2001**, *46*, 187-203.
57. Check, E., Gene therapy: A tragic setback *Nature* **2002**, *420*, 116-118.
58. Rosi, N. L.; Giljohann, D. A.; Thaxton, C. S.; Lytton-Jean, A. K. R.; Han, M. S.; Mirkin, C. A., Oligonucleotide-Modified Gold Nanoparticles for Intracellular Gene Regulation *Science* **2006**, *312*, 1027-1030.
59. Han, G.; Martin, C. T.; Rotello, V. M., Stability of Gold Nanoparticle-Bound DNA toward Biological, Physical, and Chemical Agents. *Chem. Biol. Drug Des.* **2006**, *67*, 78-82.
60. Salem, A. K.; Searson, P. C.; Leong, K. W., Multifunctional nanorods for gene delivery. *Nature Materials* **2003**, *2*, 668-671.
61. Hong, R.; Han, G.; Fernández, J. M.; Kim, B.-j.; Forbes, N. S.; Rotello, V. M., Glutathione-Mediated Delivery and Release Using Monolayer Protected Nanoparticle Carriers. *J. Am. Chem. Soc* **2006**, *128*, 1078-1079.
62. Polizzi, M. A.; Stasko, N. A.; Schoenfish, M. H., Water-Soluble Nitric Oxide-Releasing Gold Nanoparticles. *Langmuir* **2007**, *23*, 4938-4943.
63. Han, G.; You, C.-C.; Kim, B.-j.; Turingan, R. S.; Forbes, N. S.; Martin, C. T.; Rotello, V. M., Light-Regulated Release of DNA and Its Delivery to Nuclei by Means of Photolabile Gold Nanoparticles. *Angew. Chem.* **2006**, *118*, 3237-3241.
64. Lee, S. E.; Liu, G. L.; Kim, F.; Lee, L. P., Remote Optical Switch for Localized and Selective Control of Gene Interference. *Nano Lett.* **2009**, *9*, 562-570.
65. Seferos, D. S.; Prigodich, A. E.; Giljohann, D. A.; Patel, P. C.; Mirkin, C. A., Polyvalent DNA Nanoparticle Conjugates Stabilize Nucleic Acids. *Nano Lett.* **2009**, *9*, 308-311.
66. Wu, G.; Mikhailovsky, A.; Khant, H. A.; Fu, C.; Chiu, W.; Zasadzinski, J. A., Remotely Triggered Liposome Release by Near-Infrared Light Absorption via Hollow Gold Nanoshells. *J. Am. Chem. Soc* **2008**, *130*, 8175-8177.
67. Giljohann, D. A.; Seferos, D. S.; Prigodich, A. E.; Patel, P. C.; Mirkin, C. A., Gene Regulation with Polyvalent siRNA-Nanoparticle Conjugates. *J. Am. Chem. Soc* **2009**, *131*, 2072-2073.
68. Ghosh, P. S.; Kim, C.-K.; Han, G.; Forbes, N. S.; Rotello, V. M., Efficient Gene Delivery Vectors by Tuning the Surface Charge Density of Amino Acid-Functionalized Gold Nanoparticles. *ACS Nano* **2008**, *2*, 2213-2218.
69. Takahashi, H.; Niidome, Y.; Yamada, u., Controlled release of plasmid DNA from gold nanorods induced by pulsed near-infrared light. *Chem. Commun.* **2005**, 2247-2249.
70. Chen, C.-C.; Lin, Y.-P.; Wang, C.-W.; Tzeng, H.-C.; Wu, C.-H.; Chen, Y.-C.; Chen, C.-P.; Chen, L.-C.; Wu, Y.-C., DNA-Gold Nanorod Conjugates for Remote Control of Localized Gene Expression by near Infrared Irradiation. *J. Am. Chem. Soc* **2006**, *128*, 3709-3715.
71. Wijaya, A.; Schaffer, S. B.; Pallares, I. G.; Hamad-Schifferli, K., Selective Release of Multiple DNA Oligonucleotides from Gold Nanorods. *ACS Nano* **2009**, *3*, 80-86.
72. Braun, G. B.; Pallaoro, A.; Wu, G.; Missirlis, D.; Zasadzinski, J. A.; Tirrell, M.; Reich, a. N. O., Laser-Activated Gene Silencing via Gold Nanoshell-siRNA Conjugates. *ACS Nano* **2009**, *ASAP 10.1021/nn900469q*.
73. Rhim, W.-K.; Kim, J.-S.; Nam, J.-M., Lipid-Gold-Nanoparticle Hybrid-Based Gene Delivery *Small* **2008**, *4*, 1651-1655.

74. Noh, S. M.; Kim, W.-K.; Kim, S. J.; Kim, J. M.; Baek, K.-H.; Oh, Y.-K., Enhanced cellular delivery and transfection efficiency of plasmid DNA using positively charged biocompatible colloidal gold nanoparticles. *Biochim. Biophys. Acta* **2007**, *1770*, 747-752.
75. Huang, X.; Qian, W.; El-Sayed, I. H.; El-Sayed, M. A., The Potential Use of the Enhanced Nonlinear Properties of Gold Nanospheres in Photothermal Cancer Therapy. *Lasers in Surgery and Medicine* **2007**, *39*, 747-753.
76. Rhodes, D. R.; Chinnaiyan, A. M., DNA Microarrays: Implications for Clinical Medicine *Journal of Investigative Surgery* **2002**, *15*, 275-279.
77. Divne, A.-M.; Allen, M., A DNA microarray system for forensic SNP analysis. *Forensic Science International* **2005**, *154*, 111-121.
78. Niemeyer, C. M.; Blohm, D., DNA Microarrays. *Angew. Chem. Int. Ed.* **1999**, *38*, 2865-2870.
79. Li, H.; Sun, J.; Cullum, B. M., Label-free detection of proteins using SERS-based immuno-nanosensors *Nanobiotechnology* **2006**, *2*, 17-28.
80. Bell, S. E. J.; Sirimuthu, N. M. S., Surface-Enhanced Raman Spectroscopy (SERS) for Sub-Micromolar Detection of DNA/RNA Mononucleotides. *J. Am. Chem. Soc.* **2006**, *128*, 15580-15581.
81. Gearheart, L. A.; Ploehn, H. J.; Murphy, C. J., Oligonucleotide Adsorption to Gold Nanoparticles: A Surface-Enhanced Raman Spectroscopy Study of Intrinsically Bent DNA *J. Phys. Chem. B* **2001**, *105*, 12609-12615.
82. Brabec, V.; Niki, K., Raman-Scattering from Nucleic-Acids Adsorbed at a Silver Electrode. *Biophys. Chem.* **1985**, *23*, 63-70.
83. Green, M.; Liu, F.-M.; Cohen, L.; Köllensperger, P.; Cass, T., SERS platforms for high density DNA arrays. *Faraday Discussions* **2006**, *132*, 269-280.
84. Jackson, J. B.; Halas, N. J., Surface-enhanced Raman scattering on tunable plasmonic nanoparticle substrates. *PNAS* **2004**, *101*, 17930-17935.
85. Levin, C. S.; Bishnoi, S. W.; Grady, N. K.; Halas, N. J., Determining the Conformation of Thiolated Poly(ethylene glycol) on Au Nanoshells by Surface-Enhanced Raman Scattering Spectroscopic Assay. *Nano Lett.* **2006**, *7*, 3277-3281.
86. Wang, H.; Levin, C. S.; Halas, N. J., Nanosphere Arrays with Controlled Sub-10-nm Gaps as Surface-Enhanced Raman Spectroscopy Substrates. *J. Am. Chem. Soc.* **2005**, *127*, 14992-14993.
87. Lee, S. J.; Morrill, A. R.; Moskovits, M., Hot Spots in Silver Nanowire Bundles for Surface-Enhanced Raman Spectroscopy *J. Am. Chem. Soc.* **2006**, *128*, 2200-2202.
88. Levin, C. S.; Janesko, B. G.; Bardhan, R.; Scuseria, G. E.; Hartgerink, J. D.; Halas, N. J., Chain-Length-Dependent Vibrational Resonances in Alkanethiol Self-Assembled Monolayers Observed on Plasmonic Nanoparticle Substrates. *Nano Lett.* **2006**, *11*, 2617-2621.
89. Jain, P. K.; El-Sayed, M. A., Universal Scaling of Plasmon Coupling in Metal Nanostructures: Extension from Particle Pairs to Nanoshells. *Nano Lett.* **2007**, *7*, 2854-2858.
90. Oubre, C.; Nordlander, P., Optical Properties of Metallodielectric Nanostructures Calculated Using the Finite Difference Time Domain Method. *J. Phys. Chem. B* **2004**, *108*, 17740-17747.
91. Malynych, S.; Luzinov, I.; Chumanov, G., Poly(vinyl pyridine) as a universal surface modifier for immobilization of nanoparticles. *J. Phys. Chem. B* **2002**, *106*, 1280-1285.

92. Tam, F.; Moran, C.; Halas, N., Geometrical Parameters Controlling Sensitivity of Nanoshell Plasmon Resonances to Changes in Dielectric Environment. *J. Phys. Chem. B* **2004**, *108*, 17290-17294.
93. Zhang, D.; Xie, Y.; Mrozek, M. F.; Ortiz, C.; Davisson, V. J.; Ben-Amotz, D., Raman Detection of Proteomic Analytes. *Anal. Chem.* **2003**, *75*, 5703-5709.
94. Zhang, D.; Ben-Amotz, D., Enhanced Chemical Classification of Raman Images in the Presence of Strong Fluorescence Interference. *Applied Spectroscopy* **2000**, *54*, 1379-1383.
95. Seeman, N., DNA in a Material World. *Nature* **2003**, *421*, 427-432.
96. Demers, L. M.; Mirkin, C. A.; Mucic, R. C.; Reynolds, R. A.; Letsinger, R. L.; Elghanian, R.; Viswanadham, G., A Fluorescence-Based Method for Determining the Surface Coverage and Hybridization Efficiency of Thiol-Capped Oligonucleotides Bound to Gold Thin Films and Nanoparticles. *Anal. Chem.* **2000**, *72*, 5535-5541.
97. Hurst, S. J.; Lytton-Jean, A. K. R.; Mirkin, C. A., Maximizing DNA Loading on a Range of Gold Nanoparticle Sizes. *Anal. Chem.* **2006**, *78*, 8313-8318.
98. Otto, C.; Tweel, T. J. J. v. d.; Mul, F. F. M. d.; Greve, J., Surface-Enhanced Raman-Spectroscopy of DNA Bases. *Journal of Raman Spectroscopy* **1986**, *17*, 289-298.
99. Ni, F.; Sheng, R.; Cotton, T. M., Flow injection analysis and real-time detection of RNA bases by surface-enhanced Raman spectroscopy. *Anal. Chem.* **1990**, *62*, 1958-1963.
100. Petrovykh, D. Y.; Pérez-Dieste, V.; Opdahl, A.; Kimura-Suda, H.; Sullivan, J. M.; Tarlov, M. J.; Himpel, F. J.; Whitman, L. J., Nucleobase Orientation and Ordering in Films of Single-Stranded DNA on Gold. *J. Am. Chem. Soc.* **2006**, *128*, 1-2.
101. Yao, L.; Sullivan, J.; Hower, J.; He, Y.; Jiang, S., Packing structure of single-stranded DNA and double-stranded DNA thiolates on Au(111) A molecular simulation study. *J. Chem. Phys.* **2007**, *127*, 195101-195106.
102. Boozer, C.; Ladd, J.; Chen, S.; Yu, Q.; Homola, J.; Jiang, S., DNA Directed Protein Immobilization on Mixed ssDNA/Oligo(ethylene glycol) Self-Assembled Monolayers for Sensitive Biosensors. *Anal. Chem.* **2004**, *76*, 6967-6973.
103. Domke, K. F.; Zhang, D.; Pettinger, B., Tip-Enhanced Raman Spectra of Picomole Quantities of DNA Nucleobases at Au(111). *J. Am. Chem. Soc.* **2007**, *129*, 6708-6710.
104. Feig, M.; Pettitt, B. M., Sodium and Chlorine Ions as Part of the DNA Solvation Shell. *Biophys. J.* **1999**, *77*, 1769-1782.
105. Wong, E. L. S.; Gooding, J. J., The Electrochemical Monitoring of the Perturbation of Charge transfer through DNA by Cisplatin. *J. Am. Chem. Soc.* **2007**, *129*, 8950-8952.
106. Giese, B.; Mcnaughton, D., Interaction of Anticancer Drug Cisplatin with Guanine: Density Functional Theory and Surface-Enhanced Raman Spectroscopy Study. *Biopolymers* **2003**, *72*, 472-490.
107. Liedert, B.; Pluim, D.; Schellens, J.; Thomale, J., Adduct-specific monoclonal antibodies for the measurement of cisplatin-induced DNA lesions in individual cell nuclei. *Nucleic Acids Res.* **2006**, *34*, e47.
108. Kasparova, J.; pospsilova, S.; Brabec, V., Different Recognition of DNA Modified by Antitumor Cisplatin and its Clinically ineffective trans Isomer by tumor Suuppressor Protein p53. *J. Biol. Chem.* **2001**, *276*, 16064-16070.
109. Benedetti, M.; Malina, J.; Kasparkova, J.; Brabec, V.; Natile, G., Chiral Discrimination in Platinum Anticancer Drugs. *Enviornmental Health Perspectives* **2002**, *110*, 779-783.
110. Keren, K.; Krueger, M.; Gilad, R.; Ben-Yoseph, G.; Sivan, U.; Braun, E., Sequence-Specific Molecular Lithography on Single DNA Molecules. *Science* **2002**, *297*, 72-75.

111. Drummond, T. G.; Hill, M. G.; Barton, J. K., Electrochemical DNA sensors. *Nature Biotechnology* **2003**, *21*, 1192-1199.
112. Staii, C.; Alan T. Johnson, J.; Chen, M.; Gelperin, A., DNA-Decorated Carbon Nanotubes for Chemical Sensing. *Nano Lett.* **2005**, *5* (9), 1774-1778.
113. Petrovykh, D. Y.; Rez-Dieste, V. P.; Opdahl, A.; Kimura-Suda, H.; Sullivan, J. M.; Tarlov, M. J.; Himpel, F. J.; Whitman, L. J., Nucleobase Orientation and Ordering in Films of Single-Stranded DNA on Gold. *J. Am. Chem. Soc.* **2006**, *128*, 2-3.
114. Yao, L.; Sullivan, J.; Hower, J.; He, Y.; Jianga, S., Packing structures of single-stranded DNA and double-stranded DNA thiolates on Au(111): A molecular simulation study. *J. Chem. Phys.* **2007**, *127*, 195101-6.
115. Boozer, C.; Ladd, J.; Chen, S.; Yu, Q.; Homola, J.; Jiang, S., DNA Directed Protein Immobilization on Mixed ssDNA/oligo(ethylene glycol) Self-Assembled monolayers for Sensitive Biosensors. *Anal. Chem.* **2004**, *76*, 6967-6972.
116. Barhoumi, A.; Zhang, D.; Tam, F.; Halas, N. J., Surface-Enhanced Raman Spectroscopy of DNA. *J. Am. Chem. Soc.* **2008**, *130*, 5523-5529.
117. Dong, L. Q.; Zhou, J. Z.; Wu, L. L.; Dong, P.; Lin, Z. H., SERS studies of self-assembled DNA monolayer – characterization of adsorption orientation of oligonucleotide probes and their hybridized helices on gold substrate. *Chem. Phys. Lett.* **2002**, *354*, 458-465.
118. Otto, C.; Tweel, T. J. J. v. d.; Mul, F. F. M. d.; Greve, J., Surface-Enhanced Raman Spectroscopy of DNA Bases. *J. Raman Spec.* **1986**, *17*, 289-298.
119. Lal, S.; Grady, N. K.; Goodrich, G. P.; Halas, N. J., Profiling the Near Field of a Plasmonic Nanoparticle with Raman-Based Molecular Rulers. *Nano Lett.* **2006**, *6*, 2338-2343.
120. Demers, L. M.; Mirkin, C. A.; Mucic, R. C.; Reynolds, R. A.; Letsinger, R. L.; Elghanian, R.; Viswanadham, G., A Fluorescence-Based Method for Determining the Surface Coverage and Hybridization Efficiency of Thiol-Capped Oligonucleotides Bound to Gold Thin Films and Nanoparticles *Anal. Chem* **2000**, *72*, 5535-5541.
121. Seeman, N. C., DNA in a material world. *Nature* **2003**, *421*, 427-431.
122. Wang, J., Survey and Summary From DNA biosensors to gene chips *Nucleic Acids Res.* **2000**, *28*, 3011-16.
123. Niemeyer, C. M.; Blohm, D., DNA-Mikroarrays. *Angew. Chem. Int. Ed.* **1999**, *38*, 2865-69.
124. Brown, P. O.; Botstein, D., Exploring the new world of the genome with DNA microarrays. *Nat. Genet.* **1999**, *21*, 33-37.
125. Pease, A. C.; Solas, D.; Sullivan, E. J.; Cronn, M.; Holmes, C. P.; Fodor, S. P. A., Light-generated oligonucleotide arrays for rapid DNA sequence analysis. *Proc. Natl. Acad. Sci.* **1994**, *91*, 5022-26.
126. Ramsay, G., DNA chips: State-of-the art *Nat. Biotechnol.* **1998**, *16*, 40-44.
127. Taton, T. A.; Mirkin, C. A.; Letsinger, R. L., Scanometric DNA Array Detection with Nanoparticle Probes. *Science* **2000**, *289*, 1757-60.
128. Storhoff, J. J.; Elghanian, R.; Mucic, R. C.; Mirkin, C. A.; Letsinger, R. L., One-Pot Colorimetric Differentiation of Polynucleotides with Single Base Imperfections Using Gold Nanoparticle Probes. *J. Am. Chem. Soc.* **1998**, *120*, 1959-64.
129. Zhao, X.; Tapeç-Dytioco, R.; Tan, W., Ultrasensitive DNA Detection Using Highly Fluorescent Bioconjugated Nanoparticles. *J. Am. Chem. Soc.* **2003**, *125*, 11474-75.

130. Gerion, D.; Chen, F.; Kannan, B.; Fu, A.; Parak, W. J.; Chen, D. J.; Majumdar, A.; Alivisatos, P., Room-Temperature Single-Nucleotide Polymorphism and Multiallele DNA Detection Using Fluorescent Nanocrystals and Microarrays. *Anal. Chem.* **2003**, *75*, 4766-4772.
131. Chung-ShiehWu, J. M. C. a. X. F., Compact quantum dot probes for rapid and sensitive DNA detection using highly efficient fluorescence resonant energy transfer. *Nanotechnology* **2009**, *20*, 1-7.
132. Star, A.; Tu, E.; Niemann, J.; Gabriel, J.-C. P.; Joiner, C. S.; Valcke, C., Label-free detection of DNA hybridization using carbon nanotube network field-effect transistors. *Proc. Natl. Acad. Sci.* **2006**, *103*, 921-926.
133. Wirtz, R.; Walti, C.; AGermishuizen, W.; Pepper, M.; Middelberg, A. P. J.; Davies, A. G., High-sensitivity colorimetric detection of DNA hybridization on a gold surface with high spatial resolution. *Nanotechnology* **2003**, *14*, 7-10.
134. Li, H.; Rothberg, L. J., Label-Free Colorimetric Detection of Specific Sequences in Genomic DNA Amplified by the Polymerase Chain Reaction. *J. Am. Chem. Soc.* **2004**, *126*, 10958-10961.
135. Drummond, T. G.; Hill, M. G.; Barton, J. K., Electrochemical DNA Sensors. *Nat. Biotechnol.* **2003**, *21*, 1192 - 1199
136. Kneipp, K.; Kneipp, H.; Kartha, V. B.; Manoharan, R.; Deinum, G.; Itzkan, I.; Dasari, R. R.; Feld, M. S., Detection and identification of a single DNA base molecule using surface-enhanced Raman scattering (SERS). *Phys. Rev. E* **1998**, *57*.
137. Braun, G.; Lee, S. J.; Dante, M.; Nguyen, T.-Q.; Moskovits, M.; Reich, N., Surface-Enhanced Raman Spectroscopy for DNA Detection by Nanoparticle Assembly onto Smooth Metal Films. *J. Am. Chem. Soc.* **2007**, *129*, 6378-6379.
138. Fanga, C.; Agarwal, A.; Buddharajua, K. D.; Khalidb, N. M.; Salimb, S. M.; Widjaja, E.; Marc V. Garlandb; Balasubramaniana, N.; Kwonga, D.-L., DNA detection using nanostructured SERS substrates with Rhodamine B as Raman label. *Biosens. Bioelectron.* **2008**, *24*, 216–221.
139. Laura Fabris, M. D.; Braun, G.; Lee, S. J.; Reich, N. O.; Moskovits, M.; Nguyen, T.-Q.; Bazan, G. C., A Heterogeneous PNA-Based SERS Method for DNA Detection. *J. Am. Chem. Soc.* **2007**, *129* 6086-6087.
140. Barhoumi, A.; Zhang, D.; Tam, F.; Halas, N. J., Surface-Enhanced Raman Spectroscopy of DNA. *J. Am. Chem. Soc.* **2008**, *130*, 5523-5529.
141. Talley, C. E.; Jackson, J. B.; Oubre, C.; Grady, N. K.; Hollars, C. W.; Lane, S. M.; Huser, T. R.; Nordlander, P.; Halas, N. J., Surface-Enhanced Raman Scattering from Individual Au Nanoparticles and Nanoparticle Dimer Substrates. *Nano Lett.* **2005**, *5*, 1569-74.
142. Jackson, J. B.; Halas, N. J., Surface-enhanced Raman scattering on tunable plasmonic nanoparticle substrates. *Proc. Natl. Acad. Sci.* **2004**, *101*, 17930–17935.
143. Levin, C. S.; Janesko, B. G.; Bardhan, R.; Scuseria, G. E.; Hartgerink, J. D.; Halas, N. J., Chain-Length-Dependent Vibrational Resonances in Alkanethiol Self-Assembled Monolayers Observed on Plasmonic Nanoparticle Substrates. *Nano Lett.* **2006**, *6*, 2617-2621
144. Barhoumi, A.; Zhang, D.; Halas, N. J., Correlation of Molecular Orientation and Packing Density in a dsDNA Self-Assembled Monolayer Observable with Surface-Enhanced Raman Spectroscopy. *J. Am. Chem. Soc.* **2008**, *130*, 14040–41.
145. Lal, S.; Westcott, S. L.; Taylor, R. N.; Jackson, J. B.; Nordlander, P.; Halas, N. J., Light Interaction between Gold Nanoshells Plasmon Resonance and Planar Optical Waveguides. *J. Phys. Chem. B* **2002**, *106*, 5609-5612.

146. Tam, F.; Moran, C.; Halas, N., Geometrical Parameters Controlling Sensitivity of Nanoshell Plasmon Resonances to Changes in Dielectric Environment. *J. Phys. Chem. B* **2004**, *108*, 17290-17294.
147. Jean, J. M.; Hall, K. B., 2-Aminopurine fluorescence quenching and lifetimes: Role of base stacking. *Proc. Natl. Acad. Sci.* **2001** *98*, 37-41.
148. Watanabe, S. M.; Goodman, M. F., On the molecular basis of transition mutations: Frequencies of forming 2-aminopurine cytosine and adeninecytosine base mispairs in vitro. *Proc. Natl. Acad. Sci.* **1981**, *78*, 2864-68.
149. Law, S. M.; Eritja, R.; Goodman, M. F.; Breslauer, K. J., Spectroscopic and Calorimetric Characterizations of DNA Duplexes Containing 2-Aminopurine. *Biochem.* **1996**, *35*, 12329-12337.
150. Manoj, P.; Min, C.-K.; Aravindakumar, C. T.; Joo, T., Ultrafast charge transfer dynamics in 2-aminopurine modified double helical DNA. *Chem. Phys.* **2008**, *352*, 333-338.
151. Barhoumi, A.; Huschka, R.; Bardhan, R.; Knight, M. W.; Halas, N. J., Light-induced release of DNA from plasmon-resonant nanoparticles: Towards light-controlled gene therapy. *Chem. Phys. Lett.* **2009**, *482*, 171-179.
152. Holliday, R., The inheritance of epigenetic defects. *Science* **1987**, *238*, 163-70.
153. Esteller, M., Epigenetics in Cancer. *New Engl. J. Med.* **2008**, *358*, 1148-59.
154. Feinberg, A. P.; Vogelstein, B., Hypomethylation distinguishes genes of some human cancers from their normal counterparts. *Nature* **1983**, *301*, 89-92.
155. Greger, V.; Passarge, E.; Hfpping, W.; Messmer, E.; Horsthemke, B., Epigenetic changes may contribute to the formation and spontaneous regression of retinoblastoma. *Hum. Genet.* **1989**, *83*, 155-158.
156. Gonzalez-Zulueta, M.; Bender, C. M.; Yang, A. S.; Nguyen, T.; Beart, R. W.; Tornout, J. M. V.; Jones, P. A., Methylation of the 5' CpG Island of the p16/CDKN2 Tumor Suppressor Gene in Normal and Transformed Human Tissues Correlates with Gene Silencing'. *Cancer Res.* **1995**, *55*, 4531-35.
157. Y, S.; G, L.; G, E.; JM, F.; JC, C.; GA, C.; PA, J., Specific activation of microRNA-127 with downregulation of the proto-oncogene BCL6 by chromatin-modifying drugs in human cancer cells. *Cancer Cell* **2006**, *9*, 435-43.
158. Kriaucionis, S.; Heintz, N., The Nuclear DNA Base 5-Hydroxymethylcytosine Is Present in Purkinje Neurons and the Brain. *Science* **2009**, *324*, 929-30.
159. Tahiliani, M.; Koh, K. P.; Shen, Y.; Pastor, W. A.; Bandukwala, H.; Brudno, Y.; Agarwal, S.; Iyer, L. M.; Liu, D. R.; Aravind, L.; Rao, A., Conversion of 5-Methylcytosine to 5-Hydroxymethylcytosine in Mammalian DNA by MLL Partner TET1. *Science* **2009**, *324*, 930-35.
160. Nestor, C.; Ruzov, A.; Meehan, R. R.; Dunican, D. S., Enzymatic approaches and bisulfite sequencing cannot distinguish between 5-methylcytosine and 5-hydroxymethylcytosine in DNA. *BioTechniques* **2010**, *48*, 317-19.
161. Halliwell, B.; Gutteridge, J. M. C., Free Radicals in Biology and Medicine. *Oxford Science Publications, New York, NY* **1999**.
162. Kanvah, S.; Joseph, J.; Schuster, G. B., Oxidation of DNA: Damage to Nucleobases. *Acc. Chem. Res.* **2010**, *43*, 280-87.
163. Michaels, M. L.; Cruz, C.; Grollman, A. P.; Miller, J. H., Evidence that MutY and MutM combine to prevent mutations by an oxidatively damaged form of guanine in DNA. *Proc. Natl. Acad. Sci. USA* **1992**, *89*, 7022-25.

164. Thompson, H. J., DNA Oxidation Products, Antioxidant Status, and Cancer Prevention. *J. Nutr.* **2004**, *134*, 3186-87.
165. Cottrell, S.; Laird, P. W., Sensitive Detection of DNA Methylation. *Ann. N. Y. Acad. Sci.* **2003**, *983*, 120-30.
166. Harris, R. A.; Wang, T.; Coarfa, C.; Nagarajan, R. P.; Hong, C.; Downey, S. L.; Johnson, B. E.; Fouse, S. D.; Delaney, A.; Zhao, Y.; Olshen, A.; Ballinger, T.; Zhou, X.; Forsberg, K. J.; Gu, J.; Echipare, L.; O'Geen, H.; Lister, R.; Pelizzola, M.; Xi, Y.; Epstein, C. B.; Bernstein, B. E.; Hawkins, R. D.; Ren, B.; Chung, W.-Y.; Gu, H.; Bock, C.; Gnirke, A.; Zhang, M. Q.; Haussler, D.; Ecker, J. R.; Li, W.; Farnham, P. J.; Waterland, R. A.; Meissner, A.; Marra, M. A.; Hirst, M.; Milosavljevic, A.; Costello, J. F., Comparison of sequencing-based methods to profile DNA methylation and identification of monoallelic epigenetic modifications. *Nature Biotechnol.* **2010**, *28*, 1097-105.
167. Bock, C.; Tomazou, E. M.; Brinkman, A. B.; Müller, F.; Simmer, F.; Gu, H.; Jäger, N.; Gnirke, A.; Stunnenberg, H. G.; Meissner, A., Quantitative comparison of genome-wide DNANA methylation mapping technologies. *Nature Biotechnol.* **2010**, *28*, 1106-14.
168. Xu, H.; Bjerneld, E. J.; Käll, M.; Börjesson, L., Spectroscopy of Single Hemoglobin Molecules by Surface Enhanced Raman Scattering. *Phys. Rev. Lett.* **1999**, *83*, 4357-60.
169. David, C.; Guillot, N.; Shen, H.; Toury, T.; Chappelle, M. L. d. l., SERS detection of biomolecules using lithographed nanoparticles towards a reproducible SERS biosensor. *Nanotechnology* **2010**, *21*.
170. Camden, J. P.; Dieringer, J. A.; Zhao, J.; Duyne, R. P. V., Controlled Plasmonic Nanostructures for Surface-Enhanced Spectroscopy and Sensing. *Acc. Chem. Res.* **2008**, *41*, 1653-61.
171. Fabris, L.; Schierhorn, M.; Moskovits, M.; Bazan, G. C., Aptatag-Based Multiplexed Assay for Protein Detection by Surface-Enhanced Raman Spectroscopy. *Small* **2010**, *6*, 1550-57.
172. Barhoumi, A.; Zhang, D.; Tam, F.; Halas, N. J., Surface-Enhanced Raman Spectroscopy of DNA *J. Am. Chem. Soc.* **2008**, *130*, 5523-29.
173. Barhoumi, A.; Halas, N. J., Label-Free Detection of DNA Hybridization Using Surface Enhanced Raman Spectroscopy. *J. Amer. Chem. Soc.* **2010**, *132*, 12792-93.
174. Kundu, J.; Levin, C. S.; Halas, N. J., Real-Time Monitoring of Lipid Transfer between Vesicles and Hybrid Bilayers on Au Nanoshells using Surface Enhanced Raman Scattering (SERS). *Nanoscale* **2009**, *1*, 114-17.
175. Neumann, O.; Tam, F.; Zhang, D.; Halas, N. J., Label-free, aptamer-based all-optical molecular recognition. *Analytical Chemistry* **2009**, *81*, 10002-6.
176. Barhoumi, A.; Zhang, D.; Halas, N. J., Correlation of Molecular Orientation and Packing Density in a dsDNA Self-Assembled Monolayer Observable with Surface-Enhanced Raman Spectroscopy. *J. Am. Chem. Soc.* **2008**, *130*, 14040-41.
177. Ehrlich, M.; A.Gama-Sosa, M.; Huang, L.-H.; Midgett, R. M.; Kuo, K. C.; A.McCune, R.; Gehrke, C., Amount and distribution of 5-methylcytosine in human DNA from different types of tissues or cells. *Nucleic Acids Res.* **1982**, *10*, 2709-21.
178. Tucker, K. L., Methylated Cytosine and the Brain: A New Base for Neuroscience. *Neuron* **2001**, *30*, 649-52.
179. Prodan, E.; Nordlander, P., Electronic Structure and polarizability of metallic nanoshells. *Chemical Physics Letters* **2002**, *352*, 140-146.
180. Oldenburg, S. J.; Jackson, J. B.; Westcott, S. L.; Halas, N. J., Infrared extinction properties of gold nanoshells. *Appl. Phys. Lett.* **1999**, *75*, 2879-2899.

181. Lal, S.; Clare, S. E.; Halas, N. J., Nanoshell-Enabled Photothermal Cancer Therapy: Impending Clinical Impact. *Acc. Chem. Res.* **2008**, *41*, 842-1851.
182. Crothers, D. M.; Zimm, B. H., Theory of melting transition of synthetic polynucleotides - evaluation of stacking free energy. *Journal of Molecular Biology* **1964**, *9* (1), 1-9.
183. Devoe, H., Stability of helical polynucleotides - base contributions. *Journal of Molecular Biology* **1962**, *4* (6), 500-517.
184. Breslauer, K. J.; Frank, R.; Blocker, H.; Marky, L. A., Predicting DNA Duplex Stability From the Base Sequence. *Proceedings of the National Academy of Sciences of the United States of America* **1986**, *83* (11), 3746-3750.
185. SantaLucia, J.; Allawi, H. T.; Seneviratne, A., Improved nearest-neighbor parameters for predicting DNA duplex stability. *Biochemistry* **1996**, *35* (11), 3555-3562.
186. SantaLucia, J., A unified view of polymer, dumbbell, and oligonucleotide DNA nearest-neighbor thermodynamics. *Proceedings of the National Academy of Sciences of the United States of America* **1998**, *95* (4), 1460-1465.
187. Sugimoto, N.; Nakano, S.; Yoneyama, M.; Honda, K., Improved thermodynamic parameters and helix initiation factor to predict stability of DNA duplexes. *Nucleic Acids Research* **1996**, *24* (22), 4501-4505.
188. Doktycz, M. J.; Goldstein, R. F.; Paner, T. M.; Gallo, F. J.; Benight, A. S., Studies of DNA dumbbells .1. melting curves of 17 DNA dumbbells with different duplex stem sequences linked by T4 endloops - evaluation of the nearest-neighbor stacking interactions in DNA. *Biopolymers* **1992**, *32* (7), 849-864.
189. Delcourt, S. G.; Blake, R. D., Stacking energies in DNA. *Journal of Biological Chemistry* **1991**, *266* (23), 15160-15169.
190. Quartin, R. S.; Wetmur, J. G., Effect of ionic strength on the hybridization of oligodeoxynucleotides with reduced charge due to methylphosphonate linkages to unmodified oligodeoxynucleotides containing the complementary sequence. *Biochemistry* **1989**, *28* (3), 1040-1047.
191. Freier, S. M.; Kierzek, R.; Jaeger, J. A.; Sugimoto, N.; Caruthers, M. H.; Neilson, T.; Turner, D. H., Improved free energy parameters for predictions of RNA duplex stability. *Proceedings of the National Academy of Sciences of the United States of America* **1986**, *83* (24), 9373-9377.
192. Wartell, R. M.; Benight, A. S., Thermal denaturation of DNA molecules - a comparison of theory with experiment. *Physics Reports-Review Section of Physics Letters* **1985**, *126* (2), 67-107.
193. Gotoh, O.; Tagashira, Y., Stabilities of nearest-neighbor doublets in double-helical DNA determined by fitting calculated melting profiles to observed profiles. *Biopolymers* **1981**, *20* (5), 1033-1042.
194. Demers, L. M.; Mirkin, C. A.; Mucic, R. C.; Reynolds, R. A.; Letsinger, R. L.; Elghanian, R.; Viswanadham, G., A Fluorescence-Based Method for Determining the Surface Coverage and Hybridization Efficiency of Thiol-Capped Oligonucleotides Bound to Gold Thin Films and Nanoparticles. *Anal. Chem.* **2000**, *72*, 5535-5541.
195. Brewood, G. P.; Rangineni, Y.; Fish, D. J.; Bhandiwad, A. S.; Evans, D. R.; Solanki, R.; Benight, A. S., Electrical detection of the temperature induced melting transition of a DNA hairpin covalently attached to gold interdigitated microelectrodes. *Nucleic Acids Res.* **2008**, *36*.
196. Sun, Y.; Harris, N. C.; Kiang, C.-H., Melting transition of directly linked gold nanoparticle DNA assembly. *Physica A* **2005**, *350*, 89-94.

197. Meunier-Prest, R.; Raveau, S.; Finot, E.; Legay, G.; Cherkaoui-Malki, M.; Latruffe, N., Direct measurement of the melting temperature of supported DNA by electrochemical method. *Nucleic Acids Res.* **2003**, *31*.
198. Hill, H. D.; Millstone, J. E.; Banholzer, M. J.; Mirkin, C. A., The Role Radius of Curvature Plays in Thiolated Oligonucleotide Loading on Gold Nanoparticles. *ACS Nano* **2009**, *3*, 418-424.
199. Cederquist, K. B.; Keating, C. D., Curvature Effects in DNA: Au Nanoparticle Conjugates. *ACS Nano* **2009**, *3*, 256-260.
200. Langer, R., Drug delivery and targeting. *Nature* **1998**, *392* (6679), 5-10.
201. Panyam, J.; Labhasetwar, V., Biodegradable nanoparticles for drug and gene delivery to cells and tissue. *Adv. Drug Delivery Rev.* **2003**, *55* (3), 329-347.
202. Niidome, T.; Huang, L., Gene therapy progress and prospects: Nonviral vectors. *Gene Ther.* **2002**, *9* (24), 1647-1652.
203. Shea, L. D.; Smiley, E.; Bonadio, J.; Mooney, D. J., DNA delivery from polymer matrices for tissue engineering. *Nat. Biotechnol.* **1999**, *17* (6), 551-554.
204. Richardson, T. P.; Peters, M. C.; Ennett, A. B.; Mooney, D. J., Polymeric system for dual growth factor delivery. *Nature Biotechnology* **2001**, *19* (11), 1029-1034.
205. Kim, C. K.; Ghosh, P.; Pagliuca, C.; Zhu, Z. J.; Menichetti, S.; Rotello, V. M., Entrapment of Hydrophobic Drugs in Nanoparticle Monolayers with Efficient Release into Cancer Cells. *J. Am. Chem. Soc.* **2009**, *131* (4), 1360-1361.
206. LaVan, D. A.; McGuire, T.; Langer, R., Small-scale systems for in vivo drug delivery. *Nat. Biotechnol.* **2003**, *21* (10), 1184-1191.
207. Kim, S. Y.; Shin, I. L. G.; Lee, Y. M.; Cho, C. S.; Sung, Y. K., Methoxy poly(ethylene glycol) and epsilon-caprolactone amphiphilic block copolymeric micelle containing indomethacin. II. Micelle formation and drug release behaviours. *J. Controlled Release* **1998**, *51* (1), 13-22.
208. Chilkoti, A.; Dreher, M. R.; Meyer, D. E.; Raucher, D., Targeted drug delivery by thermally responsive polymers. *Adv. Drug Delivery Rev.* **2002**, *54* (5), 613-630.
209. Boussif, O.; Lezoualch, F.; Zanta, M. A.; Mergny, M. D.; Scherman, D.; Demeneix, B.; Behr, J. P., A Versatile Vector for Gene and Oligonucleotide Transfer into Cells in Culture and In-Vivo-Polythylenimine. *Proc. Natl. Acad. Sci. U S A* **1995**, *92* (16), 7297-7301.
210. Shalek, A. K.; Robinson, J. T.; Karp, E. S.; Lee, J. S.; Ahn, D. R.; Yoon, M. H.; Sutton, A.; Jorgolli, M.; Gertner, R. S.; Gujral, T. S.; MacBeath, G.; Yang, E. G.; Park, H., Vertical silicon nanowires as a universal platform for delivering biomolecules into living cells. *Proc. Natl. Acad. Sci. U. S. A.* **2010**, *107* (5), 1870-1875.
211. Chen, C. C.; Lin, Y. P.; Wang, C. W.; Tzeng, H. C.; Wu, C. H.; Chen, Y. C.; Chen, C. P.; Chen, L. C.; Wu, Y. C., DNA-gold nanorod conjugates for remote control of localized gene expression by near infrared irradiation. *J. Am. Chem. Soc.* **2006**, *128* (11), 3709-3715.
212. Takahashi, H.; Niidome, Y.; Yamada, S., Controlled release of plasmid DNA from gold nanorods induced by pulsed near-infrared light. *Chem. Commun.* **2005**, (17), 2247-2249.
213. Wijaya, A.; Schaffer, S. B.; Pallares, I. G.; Hamad-Schifferli, K., Selective Release of Multiple DNA Oligonucleotides from Gold Nanorods. *Acs Nano* **2009**, *3* (1), 80-86.
214. Braun, G. B.; Pallaoro, A.; Wu, G. H.; Missirlis, D.; Zasadzinski, J. A.; Tirrell, M.; Reich, N. O., Laser-Activated Gene Silencing via Gold Nanoshell-siRNA Conjugates. *Acs Nano* **2009**, *3* (7), 2007-2015.

215. Lee, S. E.; Liu, G. L.; Kim, F.; Lee, L. P., Remote Optical Switch for Localized and Selective Control of Gene Interference. *Nano Lett.* **2009**, *9* (2), 562-570.
216. Han, G.; You, C. C.; Kim, B. J.; Turingan, R. S.; Forbes, N. S.; Martin, C. T.; Rotello, V. M., Light-regulated release of DNA and its delivery to nuclei by means of photolabile gold nanoparticles. *Angew. Chem. Int. Ed.* **2006**, *45* (19), 3165-3169.
217. Barhoumi, A.; Huschka, R.; Bardhan, R.; Knight, M. W.; Halas, N. J., Light-induced release of DNA from plasmon-resonant nanoparticles: Towards light-controlled gene therapy. *Chem. Phys. Lett.* **2009**, *482* (4-6), 171-179.
218. Prodan, E.; Nordlander, P.; Halas, N. J., Electronic structure and optical properties of gold nanoshells. *Nano Lett.* **2003**, *3* (10), 1411-1415.
219. Wang, H.; Brandl, D. W.; Nordlander, P.; Halas, N. J., Plasmonic nanostructures: Artificial molecules. *Acc. Chem. Res.* **2007**, *40* (1), 53-62.
220. El-Sayed, I. H.; Huang, X.; El-Sayed, M. A., Selective laser photo-thermal therapy of epithelial carcinoma using anti-EGFR antibody conjugated gold nanoparticles. *Cancer Lett. (Amsterdam, Netherlands)* **2006**, *239*, 129-135.
221. Hirsch, L. R.; Stafford, R. J.; Bankson, J. A.; Sershen, S. R.; Rivera, B.; Price, R. E.; Hazle, J. D.; Halas, N. J.; West, J. L., Nanoshell-mediated near-infrared thermal therapy of tumors under magnetic resonance guidance. *Proc. Natl. Acad. Sci. USA* **2003**, *100*, 13549-13554.
222. Richardson, H. H.; Carlson, M. T.; Tandler, P. J.; Hernandez, P.; Govorov, A. O., Experimental and Theoretical Studies of Light-to-Heat Conversion and Collective Heating Effects in Metal Nanoparticle Solutions. *Nano Lett.* **2009**, *9* (3), 1139-1146.
223. Stephens, A. C.; Rivers, R. P. A., Antisense oligonucleotide therapy in cancer. *Curr. Opin. Mol. Ther.* **2003**, *5* (2), 118-122.
224. Neto, B. A. D.; Lapis, A. A. M., Recent Developments in the Chemistry of Deoxyribonucleic Acid (DNA) Intercalators: Principles, Design, Synthesis, Applications and Trends. *Molecules* **2009**, *14* (5), 1725-1746.
225. Ihmels, H.; Otto, D., Intercalation of organic dye molecules into double-stranded DNA general principles and recent developments. *Top. Curr. Chem.* **2005**, *258*, 161-204.
226. Barcellona, M. L.; Gratton, E., The fluorescence properties of a DNA probe. 4'-6-Diamidino-2-phenylindole (DAPI). *Eur Biophys J.* **1990**, *17* (6), 315-323.
227. Manzini, G.; Xodo, L.; Barcellona, M. L.; Quadrifoglio, F., Interaction of 4'-6-diamidino-2-phenylindole 2HCl with synthetic and natural deoxy- and ribonucleic acids *J. Biosci.* **1985**, *8* (3-4), 699-711.
228. Kapuściński, J.; Szer, W., Interactions of 4', 6-diamidine-2-phenylindole with synthetic polynucleotides. *Nucl. Acids Res.* **1979**, *6* (11), 3519-3534.
229. Kubista, M.; Aakerman, B.; Norden, B., Characterization of interaction between DNA and 4',6-diamidino-2-phenylindole by optical spectroscopy. *Biochemistry* **1986**, *26* (14), 4545-4553.
230. Lin, M. S.; Comings, D. E.; Alfi, O. S., Optical studies of the interaction of 4'-6-diamidino-2-phenylindole with DNA and metaphase chromosomes. *Chromosoma* **1977**, *60* (1), 15-25.
231. Jung, K. S.; Kim, M. S.; Lee, G. J.; Cho, T. S.; Kim, E. K.; Yi, S. Y., Conformation of Single Stranded Poly(dA) and Its Interaction with 4', 6-Diamidino-2-phenylindole. *Bull. Korean Chem. Soc.* **1997**, *18* (5), 510-514.

232. Breusegem, S. Y.; Clegg, R. M.; Loontjens, F. G., Base-sequence Specificity of Hoechst 33258 and DAPI Binding to Five (A/T)₄ DNA Sites with Kinetic Evidence for more than One High-affinity Hoechst 33258-AATT Complex. *J. Mol. Biol.* **2002**, *315*, 1049-1061.
233. Ochsenkuhn, M. A.; Jess, P. R. T.; Stoquert, H.; Dholakia, K.; Campbell, C. J., Nanoshells for Surface-Enhanced Raman Spectroscopy in Eukaryotic Cells: Cellular Response and Sensor Development. *Acs Nano* **2009**, *3* (11), 3613-3621.
234. Chithrani, B. D.; Ghazani, A. A.; Chan, W. C. W., Determining the size and shape dependence of gold nanoparticle uptake into mammalian cells. *Nano Lett.* **2006**, *6* (4), 662-668.
235. Giljohann, D. A.; Seferos, D. S.; Patel, P. C.; Millstone, J. E.; Rosi, N. L.; Mirkin, C. A., Oligonucleotide loading determines cellular uptake of DNA-modified gold nanoparticles. *Nano Lett.* **2007**, *7* (12), 3818-3821.
236. Dengler, W. A.; Schulte, J.; Berger, D. P.; Mertelsmann, R.; Fiebig, H. H., Development of a Propidium Iodide Fluorescence Assay for Proliferation and Cytotoxicity Assays. *Anti-Cancer Drugs* **1995**, *6* (4), 522-532.
237. Hendry, L. B.; Mahesh, V. B.; Bransome, E. D.; Ewing, D. E., Small molecule intercalation with double stranded DNA: Implications for normal gene regulation and for predicting the biological efficacy and genotoxicity of drugs and other chemicals. *Mutat. Res.* **2007**, *623*, 53-71.
238. Wheate, N. J.; Brodie, C. R.; Collins, J. G.; Kemp, S.; Aldrich-Wright, J. R., DNA intercalators in cancer therapy: Organic and inorganic drugs and their spectroscopic tools of analysis. *Mini-Rev. Med. Chem.* **2007**, *7* (6), 627-648.